Ana Rita da Fonseca Ricardo

Licenciatura Engenharia Biotecnológica

Modelling and optimization of the Ion Exchange Membrane Bioreactor for removal of anionic pollutants from drinking water streams

Dissertação para obtenção do Grau de Doutor em Engenharia Química, especialidade de Engenharia Bioquímica

Orientador:	João Paulo Crespo, Professor Catedrático, FCT-UNL
Co-orientadores:	Maria Ascenção M. Reis, Professora Associada, com Agregação, FCT-UNL
	Svetlozar Velizarov, Investigador Requimte, FCT-UNL

Júri:

Presidente:	Prof. Doutor Fernado Jorge da Silva Pina
Arguentes:	Prof. Doutor Jack Gilron
	Prof. Doutor Eugénio Manuel de Faria Campus Ferreira
Vogais:	Prof. Doutora Paula Maria Lima e Castro
	Prof. Doutor João Paulo Serejo Goulão Crespo
	Prof. Doutora Maria da Ascensão C. F. Miranda Reis
	Prof. Doutor Svetlozar Gueorguiev Velizarov

FACULDADE DE CIÊNCIAS E TECNOLOGIA
UNIVERSIDADE NOVA DE LISBOA

Dezembro, 2011

Modelling and optimization of the Ion Exchange Membrane Bioreactor for removal of anionic pollutants from drinking water streams

Agradecimentos

Em primeiro lugar gostaria de agradecer ao Professor Doutor João Goulão Crespo e à Professora Doutora Ascensão Reis por terem acreditado nas minhas capacidades apenas com uma conversa de 30 minutos. Agradeço a disponibilidade, os ensinamentos, o rigor científico e a criatividade demonstrada ao longo deste trabalho científico. O meu agradecimento também pela amizade e por todo o apoio pessoal dado ao longo destes anos. Um doutoramento é um período de crescimento e vocês foram concerteza os catalizadores desse processo.

Ao Doutor Svetlozar Velizarov, co-orientador deste trabalho, agradeço o enorme apoio prestado na execução deste trabalho científico. O seus conhecimentos, rigor científico e apurado espírito crítico foram essenciais para a tese que hoje apresento.

Agradeço ao Professor Doutor Rui Oiveira pelo opoio prestado na realização dos modelos, quer estatítisticos quer mecanísticos. Muito obrigado pela disponibilidade e pelas explicações.

Agradeço também ao Doutor João Dias pela ajuda no MatLab, principalmente no início quando o afundava em questões sem fim.

À Doutora Gilda Carvalho agradeço os ensinamentos e a ajuda na execução das análises de FISH. É sempre compensador trabalhar com pessoas que adoram aquilo que fazem e que tem um grande espírito de entreajuda.

Agradeço à Doutora Carla Portugal pela ajuda com as medições de fluorescência e pela sua sempre boa disposição e amizade.

O meu muito obrigada à Doutora Cristina Matos, que para além da sua valiosa amizade, me passou o testemunho de estudar o IEMB. Sem os seus ensinamentos não seria possível completar este trabalho.

Agradeço o apoio financeiro da Fundação para a Ciência e Tecnologia através de minha bolsa de doutoramento SFRH/BD/25275/2005.

Agradeço à Rita Valério pela ajuda no trabalho com o módulo de Plexiglas, assim como toda a paciência para os problemas que surgiram na execução deste trabalho.

A todo o grupo Bioeng deixo o meu profundo agradecimento. Convosco partilhei o dia-a-dia destes últimos anos com boa disposição e espírito de entreajuda. Em especial queria agradeçer à Andreia, pela disponibilidade em sempre ajudar os outros. Obrigado também pelos momentos

de boa disposição e alegria. Agradeço também à Joana Fradinho pelos "brainstorming" de ideias e pelas conversas na boleia para casa.

Muito obrigada à Luísa Neves pela sua alegria, optimismo e preocupação. É de facto a pessoa mais atenciosa que conheço e levo comigo os bons momentos que partilhamos juntas quer no laboratório quer nas conferências.

Ao "gang da marmita" por ter partilhado comigo valiosos momentos de descontração. À Claúdia, Rita, Filipa e Graça, obrigado por me ouvirem e me darem opoio em momentos essenciais, quer relacionados com o trabalho quer relacionados com a minha vida pessoal.

Em especial agradeço à Ana, por tudo aquilo que me ensinou e por me ensinar que devemos sempre lutar pelos nossos sonhos, mesmo quando apenas nós acreditamos. Obrigada pelas grandes conversas que tivemos e por acreditares em mim.

Não posso deixar de agradecer a todos os meus amigos, em especial à Tatiana pela sua grande amizade e compreensão. Obrigada pelas palavras de apoio e pela paciência em ouvir os meus problemas.

Agradeço também os meus pais pelo enorme apoio que sempre me deram e em especial por terem ficado com o Tiago para eu poder trabalhar fora-de-horas. Obrigada também aos meus sogros pela confiança que depositaram em mim.

Em especial queria agradecer ao meu grande homem, Tiago, por acreditar que a mamã é a melhor mulher do mundo. O seu olhar dá-me uma força imensa e fez-me acreditar que eu sou uma super mulher. Obrigada por seres quem és.

Por último, um muito obrigada ao meu marido Paulo por me ter apoiado sempre e por me aturar ao longo destes anos. Sem o seu amor, ajuda, carinho e incentivo, este trabalho não seria possível.

Resumo

Neste trabalho pretendeu-se estudar a remoção biológica de nitrato e perclorato de água usando um reactor de membranas de permuta iónica (IEMB,"Ion Exchange Membrane Bioreactor"). Este sistema combina o transporte destes iões, através de uma membrana de permuta aniónica, com respectiva redução biológica. No IEMB o transporte não é apenas dependente das propriedades da membrana mas também das condições do compartimento biológico. Utilizando análise estatística multivariada, foi possível verificar que as variáveis mais importantes estavam relacionas quer com a composição da água poluída, quer com a composição do meio de alimentação ao bio-compartimento. A combinação deste modelo estatístico com um modelo mecanístico numa estrutura híbrida permite prever o transporte de aniões através da membrana, mesmo em condições em que a taxa de redução biológica é limitante. Verificou-se que devido à presença de nitrato numa maior gama de concentração, a taxa de redução biológica foi maioritariamente controlada pela cinética de redução de perclorato. Esta diferença foi responsável pela distribuição da comunidade microbiana no biofilme permitindo a redução sequencial dos dois poluentes, evitando assim inibição na redução de perclorato pela presença de nitrato.

A eficiência deste processo foi demonstrada previamente no tratamento de água contaminada com estes micropoluentes. No entanto, considerando uma possível aplicação industrial, é essencial identificar a forma como as variáveis importantes de processo afectam o desempenho deste bio-reactor. Deste modo, investigou-se o desempenho do IEMB, operado com água contaminada com perclorato e nitrato, utilizando um módulo constituído por diversas membranas dispostas em série (configuração "plate-and-frame"). Verificou-se que a água contaminada é tratada eficazmente e que a contaminação secundária pode ser evitada com a utilização de um protocolo de aumento gradual da concentração de etanol no meio de alimentação do bio-compartimento.

Palavras-chave

Reactor de membrana de permuta iónica; Tratamento de água; Nitrato e Perclorato; Cultura mista; Análise Estatística Multivariada; Modelação híbrida

Abstract

The present work aimed at studying the treatment of drinking water supplies contaminated with perchlorate and nitrate, using the Ion Exchange Membrane Bioreactor (IEMB) concept. This system combines the transport of these two anions from contaminated water, through an anion exchange membrane, with their biological reduction in a separate compartment. In the IEMB, the mass transport is dependent not only from membrane properties but also from the biocompartment conditions. Multivariate statistical techniques allowed determining the most important process parameters related mainly to the compositions of the polluted water stream and biomedium and to the fluid dynamics operating conditions. The combination of statistical techniques with mechanistic modelling was a major achievement since the counterion transport across the membrane was successfully simulated and predicted under biological reactions rate-limiting conditions. Since nitrate is present in the contaminated water in much higher concentration than that of perchlorate, the IEMB process rate was mainly limited by the perchlorate bioreduction kinetics. This difference influenced organisation of microbial communities in the biofilm. This organization allows sequentially reduction of nitrate and perchlorate thus minimizing perchlorate inhibition by nitrate.

Considering a possible large-scale application, it is essential to determine the effect of the key process variables. In this work, the performance of a plate-and-frame module configuration, consisting of a series of anion-exchange membranes was investigated. It was found that contaminated water streams are effectively treated and that secondary contamination of treated water by the carbon source used was avoided by a start-up procedure involving a gradual increase of ethanol feeding to the IEMB biocompartment.

Keywords

Ion-exchange membrane bioreactor; Water treatment; Nitrate and Perchlorate; Mixed microbial culture; Multivariate statistical modelling; Hybrid modelling

Table of Contents

x

Table of Figures

Table Index

List of Abbreviations, Variables and Notations

A	membrane area (m^2)
AEM	anion exchange membrane
AIC	Akaike Information Criterion parameter
A/V_b	membrane area per bioreactor volume (m^2/L)
b	endogeneous decay rate (d^{-1})
B	matrix of regression coefficients of Y
C	Y-weight matrix
C_i	target counterion molar concentration (mmol/L)
C_{bulk}	bulk counterion molar concentration (mmol/L)
CCL	candidate contaminants list
CFD	computation fluid dynamics
CV	cross validation
D	diffusion coefficient (m^2/h)
DWEL	drinking water equivalent level
E	matrix of X-residuals
EU	European Union
EPS	extracellular polymeric substances
EEMs	excitation-emission matrices
Ex/Em	excitation / emission
F	matrix of Y-residuals
F/A	water flow rate per membrane area ($L/m^2.h$)
g_1	result of 'softmax' function for the mechanistic model
g_2	result of 'softmax' function for the PLS model
HRT	hydraulic retention time (d)
IEMB	ion-exchange membrane bioreactor
J_i	flux of species *i* across the membrane (g/m^2h; mg/m^2h)
K	half-saturation constants (mg/L)
L	membrane thickness (μm)
LV	latent variables
MABs	membrane-attached biofilms
MCL	maximum contaminant level
MOE	mixture of Experts

nar	nitrate reductase
nir	nitrite reductase
nor	nitric oxide reductase
nos	nitrous oxide reductase
N	number of observations
NOM	natural organic matter
p_m	number of model parameters
P	matrix of X-loadings
P_m	membrane permeability (m^2/s)
PLS	projection to latent structures
q_{max}	maximum specific reduction rate (mg/mgVSS.d)
Q	matrix of Y-loadings
Q_m	membrane ion exchange capacity (meq/g)
R^2	correlation coefficient
Re	Reynolds number
RMSEP	root-mean-square-error-of-prediction
SEM	scanning electron microscopy
t	time
T	scores matrix
TNP	total number of parameters
USEPA	United States Environmental Protection Agency
VSS	volatile suspended solids (mg/L)
w	weights of 'softmax' function
W	X-weight matrix
x	predictor variable
X	matrix of predictor variables
X_b	biomass concentration (mgVSS/L)
y	response variable
Y	matrix of response variable
β_i	regression coefficient of predictor i
δ	standard deviation
δ_1	thickness of the boundary layer in the water compartment (μm)
δ_2	thickness of the boundary layer in the biocompartment (μm)

Subscripts

b	bioreactor
B	biocompartment
bulk	bulk counterion
exp	response variable experimental results
F	biofeed
i	trace counterion
model	response variable estimated results
n	nitrate
p	perchlorate
W	polluted water stream

Chapter

1

Introduction

1.1. Background

The drinking water disinfection implemented during the 20th century was a major public health accomplishment. Before this procedure, millions of people died infected with waterborne diseases such as typhoid and cholera [1]. Following the use of chemical disinfection, in the early 1900s, the concern with drinking water quality is nowadays of major importance. During the 20th century, regulation about drinking water quality was introduced and treatment water facilities were implemented and designed in order to fulfill the requirements. However, after the World War II, during a period designated as a "chemical revolution", new synthetic chemicals have been introduced in the environment [2]. Afterwards, new emerging contaminants have been discovered that can be potential threats to both environment and to human health. This was possible mainly due to the development of advanced analytical techniques that are now able to detect contaminants present in extremely low concentrations in drinking water sources. For some of the emerging contaminants, it is unfeasible to use conventional treatment methods that are already implemented in the field for their removal [3]. This study is focused on the development of a technology for the removal of two of such pollutants: perchlorate and nitrate. Perchlorate is an inorganic contaminant that, due to its high solubility in water and chemical stability, becomes a challenge to remove [4]. Nitrate is often found as a co-contaminant with perchlorate of drinking water sources and is one of the most common contaminants in rural and suburban areas due to its high solubility in water [4].

1.1.1. Perchlorate

Perchlorate was first detected in the 1980's in California and Nevada's groundwater [5]. However, the severity of the perchlorate contamination was only recognized in 1997 after the development of a more sensitive analytical technique that allowed for detecting perchlorate down to 4 μg/L [4]. In the United States, federal and state agencies identified more than 400 sites (surface and ground waters and soil) that were contaminated with perchlorate, thus affecting more than 35 states (see Figure 1.1) and more than 20 million persons [6]. Although the United States of America were the leading center of perchlorate contamination, perchlorate has also been detected in other countries. In Israel, perchlorate contamination has been found in the vadose zone near an ammonium perchlorate manufacturing plant north of Tel Aviv located above the central part of Israel's coastal aquifer [7]. Perchlorate was detected at 1200 mg perchlorate/kg sediment in a sample taken at 40 m below the soil surface [7]. In China, a recent study of Beijing water quality also detected perchlorate, 0.1 - 6.8 μg/L in the finish drinking water which variation was season-dependent [8]. On the other hand, higher levels of perchlorate were also detected in different types of foods and beverages [9, 10]. In Japan, cow's milk samples presented even higher perchlorate concentrations (9.4 ± 2.7 μg/L) than samples from US dairy milk reported by Food and Drug Administration (FDA) in 2004 (5.9 ± 1.8 μg/L) [10].

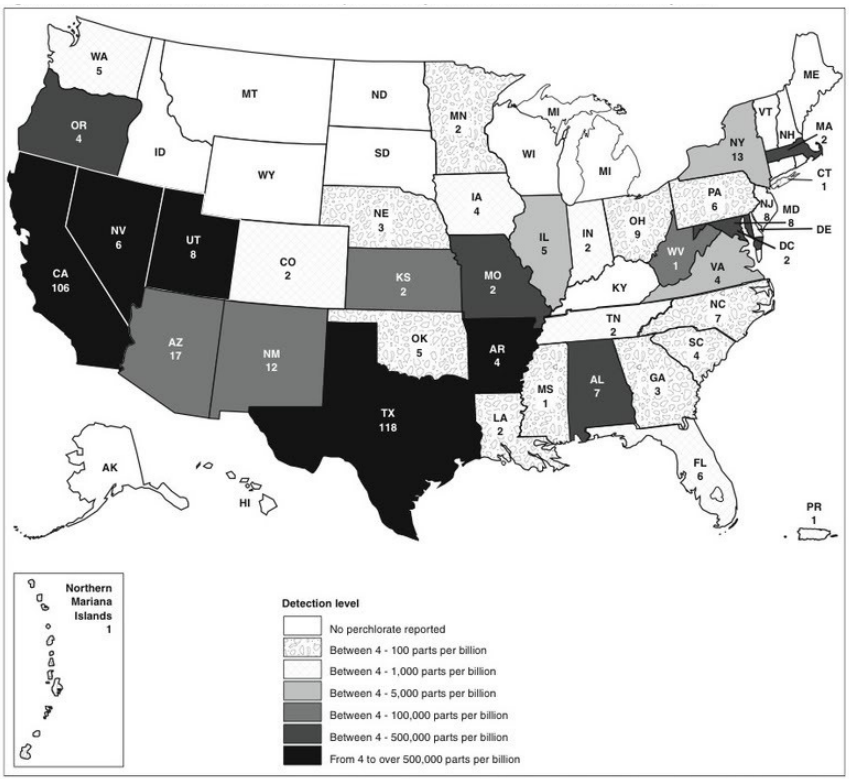

Figure 1.1: Maximum perchlorate concentrations reported in both water and soil samples and number of sites analyzed in USA (January 2005). Source: US GAO [6].

The main source of contamination came from disposal practices of aerospace industries and military facilities, where synthetically manufactured ammonium perchlorate was used as a fuel for rockets and solid missiles [5]. Perchlorate is also widely used in firework formulation since it is used as an oxidizer agent [11]. In the period before perchlorate regulation, processing waters and wastewaters from the disposal treatment of perchlorate-containing fuels were discharged directly to soil or into evaporation ponds [4]. Consequently, it is common to find perchlorate contamination near perchlorate manufacturing plants.

Perchlorate also occurs naturally in the environment. It has been detected in nitrate deposits in Chile that were used in some fertilizers [12]. These fertilizers were widely used and are still exported to the United States [4]. In the period of 1909 to 1929, 13 million of tons of nitrate were imported by USA from Chile [11]. About 65% was used as a fertilizer, resulting in approximately 30 tons of perchlorate that have been applied into the agricultural soil during that period [11]. More recently, perchlorate was also discovered in the southwestern part of the United States in natural phosphorous minerals that are formed through evaporation processes at levels as high as 3700 mg/kg [4].

Perchlorate contamination in drinking water and food supplies is a serious problem due to its adverse impact on the human health, particularly on the thyroid gland. Perchlorate inhibits the thyroid functioning since it competes with the iodine uptake by the thyroid gland [13]. This inhibition causes hypothyroidism that affects human vital functions such as growth, development, metabolism and reproduction [14]. Moreover, chlorate and chlorite, produced during perchlorate reduction, can also cause a severe toxicity in microorganisms, plants and laboratory animals [14].

1.1.2. Nitrate

Nitrate is not classified as a drinking water emerging contaminant given that it is regulated since 1980 in Europe and 1992 in the United States of America [15, 16]. It was introduced in the Safe Drinking Water Act approved by the USA congress in 1974, but only in 1992 the US EPA made the regulation for nitrate effective [16].

While the primary toxicity of nitrate is considered to be low, its conversion to nitrite or to nitrosamides can cause serious health risks [17]. In fact, concentrations of nitrate in drinking water above 10 mg/L can be fatal to infants under six months old, since nitrite formed during denitrification combines with hemoglobin in the blood and form methemoglobin, which affects oxygen uptake [18]. This condition is usually referred to as a “blue baby syndrome”. It is most often detected in infants with less than six months of age mainly because they possess much less oxidizable hemoglobin than adults. Moreover, due to the immaturity of certain enzymes, nitrate remains longer in the infants bodies since they have less ability to excrete nitrate by the kidneys as adults do. In fact, the maximum contaminant level (MCL) defined by US EPA was decided

based on 214 methemoglobinemia cases reported by the American Public Health Association [18].

Several reports have also suggested a correlation between nitrate consumption and spontaneous abortions, intrauterine growth restrictions and diverse birth defects [18]. Furthermore, many studies described a relation between stomach and gastrointestinal cancer and nitrate water intake [19]. However, in these studies the evidence of nitrate exposure effect is inconclusive since this factor can not be isolated from other exposure agents [18]. Nevertheless, there is a consensus on the carcinogenic effect of N-nitroso compounds formed after nitrate ingestion.

Nitrate can occur naturally in the soil and water since it is the primary source of nitrogen for plants. However, in the past 50 years, the rate of nitrogen deposition onto land duplicated due to the use of nitrogen rich fertilizers, the fossil fuels burning and the replacement of natural vegetation with nitrogen-fixing crops [17]. Together with the uncontrolled discharge of raw and treated wastewaters, nitrate concentration in groundwater increased to contaminant levels. This limited a direct use of groundwater for human consumption in several parts of the world, including India, China, Japan, USA and some parts of Europe [17]. In 1992, a study performed by US EPA showed that 1.2 % of public and 2.4 % of private domestic wells, from samples taken in 50 states, had values exceeding the MCL of 45 mg/L [18]. These results indicate that more than 4 million people could be consuming water with toxic levels of nitrate [18].

In Europe, a recent report from 2011 showed that 34 % of the 31 000 analyzed groundwater wells in 15 countries of the European Union, had an average nitrate concentration above 25 mg/L in which 15 % were above the MCL of 50 mg/L [20] (see Figure 1.2). These results showed that a stable and decreasing trend in groundwater nitrate concentration is documented when comparing with values reported for the period of 2000-2003 for the European Union composed by 15 countries [20]. However, in 34% of the monitoring stations, a trend of increasing nitrate concentrations was still detected. This trend was detected in countries like Belgium, France, Spain, Portugal, Germany, Ireland, Italy, Estonia and United Kingdom [20]. For this reason, all EU member states have already implemented actions programmes to assure full conformity with the requirements of the EU nitrates directive.

Nitrate is also often found as a co-contaminant with perchlorate since ammonium nitrate is an important component of explosives [21]. Nitrate concentration in contaminated groundwater is usually 2-5 orders of magnitude higher than that of perchlorate [21]. Moreover, due to their similar chemical characteristics, nitrate can decrease perchlorate removal efficiency in both physical and biological treatment processes. On one hand, nitrate may compete with perchlorate for binding on ion exchange resins or for transport in membrane-based processes. On the other hand, the close similarity in the redox potential of NO_3^-/N_2 pair (E^o = 1.25 V) with the ClO_4^-/Cl^- pair (E^o =1.28 V) makes nitrate an excellent competitor in biological treatment processes [14]. In fact, nitrate has been described as an inhibiting agent of perchlorate biological reduction by

several authors [21-23]. Therefore, the feasibility of a perchlorate treatment technology should be evaluated in the presence of nitrate.

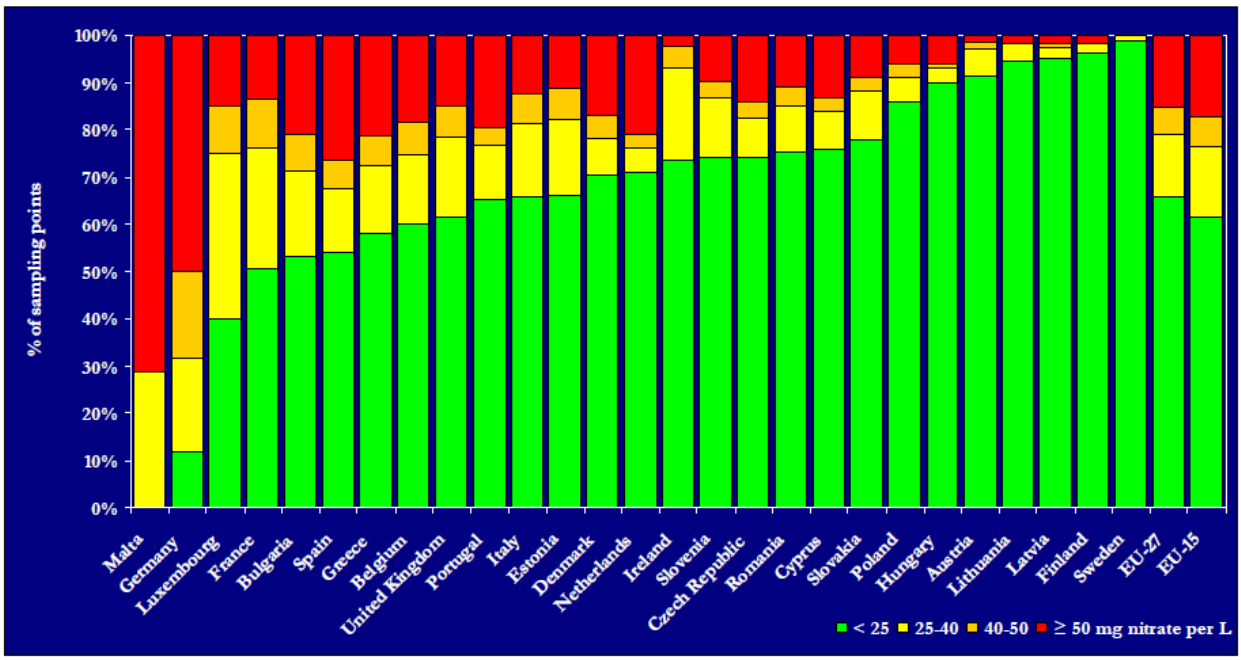

Figure 1.2: Frequency diagram of percentage of sampling points per groundwater quality class. i) nitrate values measured below 25 mg/L; ii) between 25 and 40 mg/L; iii) between 40 and 50 mg/L; iv) above 50 mg/L. Source: European Union [20]

1.1.3. Regulation

Since 1998, perchlorate has been included in the US EPA drinking water candidate contaminants list (CCL) under the Safe Drinking water Act [24]. This law, approved in 1974 by the US congress, ensures the quality of drinking water and recommends EPA to set standards for drinking water parameters. Accordingly, in 2005 the EPA defined the safe level of perchlorate as a reference dose of 0.7 µg perchlorate/kg body weight.day [25]. This value corresponds to a drinking water equivalent level (DWEL) of 24 µg/L, assuming water as the unique perchlorate source [25]. In 2009, the DWEL was reduced to 15 µg/L after EPA considered also the possibility of perchlorate exposure from food sources, as documented by several studies [9, 10]. A perchlorate MCL is still not available at the present time, however, a number of different states have already defined their own action levels for acceptable perchlorate levels in drinking water ranging between 1 and 18 µg/L [14]. For those with no state applicable law, 15 µg/L of perchlorate is the recommended cleanup target [26]. In Europe, no regulation is yet defined for perchlorate in drinking water sources.

After the Safe Drinking Water Act, a nitrate maximum contaminant level goal for drinking water has been set to 45 mg/L (10 mg N/L) in the United States [16]. This value was adopted as

the MCL in 1992 and is still in force nowadays, since the MCL is maintained at 45 mg/L, a value that the EPA considers to be safe for human health. The World Health Organization and the European Union have established a MCL of 50 mg/L in drinking water since 1980 and 1993, respectively [15, 27]. This value was reconfirmed in 2004 by the World Health Organization [28]. Nevertheless, EU recommends a level below 25 mg/l in treated water [15]. Nitrite, an intermediate of nitrate reduction, is also regulated with a MCL in drinking water of 0.5 mg/L in Europe and 3.3 mg/L in USA [15, 16].

1.2. Treatment technologies

The perchlorate and nitrate physical and chemical characteristics, especially their low reactivity and high water solubility, make them very difficult to be removed by traditional water treatment methods, such as flocculation, coagulation, sedimentation and filtration [5, 21]. Therefore, a variety of other physiochemical and biological treatment processes are now being used to remove nitrate and perchlorate.

1.2.1. Physicochemical processes

The most commonly used technology for the treatment of water contaminated with nitrate and perchlorate is anion-exchange [14, 29]. This process involves the passage of contaminated water through a strongly basic anion exchange resin, in which perchlorate and/or nitrate are exchanged for chloride or bicarbonate ions [30]. These resins are typically organic polymers with strong positively-charged functional groups such as e.g. quaternary amines (R_4N^+) [31]. After anion-exchange, nitrate and perchlorate remain bonded to the functional groups, whereas chloride (or bicarbonate) ions flow out:

$$R_4N^+Cl^- + NO_3^- \Leftrightarrow R_4N^+NO_3^- + Cl^- \quad (1.1)$$

$$R_4N^+Cl^- + ClO_4^- \Leftrightarrow R_4N^+ClO_4^- + Cl^- \quad (1.2)$$

A broad variety of anion-exchange resins that present a high selectivity for nitrate and/or perchlorate have been developed. When all the resin's functional groups have been exchanged, the resin becomes saturated and requires regeneration. This regeneration is usually performed with a saturated sodium chloride brine solution. The main drawback of this technology is the need for resin regeneration and the costs associated with the disposal of the spent regenerant that contains high concentrations of contaminants. Moreover, the competition of other anions

present in the water such as sulphate, chloride and phosphate can decrease the resin selectivity for the target pollutants.

Alternatively to anion exchange, activated carbon adsorption, electrodialysis, nanofiltration and reverse osmosis are also commonly used [32-34]. Adsorption on granular activated carbon is a technology widely implemented in drinking water treatment facilities. However, virgin granular activated carbon has to be tailored with cationic surfactants to be effective for perchlorate removal [32]. This makes it more expansive and also affects its adsorption capacity for other contaminants [31].

Membrane processes for water treatment, such as nanofiltration or reverse osmosis, are based on the use of a semi-permeable membrane that retains low-molecular weight solutes, such as nitrate and perchlorate [33]. In this processes, water is forced to cross the membrane, while the pollutants remain in the contaminated stream, thus forming concentrated brine. The driving force for mass transport is imposed by the difference of pressure across the membrane. Despite the production of water of high quality, large volumes of rejected streams highly concentrated in pollutans are produced. Furthermore, the selectivity of pressure-driven membrane technologies to different compounds of similar molecular weight and physicochemical characteristics is relatively low [31].

Electrodialyis has also been found to be suitable for removal of nitrate and perchlorate from water streams [34]. In this process, an electrical potential difference is used as the driving force for the removal of charged pollutants from polluted water. The membrane modules used consist of a series of anion- and cation-exchange membranes arranged in an alternating mode. As water flows between these membranes, under the applied electrical potential, perchlorate and/or nitrate ions, being negatively-charged, accumulate at the cation-exchange membrane and are eventually collected as concentrate. Similarly, positive ions accumulate at the anion-exchange membrane. This method produces two types of streams: a water pollutant free and a stream containing a high concentration of pollutants. Once more, the major drawback of this process is the production of a rejected stream.

A technology that completely degrades nitrate and perchlorate to harmless products is preferable since most physical processes only transfer perchlorate from one phase to another, necessitating its subsequent treatment and disposal. Thus, an alternative is to use degradation technologies since thermodynamics favor reduction of nitrate and perchlorate to nitrogen and chloride, respectively [35]:

$$NO_3^- + H^+ + 2.5\ H_2 \Leftrightarrow 0.5\ N_2 + 3H_20 \qquad \Delta G^o = -112\ KJ/e^- \qquad (1.3)$$

$$ClO_4^- + 4H_2 \Leftrightarrow Cl^- + 4H_20 \qquad \Delta G^o = -118\ KJ/e^- \qquad (1.4)$$

Despite perchlorate reduction being thermodynamically favored, perchlorate reduction capability is affected by the high activation energy (120 KJ/mol). This energy is derived from the atomic structure, in which a central chlorine atom is surrounded by four oxygen atoms in a tetrahedral configuration. Nitrate has a lower activation energy (47 KJ/mol) since the binding forces of oxygen atoms to the central nitrogen are weaker. Therefore, slower reduction rates were observed for both chemical and electrochemical reduction of perchlorate, which makes these techniques unfeasible for their practical implementation [31]. Moreover, chemical reduction requires the use of a catalyst that usually contains heavy metals [31].

1.2.2. Biological processes

Removal of perchlorate and nitrate by microbial reduction has been proven to be a feasible technology [5]. Their high oxidation states and high activation energies makes nitrate and perchlorate suitable as electron acceptors for microbial reduction. Therefore, under anoxic conditions some microorganisms can use perchlorate or nitrate as electron acceptors given that an electron donor is available.

The perchlorate reduction pathway consists in three steps: the first two steps are catalyzed by a (per)chlorate reductase, which sequentially reduces perchlorate (ClO_4^-) to chlorate (ClO_3^-), which in turn is reduced to chlorite. The third step splits chlorite to chloride and oxygen by a chlorite dismutase (see Figure 1.3) [36].

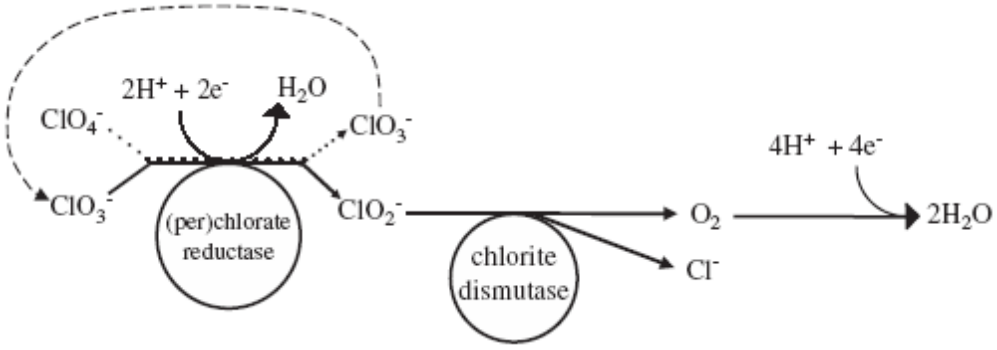

Figure 1.3: Schematic representation of perchlorate-reducing pathway. Source: Nerenberg et al., 2006 [36].

The ubiquity of (per)chlorate reducing-bacteria was shown by isolation of organisms from a variety of wastewaters, soils and sediments [12]. These organisms belong to *Alfa*, *Beta*, *Gamma*, and *Epsilon* subclasses of proteobacteria. All (per)chlorate reducers are also chlorate reducers, but the opposite is not always true.

Besides chlorate and perchlorate, (per)chlorate reducing bacteria can utilize oxygen and nitrate as electron acceptors. In the presence of oxygen, the (per)chlorate reductase in almost all (per)chlorate reducing bacteria is inhibited and (per)chlorate reduction stops [37]. An exception is *Pseudomonas sp.* PDA that is able to consume chlorate in the presence of oxygen [38].

(Per)chlorate reducing bacteria can also use nitrate as an electron acceptor. However, under the presence of both substrates, a competition for nitrate and perchlorate may occur. The effect of nitrate on (per)chlorate reduction rate depends on the species under study [39]. In some species, perchlorate and nitrate are reduced simultaneously, whereas in other species perchlorate reduction only starts after complete perchlorate reduction [12].

Under anoxic conditions, nitrate can be reduced to gaseous nitrogen-containing species, principally nitrogen, by a process referred to as denitrification. The production of nitrogen gas through denitrification closes the nitrogen cycle in nature via nitrogen fixation, since the ammonia produced during nitrogen fixation, can be converted into nitrite and nitrate. Full denitrification occurs in a multi-step process with four enzymatic steps, catalyzed by four metalloproteins: nitrate reductase, nitrite reductase, nitric oxide reductase and nitrous reductase (Table 1.1).

Table 1.1: Overview of the denitrification process. nar: nitrate reductase; nir: nitrite reductase; nor: nitric oxide reductase; nos: nitrous oxide reductase. Source: Shapleigh, 2006 [40]

Overall reaction:		
$NO_3^- \xrightarrow{nar} NO_2^- \xrightarrow{nir} NO \xrightarrow{nor} N_2O \xrightarrow{nos} N_2$		
Separate reactions:		
$NO_3^- + 2e^- + 2H^+ \rightarrow NO_2^- + H_2O$	ΔG_0' = -161 kJ/mol	E_0' = +420 mV
$NO_2^- + e^- + 2H^+ \rightarrow NO + H_2O$	ΔG_0' = -76.2 kJ/mol	E_0' = +374 mV
$2NO + 2e^- + 2H^+ \rightarrow N_2O + H_2O$	ΔG_0' = -306.3 kJ/mol	E_0' = +1177 mV
$N_2O + 2e^- + 2H^+ \rightarrow N_2 + H_2O$	ΔG_0' = -339.5 kJ/mol	E_0' = +1352 mV

Denitrifying bacteria are found in *Alfa*, *Beta*, *Gamma*, and *Epsilon* subclasses of proteobacteria, *Firmicutes*, and *Bacteroidetes*, with more than 130 bacterial species already identified [41]. In some of the isolated bacteria, only parts of the denitrification electron transport chain are expressed. This can be advantageous since each step of denitrification can be carried out individually due to its positive reduction potential.

Both perchlorate and nitrate biological reduction based processes have been applied in water treatment. The systems developed utilize either suspended-cell reactors or fixed-film reactors. The first are common in wastewater treatment, whereas fixed-film systems, in which

metabolizing cells are organized in a biofilm supported to a solid media, are commonly used to treat dilute contaminated streams and to increase process efficiency in wastewater treatment.

The first bioreactor applied for perchlorate treatment was based on a suspended-cell culture and was developed in the early 1990s for the treatment of wastewater from the Air Force Research Laboratory [42]. With this configuration, water bioremediation from a stream containing 5000 mg/L of ClO_4^- down to ~ 400 µg/L was achieved [42].

For groundwater treatment, two different fixed-bed designs have been investigated: packed-bed reactors and fluidized-bed reactors. In the first type, microbial cells grow mainly in a biofilm at the surface of the packing material (e.g., coarse sand, ring packing). With this configuration, a higher number of organisms can be maintained within the reactor when comparing with the suspended cells reactor. A pilot-scale unit using the packed-bed design was implemented in California and was able to reduce both perchlorate and nitrate to bellow 4 µg/L perchlorate and 0.1 mg/L nitrate, respectively [43].

Several full-scale fluidized-bed reactors are currently treating perchlorate in several locations in the United States [4]. In these systems, the biological medium is fluidized within the reactor by an upward flow of water, whereas the microbial population growth is supported by suspended media particles like sand or granular activated carbon [44]. Within this system, no clogging problems are observed as in packed-bed reactor. However, this configuration requires stronger pumps to maintain the flow rates required for bed fluidization, leading to higher energy consumption.

Biological denitrification is commonly used for the treatment of both municipal and wastewater, with several full-scale plants operating all over the world [30]. The most developed system is a two-stage process combining nitrification/denitrification, in which ammonia is oxidized to nitrite and subsequently to nitrate by nitrifying bacteria. Then, reduction of nitrate to molecular nitrogen is carried out by denitrifying bacteria, using either substrates from the wastewater or external organic carbon sources as electron donors [45].

Despite the ecological and cost-effective advantages of biological treatment of nitrate and perchlorate contaminated water over physico-chemical processes, drawback is that bacterial cells as well as their metabolic by-products have to be removed from the treated water. Moreover, the majority of biological processes are based on heterotrophic denitrifying and perchlorate reducing bacteria, which implies the addition of an organic carbon source to the water to be treated. The fine tunning of carbon fed to the bioreactor is required in order to avoid secondary contamination of treated water. Therefore, following the bioreduction, water post-treatment processes including filtration steps and disinfection are required.

1.2.3 Integrated processes: membrane-supported biofilm reactors

Different hybrid processes combining membranes and biological processes have been developed: the hydrogen-based membrane biofilm reactor [46-48], the dialysis membrane biofilm reactor [49] and the ion exchange membrane bioreactor [50]. In these processes, active reducing bacteria grow, as a biofilm, on the outside of a permeable membrane that delivers nutrients to the bacteria. A biofilm is defined as a consortium of cells immobilized at a substratum involved in an organic polymer matrix of microbial origin denominated extracellular polymeric substances (EPS) [51]. The initial events for biofilm formation result from the transport of cells to the substratum used as a supporting solid material, adsorption to the substratum and cell proliferation. The biofilm structure results from interactions between environmental factors, such as the mass transfer across the biofilm, the cell growth rate, the cell detachment rate, and the hydrodynamic shear stress [51].

Advantages of biofilm systems include organization of cells that favor community interactions between microorganisms [52]. For this reason, cell activity may alter microenvironments (e.g., pH, concentrations of oxygen, metabolites, biocides, etc.) which may allow for growth of microorganisms that cannot be cultivated in suspension. By using a biofilm reactor, it becomes possible to decouple solids retention time from hydraulic retention time, which allows for processing large volumes of liquid.

The membrane biofilm reactor differs from the conventional biofilm reactors since the substrates (electron donor or acceptor) diffuse into the membrane-attached biofilm from opposite sides (counter-diffusion) (see Figure 1.4), whereas in conventional biofilm reactors substrates enter into the biofilm from the same side (co-diffusion) [53]. In this system, the mass transfer across the biofilm may control the cell metabolic activity, thus leading to biofilm stratification, different from that in conventional biofilm processes, in which substrates are supplied by co-diffusion.

Membrane-supported biofilm reactors have been mainly applied for gas delivery (oxygen, hydrogen) since they allow for a more efficient gas transport to attached cells than the classical gas sparging devices [54]. For the treatment of nitrate and perchlorate contaminated water streams, a hydrogen-based membrane biofilm reactor has been proposed [46-48]. In the hydrogen-based membrane biofilm reactor, hydrogen gas is delivered to the microbial culture by hollow-fibers, thus reducing the primary risks of its high flammability and volatility [46]. In this process, the bioreduction is accomplished by autotrophic bacteria that use carbon dioxide as carbon source and hydrogen as electron donor. This process was successfully applied for nitrate removal [46] as well as for simultaneous nitrate and perchlorate removal [47]. However, in this process, secondary contamination of the treated water by microbial cells cannot be avoided.

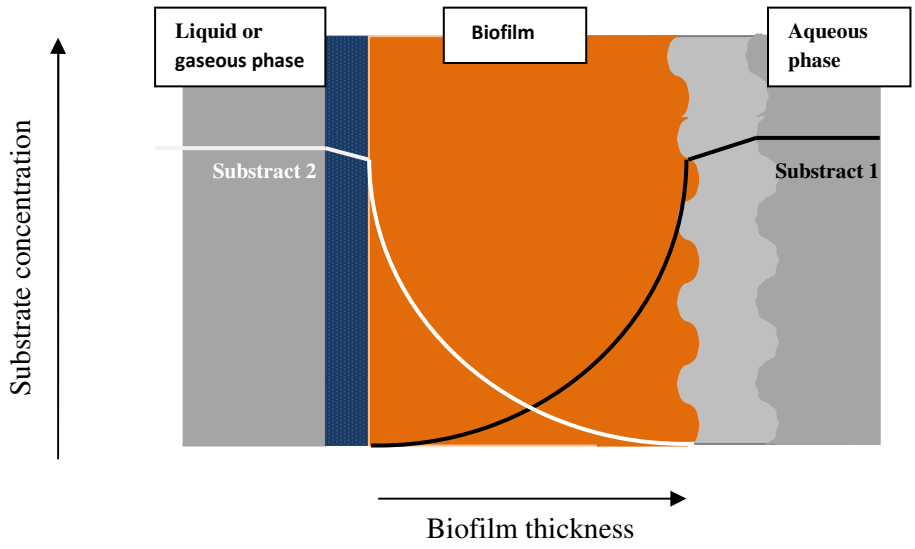

Figure 1.4: Illustration of substrates mass transfer by counter-diffusion in a membrane biofilm reactor.

An alternative membrane biofilm reactor developed for nitrate removal from drinking water sources uses a dialysis porous membrane to separate the biological reduction zone from the water stream, thus avoiding secondary contamination of water by microbial cells [49]. Nevertheless, the dialysis membrane used permitted the transport of carbon source and other nutrients from the bioreactor to the treated water.

The ion-exchange membrane bioreactor (IEMB) combines the transport of nitrate and perchlorate through a dense anion-exchange membrane with biological reduction in a separate compartment (biocompartment) [50]. The biological reduction takes place in the biofilm developed on the membrane surface contacting the biological compartment. The membrane is a physical barrier between the water and the bioreactor compartment and due to its dense properties, contamination of the treated water by a non-charged and non-fermenting carbon source (e.g. ethanol) can be minimized [55]. Moreover, the biofilm formed on the membrane surface contacting the biological compartment can act as a reactive barrier to the transport of excess carbon source to the water compartment. These features assure that secondary contamination of treated water by microorganisms, metabolic by-products and excess carbon source can be avoided and/or minimized if proper operating IEMB conditions are assured. Furthermore, since the transport is governed by Donnan dialysis, the transport of target anionic pollutants is possible even against their own concentration gradients by using a higher concentration of chloride as the "driving" counter-ion for their transport [50]. A high concentration of chloride in the biocompartment forces the target anions to diffuse from the water compartment (in the opposite direction to the chloride transport) to maintain the electroneutrality in the system (see Figure 1.5). Once in the biological compartment, anionic

micropollutants are reduced to innocuous species by a suitable mixed microbial culture under anoxic conditions. As the microbial culture performs nitrate and perchlorate reduction, only the driving force for transport of these two compounds is kept high since other ions transported are not biologically converted [50]. This characteristic guarantees that an adequate water composition is maintained since water is not demineralised (as occurs in some physical water treatment processes, such as reverse osmosis).

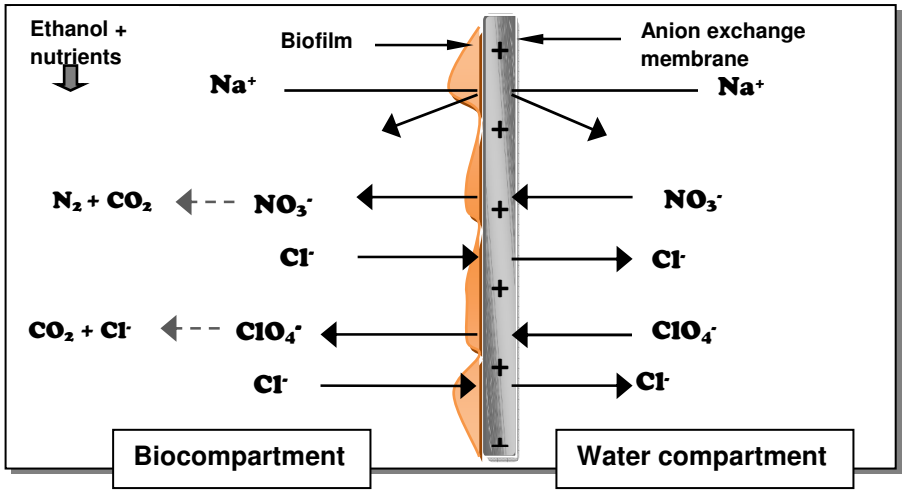

Figure 1.5: Schematic diagram of counter-ion transport and nitrate and perchlorate bioreduction in the IEMB process.

1.3. Motivation and work objectives

The Ion-Exchange Membrane Bioreactor (IEMB) concept, developed by the host research group, was first patented in Portugal in 1999 [56] and an international patent was granted in 2001 [57]. Initially, the IEMB was studied for denitrification of contaminated drinking water streams [58-60] and proved to be an efficient process for water contaminated with nitrate, since it was able to treat up to 30 L/m^2.h of polluted water containing up to 150 mg/L of nitrate [58, 59]. Later on, the feasibility of the IEMB to remove simultaneously nitrate and perchlorate from contaminated water stream was proved [55, 61]. In these experiments, ethanol, used as carbon source and electron donor was not detected in the treated water compartment, even when its concentration in the biocompartment was as high as 250 mg/L [55]. Moreover, the treated water composition, concerning other ions, was preserved [55].

A mechanistic mathematical model for the prediction of the flux of target charged pollutant(s) from the water to the biocompartment was developed [62]. The model considers the transport of a trace polluting counter-ion (present in the water compartment) against an excess of a major

bulk “driving” counter-ion (added to the biocompartment) in the frame of the resistances-in-series steady-state modeling approach. This model is based on various assumptions (see chapter 2 for details), the most important of which being the assumption that the overall process is controlled solely by mass transfer steps, thus presuming that the biological conditions are not limiting the process.

The IEMB concept was extended to the treatment of water contaminated with bromate, and ionic mercury [63-65]. Bromate which is a genotoxic carcinogen, was studied with co-contamination of nitrate [63] and with co-contamination of nitrate and perchlorate [64]. The results showed that a water stream contaminated with 60 mg/L of nitrate, 100 μg/L of perchlorate and 200 μg/L of bromate was efficiently treated to levels below the recommended limits for the three anions since the final water stream contained 0.3 mg/L of nitrate, 3.6 μg/L of perchlorate and 18 μg/L of bromate [64]. In the biocompartment, the mixed microbial culture was able to reduce nitrate, perchlorate and bromate to values below their detection limits (0.3 mg/L for nitrate, 10 μg/L for perchlorate and 10 μg/L for bromate) [64].

The IEMB concept was also extended for the treatment of nitrate in water with high salinity. Nitrate, accumulated to 251 mg/L in the water of the oceanarium of Lisbon, was removed to 27 mg/L, which is below the toxic levels for marine life [66]. To enhance nitrate transport through the membrane and to prevent possible co-transport of other anions, the composition of the receiving solution in the biocompartment (except for nitrate) was identical to that in the water compartment. It was demonstrated that even under such high salinity conditions, denitrification was efficient since the biocompartment effluent was almost free of nitrate (< 1 mg/L) [66].

Previous IEMB studies were, however, focused mainly on the understanding of the transport mechanism and were performed in laboratory-scale modules. Therefore, this PhD project is focused on other important issues such as the biocompartment conditions contribution to the IEMB performance as well as on the up-scaling challenges for a practical implementation of the IEMB process.

By guaranteeing proper operating conditions, i.e., anoxic conditions and no nutrient limitations, biological reduction of nitrate and perchlorate was found to be complete [55]. Under such conditions, the rates of nitrate and perchlorate removal from the treated water are mainly limited by the transport resistances of the membrane and of the liquid boundary layer contacting the water compartment. In this PhD project, a broader range of operating conditions was tested, in order to evaluate the effect of biological reactions kinetics on the IEMB process performance. With the obtained data, this PhD project aims to developed mathematical models capable of describing and predicting the transport rates not only in mass transfer limited situations, but also in situations of a biological reactions kinetics limitation. Furthermore, biological component of the IEMB was studied to characterize nitrate and perchlorate biological reduction. This

characterization is highly desirable for acquiring deeper process knowledge, required for a better rationalization and interpretation of the IEMB operating data, as well as for optimization and process control purposes. Finally, the consequences of process up-scaling were investigated in a plate-and-frame membrane module configuration.

This work is composed by three main parts with the following particular objectives:

a) Development of an integrated mathematical model for anionic flux prediction;
b) Characterization of biological kinetics and biofilm organization in the IEMB;
c) Evaluation of an up-scaling procedure and associated operating conditions.

a) *Development of an integrated model for anionic flux prediction*

The mechanistic model previously developed has the merit of being a straightforward and an easy tool for predicting steady-state nitrate and perchlorate fluxes in mass-transfer limited situations [55]. However, it has a limited range of validity if the biological conditions have a higher impact on the overall process performance. This is particularly critical in situations of a nutrient limitation or during the start-up period, in which the membrane biofilm is still not fully developed. Under such conditions, the rates of biological conversion of target pollutants may limit the overall process and should be accounted for by the model. Therefore, the first objective of this PhD thesis was to develop a mathematical model that covers a broader range of operating conditions, especially when the process is limited by the biological reactions kinetics (Chapter 2 and 3).

Due to the intrinsic complexity of cell metabolism, which is additionally complicated by the fact that a mixed microbial culture is used, modelling of all relevant phenomena in the IEMB can be extremely difficult. Therefore, the biological reactions contribution to the mass transfer was accounted for by multivariate statistical modelling. Two different approaches were followed: a purely statistical (in Chapter 2) and a hybrid modeling (in Chapter 3). In both cases, a multivariate statistical analysis was used to obtain relations between transport of counter-ions through the membrane and physicochemical process operation conditions, including those inherent to the biological process. Statistical methods, such as Projection to Latent Structures (PLS) [67] were tested to capture the underlying mechanisms from IEMB process operating data.

In the hybrid model, the previously developed mechanistic model [62] was combined with the PLS model in a mediated structure. It was expected that with this combination, the predictive power of the mechanistic model could be improved, assuming that the statistical component may account for effects not considered by the mechanistic model. Moreover, this arrangement might combine the best of both approaches, since it allows for a certain mechanistic interpretation provided by the mechanistic model together with the inclusion of effects, which are not considered by the mechanistic model.

Considering that the membrane used in the IEMB allows for transport of anions, the model developed was designed not only for predicting nitrate and perchlorate fluxes but also for prediction of fluxes of other counter-ions that could potentially cross the membrane due to their presence in the water stream, in the biocompartment, or simultaneously in both compartments (e.g., phosphate, sulphate, bicarbonate).

b) Characterization of biological kinetics and biofilm organization in the IEMB

This study aimed at understanding the control mechanism(s) for biological reduction of nitrate and perchlorate in the biofilm formed at the membrane surface contacting the biocompartment. As already mentioned, the IEMB process is limited by counter-ion mass transfer across the membrane as long as proper operation conditions assure the complete biological reduction of the transported ionic species. Since the IEMB operates as a membrane supported biofilm reactor, the rate of bioreduction in the biofilm is controlled by the transport of nitrate and perchlorate through the membrane, as long as sufficient content of electron donor and other growth cofactors are available in the biocompartment. However, in particular situations (e.g., during the process start-up period and in situations of substrate/nutrient limitation) the rate of biological reaction may become slower than the rate of transport of nitrate and/or perchlorate incoming from the membrane. Moreover, since the biofilm is composed by a mixed microbial population, a biofilm organization may also mediate multiple biological conversions, which may result in a different profile of nitrate and perchlorate reduction. In fact, due to a typically 2-3 orders of magnitude higher concentration of nitrate than perchlorate in polluted water, the IEMB process efficiency may became limited by the rate of transport of perchlorate and its bio-reduction kinetics. Moreover, nitrate is often described as an inhibitory agent of perchlorate reduction even when present in equal amounts [39]. Thereby, the work described on Chapter 4 aims to characterize the biological reduction process within the biofilm and to identify the mechanisms that regulate nitrate and perchlorate reduction rate in the IEMB.

c) Evaluation of an up-scaling procedure and associated operating conditions

The final objective of this PhD project was to evaluate the up-scaling of the IEMB system. The IEMB concept was previously operated and validated in a single-membrane module with two rectangular channels [55, 61]. However, when considering its potential industrial application, a commercial membrane configuration needs to be tested and validated. Until now, the practical implementation of the IEMB process has been constrained by the lack of commercial anion-exchange membranes developed for this type of application. The IEMB process requires a membrane with a low membrane resistance to the transport of counterions combined with a high resistance to the possible transport of the carbon source (ethanol) from the biological to the water compartment [50].

Chapter 5 evaluates the applicability of a plate-and-frame IEMB configuration for the removal of nitrate and perchlorate from contaminated drinking water streams. Since ion exchange membranes are currently supplied only as flat membranes (for electrodialysis processes), the IEMB was tested in a plate-and-frame configuration.

An important concern when scaling-up the process is related to the control of the fluid dynamic conditions in the IEMB water and biological compartments. In the water stream side, adequate fluid dynamic conditions should be guaranteed to assure a reduced mass transfer resistance by the use of appropriate spacers and flow regime. The spacers should assure not only a low mass transfer resistance but also a low pressure drop. On the other hand, the spacers design should not potentiate membrane fouling by accumulation of particles within its mesh.

In the biocompartment, the channel height was increased to avoid possible channel clogging by the biofilm. Since the majority of the biological activity takes place on the biofilm, the up-scaling of contaminant-reducing bacteria density is achievable by increasing the specific surface area for biofilm attachment. Therefore, the IEMB system must be operated with a high ratio of membrane area per bioreactor volume (A/V_b). This up-scaling strategy may cause serious implications in the IEMB operating conditions. In this work, these implications were evaluated and the IEMB operating conditions were adjusted.

With the rise in bacteria density it is expectable higher nutrient requirements as well as higher accumulation of metabolic products. Therefore, it is important to define a proper nutrient feeding strategy to avoid situations of starvation and excess of nutrients, especially of carbon source that can potentially cross the membrane to the water compartment and cause secondary contamination of treated water and membrane fouling.

1.4. Structure of dissertation

This PhD thesis is divided in six chapters.

Chapter 1 includes state of the art, describes the motivation for this research project, and identifies the objectives of the study.

Chapters 2, 3, 4 and 5 provide approaches and solutions to specific objectives. Each chapter includes a short state of the art, describes the materials and methods used, presents and discuses the results obtained and the main conclusions drawn.

Chapters 2 and 3 focus on the modeling of the anion transport across the membrane in an operating IEMB. In Chapter 2, the modeling approach followed is completely non-parametric, whereas in Chapter 3 the mathematical model developed is based on hybrid approaches combining a previously developed mechanistic model with a statistically based model. Chapter 4 examines the degradation kinetics of nitrate and perchlorate by the mixed microbial

population selected in this study. In this chapter, the distribution of microorganisms across the biofilm thickness is investigated.

The effects of the up-scaling design in the IEMB performance are finally evaluated in Chapter 5. In this chapter, the IEMB is operated in a plate-and-frame configuration.

The results presented in Chapters 2, 3 and 4 were, respectively, submitted as dedicated papers to three scientific journals. The content of Chapter 2 is already published (Process Biochemistry (2011) 46: 1981–1992) and the articles related to Chapters 3 and 4 were recently submitted for publication on Biochemical Engineering Journal and on Water Research, respectively. The content of Chapter 5 will be submitted after the defense of this thesis.

Chapter 6 includes a summary of the principal results obtained as well as the major conclusions of this thesis. Remaining challenges and suggestions for future research are also presented.

1.5. References

1 Susan, D., Richardson, S.D., 2003. Disinfection by-products and other emerging contaminants in drinking water. Trends Anal. Chem. 22 (10): 666-684.

2 Pontius, F.W., 2003. Drinking water regulation and health. John Wiley & Sons, New York, p. 1029.

3 Speth, T.F., Schock, M.R., 2007. Removing esoteric contaminants from drinking waters: impacts of treatment implementation. J. Environ. Eng., 133(7): 665-669.

4 Hatzinger, P.B., 2005. Perchlorate biodegradation for water treatment. Environ. Sci. Tecnol. 39: 239A–247A.

5 Urbansky, E.T., 1998. Perchlorate chemistry: implications for analysis and remediation. Bioremediation. J. 2: 81-95.

6 United States Government Accountability Office (US GAO), 2007. EPA actions could reduce the availability of environmental information to the public. GAO-07-464T: 22-26.

7 Gal, H., Ronen, Z., Weisbrod, N., Dahan, O., Ronit, N., 2008. Perchlorate biodegradation in contaminated soils and the deep unsaturated zone. Soil Biol. Bioch. 40: 1751-1757.

8 Liu, Y.J., Mou, S.F., Liu, A.W., Du, B., 2004. Investigation of bromated, haloacetic acids and perchlorate in Beijing's drinking water. Environ. Sci. 25: 51-55.

9 Kirk, A.B., Smith, E.E., Tian, K., Anderson, T.A., Dasgupta, P.K., 2003. Perchlorate in milk. Environ. Sci. Technol. 37: 4979-4981.

10 Dyke, J.V., Ito, K., Obitsu, T., Hisamatsu, Y., Dasgupta. P.K., Blount, B.C., 2007. Perchlorate in dairy milk. Comparison of Japan *versus* the United States. Environ. Sci. Technol. 41: 88-92.

11 Aziz, C., Borch, R., Nicholson, P., Cox, E., 2006. Alternative causes of wide-spread, low concentrate perchlorate impacts to groundwater, Chapter 4, In: Perchlorate: environmental occurrence, interactions and treatment, B. Gu and J. Coates (eds), Springer, New York, pp. 71-92.

12 Coates, J., Achenbach, L.A., 2004. Microbial perchlorate reduction: rocket-fuelled metabolism. Nature Reviews Microb. 2: 569-580.

13 Clewell, R.A., Meriill E.A., Narayanan, L., 2004. Evidence of competitive inhibition of iodide uptake by perchlorate and translocation of perchlorate into the thyroid. Int. J. Toxicol. 23:17-23.

14 Bardiya, N., Bae, J.H., 2011. Dissimilatory perchlorate reduction: a review. Microbiol. Res. 166(4): 237-54.

15 E.U. Council directive of 15 July 1980 relating to the quality of water intended for human consumption. Off. J. Eur. Commun., 23 (L229): 11-23.

16 U.S. Environmental Protection Agency, 1992. Drinking water regulations and health advisory. Office of water, U.S. Environmental Protection Agency, Washington, DC, December 1992.

17 Gray, N. F., 2008. Drinking water quality: problems and solutions. 2nd Edition, Cambridge University Press, Cambridge. p. 520.

18 Manassaram, D.M., Backer, L.C., Moll, D.M., 2006. A review of nitrates in drinking water: maternal exposure and adverse reproductive and developmental outcomes. Environ. Health Perspect., 114 (3): 320-327.

19 Canada commission on nitrate in groundwater 2008. The report of the commission on nitrates in groundwater. http://www.gov.pe.ca/photos/original/cofNitrates.pdf (consulted on October, 2011)

20 European Community, 2011. Report from the commission to the council and the European parliament on implementation of Council Directive 91/676/EEC concerning the protection of waters against pollution caused by nitrates from agricultural sources based on Member State reports for the period 2004-2007. SEC 913, Brussels, 13/07/2011

21 Van Ginkel, S.W., Ahn, C.H., Badruzzaman, M., Roberts, D.J., Lehman, S.G., Adham, S.S., Rittmann, B.E., 2008. Kinetics of nitrate and perchlorate reduction in ion-exchange brine using the membrane biofilm reactor (MBfR). Water Res. 42: 4197-4205.

22 Choi, H., Silverstein, J., 2008. Inhibition of perchlorate reduction by nitrate in a fixed biofilm reactor. J. Hazar. Mat. 159: 440-445.

23 Pakzadeh, B., Batista, J.R., 2011. Impacts of cocontaminants on the performances of perchlorate and nitrate specialty ion-exchange resin. Ind. Eng. Chem. Res. 50 (12):7484–7493.

24 U.S. Environmental Protection Agency, 1998. Announcement of the drinking water contaminant candidate list: notice. Federal Register, 63 (40): 10274–10287.

25 U.S. Environmental Protection Agency, 2003. Memorandum from January 2006 regarding Status of EPA's Interim Assessment Guidance for Perchlorate.

26 US Environmental Protection Agency (USEPA), 2011. Drinking water: regulatory determination on perchlorate. Federal Register. 76(29): 7762-7767.

27 World Health Organization, 1993. Guidelines for drinking water quality, vol I. WHO, Geneva, Switzerland.

28 World Health Organization, 2004. Rolling revision of the WHO guidelines for drinking-water quality: nitrates and nitrites in drinking-water. Geneva, Switzerland.

29 Gu, B.; Brown, G.M., 2006. Field demonstration using highly selective, regenerable ion exchange and perchlorate destruction technologies for water treatment, Chapter 11, In: Perchlorate Environmental Occurrences, Interactions, and Treatment, Gu, B., Coates, J. D., (eds.), Springer, New York, pp. 253-278.

30 Kapoor, A., Viraraghava, T. 1997. Nitrate removal from drinking water – review. J. Environ. Eng. 123: 371–380.

31 Srinivasan, R., Sorial, G.A., 2009. Treatment of perchlorate in drinking water: a critical review. Sep. Pur. Techn. 69: 7-21.

32 Parette, R., Cannon, F.S., 2006. Perchlorate removal by modified activated carbon, Chapter 15, In: Perchlorate Environmental Occurrences, Interactions, and Treatment, Gu, B., Coates, J. D., (eds.), Springer, New York, pp. 344-372.

33 Amy, G., Yoon, Y., Yoon, J., Song, M., 2003. Treatability of perchlorate-containing water by RO, NF and UF membranes. AWWA Research Foundation, USA.

34 Roquebert, V., Booth, S., Cushing, R.S., Crozes, G., Hansen, E., 2000. Electrodialysis reversal (EDR) and ion exchange as polishing treatment for perchlorate treatment. Desalination 131: 285-291.

35 Nerenber, R., Rittman, B.E., 2004. Hydrogen-based, hollow-fiber membrane biofilm reactor for reduction of perchlorate and other oxidized contaminants. Water Sci. Technol. 49 (11-12): 223-230.

36 Nerenberg, R., Kawagoshi, Y., Rittman, B.E., 2006. Kinetics of a hydrogen-oxidizing, perchlorate –reducing bacterium. Water Res. 40: 3290-3296.

37 Rikken, G.B., Kroon, A.G.M., Van Ginkel, C.G., 1996. Transformation of (Per)chlorate into Chloride by a Newly Isolated Bacterium: Reduction and Dismutation. Appl. Microbiol. Biotechnol. 45: 420-426.

38 Xu, J., Trinble, J.J., Steinberg, L., Logan, B.E., 2004. Chlorate and nitrate reduction pathways are separately induced in the perchlorate-reducing bacterium *Dechlorosoma* sp.

KJ and the chlorate-respiring bacterium *Pseudomona*s sp. PDA. Water Res. 38: 673-680.

39 Sun, Y., Gustavson, R.L., Ali, N., Weber, K.A., Westphal, L.L., Coates, J.D., 2009. Behavioral response of dissimilatory perchlorate-reducing bacteria to different electron acceptors. Appl. Microbiol. Biotechnol. 84: 955-963.

40 Shapleigh, J.P., 2006. The denitrifying prokaryotes, Chapter 23, In: The prokaryotes: an evolving electronic resource for the microbiological community, M. Dworkin, S. Falkow, E. Rosemberg, K.-H. Schleifer, E. Stackebrand (eds.), 3rd edition, Springer-Verlag, New York, pp. 769-792.

41 Zumft, W.G., 1992. The denitrifying prokaryotes, In: The Prokaryotes- A handbook on the biology of bacteria: ecophysiology, isolation, identification, applications, A. Balows, H.G. Trüper, M. Dworkin, W. Harder, K-H. Schleifer (Eds.), 5nd ed., vol. 1. Springer-Verlag, New York, pp. 554-582

42 Attaway, H., Smith, M.D., 1994. Propellant wastewater treatment process. U.S. Patent 5,302,285.

43 Min, B., Evans, P.J., Chu, A.K., Logan, B.E., 2004. Perchlorate removal in sand and plastic media bioreactors. Water Res. 38: 47–60.

44 Sutton, P.M., Mishra, P.N., 1994. Activated carbon based biological fluidized beds for contaminated water and wastewater treatment: a state-of-the-art review. Water Sci. Technol. 29: 309–317.

45 Fuerhacker, M., Bauer, H., Ellinger, R., Sree, U., Schmid, H., Zibuschka, F., Puxbaum, H., 2000. Approach for a novel control strategy for simultaneous nitrification/denitrification in activated sludge reactors. Water Res. 34 (9): 2499-2506.

46 Haugen, K.S., Semmens, M.J., Novak, P.J., 2002. A novel in situ technology for the treatment of nitrate contaminated groundwater. Water Res. 36: 3497–3506.

47 Nerenberg, R., Rittmann, B.E., Gillogly, T.E., Lehman, G.E., Adham S.S., 2003. Perchlorate reducing using a hollow-fiber membrane biofilm reactor: kinetics, microbial ecology and pilot-scale studies. Proceedings on the seventh International in situ and on-site Bioremediation Symposium, Orlando, Florida, USA.

48 Ziv-El, M.C., Rittman, B.E., 2009. Systematic evaluation of nitrate and perchlorate bioreduction kinetics in groundwater using a hydrogen-based membrane biofilm reactor. Water Res. 43: 173-181.

49 Fuchs, W., Schatzmayr, G., Braun, R. 1997. Nitrate removal from drinking water using a membrane-fixed biofilm reactor. Appl. Microbiol. Biotechnol. 48: 267-274.

50 Velizarov, S., Reis, M.A., Crespo, J.G., 2011. The Ion-Exchange Membrane Bioreactor: developments and perspectives in drinking water treatment, Chapter 4, In: Water purification and management, J. Coca-Prados and G. Gutiérrez-Cervelló (Eds.), NATO

Science for Peace and Security Series C: Environmental Security, Springer, pp. 119-145.

51 Characklis, W.G., Marshall, K.C., 1990. Biofilms. John Wiley & Sons, p. 796.

52 Wanner, O., Eberl, H., Morenroth, E., Noguera, D., Picioreanu, C., Rittman, B., Van Loosdrecht, M.C.M., 2006. Mathematical modeling of biofilms. IWA Scientific and Technical Report n.18, IWA Publishing, 199 p.

53 Casey, E., Glennon, B., Hamer, G., 1999. Review of membranes aerated biofilm reactors, Resour. Conserv. Recy. 27: 203-215.

54 Rittman, B. E., 2007. The membrane biofilm reactor is versatile platform for water and wastewater treatment. Environ. Eng. Res. 12(4): 157-175.

55 Matos, C.T., Velizarov, S., Crespo, J.G., Reis, M.A.M., 2006. Simultaneous removal of perchlorate and nitrate from drinking water using the ion exchange membrane bioreactor concept. Water Res. 40: 231-240.

56 Crespo, J.G., Reis, A.M., Fonseca, A.D., Almeida, J.S., 1999. Ion exchange membrane bioreactor for denitrification of water (Reactor de membrana de permute iónica para desnitrificação de água). Portuguese National Patent No. 102 385 N.

57 Crespo, J.G., Reis, A.M., 2001. Treatment of aqueous media containing electrically charged compounds, Patent WO 01/40118 A1.

58 Velizarov, S., Crespo, J.G., Reis, A.M., 2002. Ion exchange membrane bioreactor for selective removal of nitrate from drinking water: Control of ion fluxes and process performance. Biotechnol. Progress 18: 296–302.

59 Velizarov, S., Reis, A.M., Crespo, J.G., 2003. Removal of trace mono-valent inorganic pollutants in an ion exchange membrane bioreactor: analysis of transport rate in a denitrification process. J. Membr. Sci. 217: 269–284.

60 Fonseca, A.D., 2002, PhD Thesis, Universidade Nova de Lisboa, Portugal.

61 Matos, C.T., Fortunato, R., Velizarov, S., Reis, M.A.M, Crespo, J.G., 2008. Removal of monovalent oxyanions from water in an ion exchange membrane bioreactor: influence of membrane permselectivity. Water Res. 42: 1785–1795.

62 Velizarov, S., Reis, M.A., Crespo, J.G., 2002. Ion exchange membrane bioreactor for selective removal of nitrate from drinking water: control of ion fluxes and process performance. Biotechnol. Progr. 18: 296-302.

63 Matos, C.T., Velizarov, S., Reis, M.A.M., Crespo, J.G., 2008, Removal of bromate from drinking water using the ion exchange membrane bioreactor concept. Environ. Sci. Technol. 42: 7702–7708.

64 Velizarov, S., Matos, C.T., Oehmen, A., Serra, S., Reis, M.A.M., Crespo, J.G., 2008. Removal of inorganic charged micropollutants from drinking water supplies by hybrid ion exchange membrane processes. Desalination 223: 85–90.

65 Oehmen, A., Viegas, R., Velizarov, S., Reis, M.A.M., Crespo, J.G., 2006. Removal of heavy metals from drinking water supplies through the ion exchange membrane bioreactor. Desalination 199: 405–407.

66 Matos, C.T., Sequeira, A.M., Velizarov, S., Crespo, J.G., Reis, M.A.M., 2009. Nitrate removal in a closed marine system using the ion exchange membrane bioreactor. J. Hazard Mater. 166: 428–434.

67 Wold, S., Sjöström, M., Eriksson, L., 2001. PLS-regression: a basic tool of chemometrics. Chemom. Intell. Lab. Syst. 58: 109-130.

Chapter

2

Multivariate statistical modelling of mass transfer in a membrane-supported biofilm reactor[1]

Summary

The main objective of this work is to develop an overall mass transfer model applicable to a particular case of membrane supported biofilm, the Ion-exchange Membrane Bioreactor (IEMB). A multivariate Projection to Latent Variables (PLS) model of the anionic membrane transport in an IEMB was developed and analysed to establish the mass transfer limiting variables for the removal of anionic pollutants (nitrate and perchlorate) from drinking water. The proposed PLS model accounts for the biological contribution to the mass transfer and predicts the anionic fluxes across the ion-exchange membrane with a prediction improvement of at least 50 % when compared with a simplified mechanistic Donnan dialysis-based transport model. The PLS model allowed for predicting the transport of target anions using only operational physicochemical data, therefore, the use of several assumptions as in mechanistic model building was avoided as well as the need for biofilm characterization. To decrease the model complexity, several techniques which select the most informative predictors were also successfully used. The analyses of important predictors to each anionic transport model show that transport driving force related variables were the

1 Published on: Process Biochemistry (2011) 46:1981–1992.

most important. Moreover, at least 30 % of the model information is related with biocompartment bulk variables.

2.1. Introduction

Membrane supported biofilm reactors combine the use of a membrane for transport of nutrients and/or products and for biofilm growth. These systems have been mainly applied for gas delivery, since they provide economical and operational advantages compared with traditional gas diffusers [1-3]. Moreover, due to the possibility for physical separation of the biofilm compartment from toxic streams, membrane supported biofilm reactors have been also applied in wastewater treatment [4, 5].

The Ion Exchange Membrane Bioreactor (IEMB) is a hybrid system integrating the use of an ion exchange membrane and a microbial culture [6]. This process is based on a membrane-supported biofilm, in which ionic micropollutants such as nitrate and perchlorate can be metabolized. In this process, the ionic transport is governed by Donnan dialysis, by adding an excess of driving counter-ion (e.g., chloride) in the stripping (biological) compartment (Figure 2.1). The IEMB process offers a number of advantages in relation to traditional technologies. One of the most relevant advantages is the fact that no contaminant-rich brine is produced, as happens in classical ion exchange based processes [7, 8]. Furthermore, since the biological culture is physically separated from the water compartment, no secondary contamination of the treated water by microbial cells, nutrients and/or metabolic by-products occurs as in typical biological treatment systems [9, 10].

The mechanism of transport of ionic micropollutants in the IEMB was extensively studied [11-13] and a resistances-in-series trace counter-ion transport model was previously developed [12]. This mechanistic model predicts accurately counter-ion transport fluxes on the basis of physicochemical and hydrodynamic data, assuming that the process is mass-transfer limited and controlled. This assumption presupposes non-limiting biological conditions for bioreduction of the micropollutants in the biocompartment [14] and neglects possible mass transfer limitations across the biofilm. Under optimized conditions, nitrate and perchlorate are completely reduced within the biofilm and the mechanistic transport model can be applied successfully. However, under specific operating conditions (e.g., during the IEMB start-up when the biofilm is still not developed or in situations of nutrient limitation), the biological conversion of these ionic pollutants may limit the process rate.

The mechanisms of ionic transport through ion exchange membranes (IEM) have been extensively studied [15-20]. So far, the most widely used models to describe the transport in IEM are based on the Nernst-Planck formalism [16-18]. These models are mainly applied to bi-

ionic systems and presuppose constant diffusion coefficients. The transport through IEM can be more rigorously described using the Stefan-Maxwell formalism [19] or through space charge based constraints [20], but it adds additional complexity to the system.

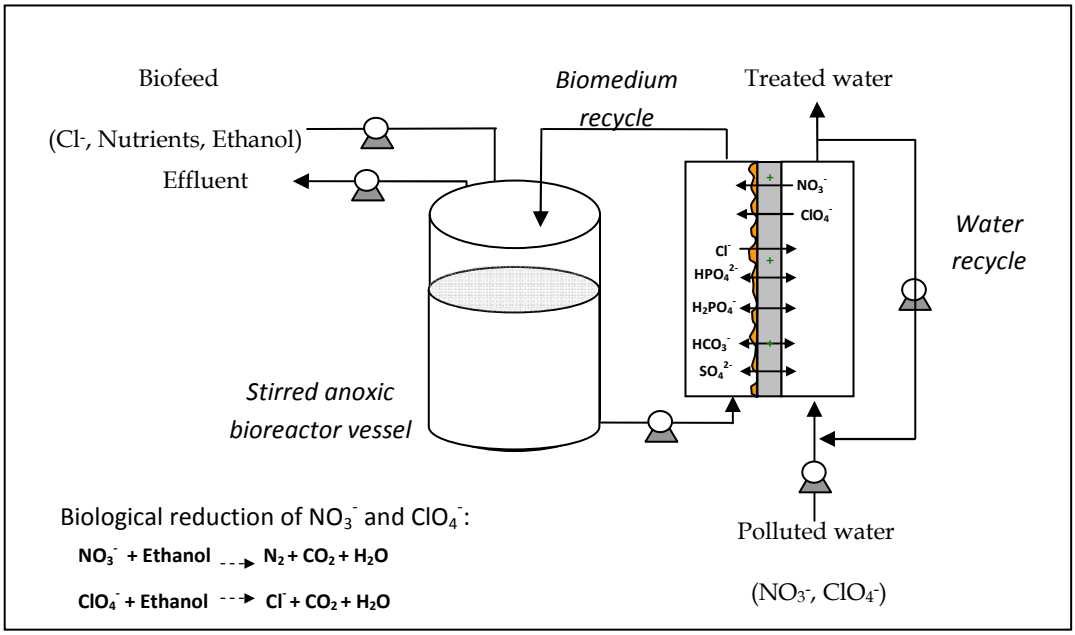

Figure 2.1: Schematic diagram of the experimental set-up and ion transport mechanism in the ion-exchange membrane bioreactor (IEMB).

The IEM transport modelling becomes more complex when the process involves (bio)chemical reactions. Prado-Rubio *et al* [18], modeled a Donnan dialysis system for separation of carboxylic acid anions from fermentation broths based on the irreversible thermodynamics approach. A reaction term was introduced in the dynamic mass balance to take into account the carboxylic acid dissociation and the pH buffering effect. Accounting for biological kinetics effects could be expected to be even more complex. Probably due to this reason, no model has been suggested so far for hybrid systems combining Donnan dialysis and biological reaction, and only few models have been proposed to represent the performance of membrane biofilm reactors. These models assumed constant biofilm density and diffusivity and uniform biofilm thickness. However, these assumptions are far away from reality, especially in the first phase of biofilm development. On the other hand, biofilms can be viewed as non-linear moving boundary problems [21], since the biofilm thickness changes over-time due to the cell growth.

The main objective of this work was to develop an overall mass transfer model applicable to a particular case of membrane supported biofilms, the Ion-exchange Membrane Bioreactor. This model must be able to cover a broad range of operating conditions, especially when the process is limited by the biological reactions kinetics. Due to the complexity of this hybrid process, multivariate statistical modelling was the approach used to identify the relationship between

transport of counter-ions through the membrane and physicochemical process operation conditions, including those inherent to the biological process.

Within the multivariate regression analysis, Projection to Latent Structure (PLS) was the chosen technique, since it is able to decompose the X matrix (input predictor matrix) into latent uncorrelated variables in the sense of maximizing the explained variance of Y matrix (target outputs) [22]. As a result, a linear model may be obtained between process operation conditions and the counter-ion fluxes across the membrane with maximum predictive power.

Although the PLS model can easily deal with numerous and multicollinear data, the selection of important variables in multivariate analysis is a crucial step since it influences model calibration. In the present study, a routine was created that selects the best model with the lowest complexity using several techniques for eliminating non-informative data without losing important information.

2.2. Materials and Methods

2.2.1. Experimental set-up

The IEMB studies were performed in a flat parallel-plate module with two identical rectangular channels separated by an anion exchange membrane with an area of 34.5 cm^2 (Figure 2.1). One of the channels was linked to a vessel (water compartment) in which the water was recirculated in order to guarantee a Reynolds number of 3000. Polluted water was continuously fed to this compartment changing its composition in terms of nitrate and perchlorate concentration, according to the design of experiments (Table 2.1). The polluted water was prepared by supplementing tap water, from the Lisbon public distribution network, with nitrate and perchlorate. The other channel of the module was connected to a vessel, designated as biocompartment, to which a pre-selected mixed anoxic microbial culture was added and continuously fed with a nutrient medium (biofeed) with different composition, depending on the experimental design. Ethanol was used as the electron donor and its concentration in the biofeed was maintained at 0.56 g/L. Two hydraulic retention times (HRT) were tested for the biocompartment: 5 days and 10 days. To maintain the same nutrient load to the biocompartment, the concentration of nutrients in the biofeed was adjusted to the set HRT. In the biocompartment, the recirculation flow rate was varied (Reynolds number of 150 and 3000) in order to investigate the effect of the hydrodynamic conditions on the target anion(s) transport.

Table 2.1: Performed experiments: Plackett-Burman experimental design (experiments 2-7 and 9-10) and experiment 1 and 8 according to reference conditions [11]

Exp No.	PO_4^{3-}	NH_4^+	SO_4^{2-}	Cl^-	$HRT_{Biocomp}$	$Re_{Biocomp}$	NO_3^- + ClO_4^- polluted water
1	958 mg/L	78 mg/L	40 mg/L	3700 mg/L	5.84 days	3000	60 mg/L + 100 µg/L
8	958 mg/L	78 mg/L	40 mg/L	3700 mg/L	5.84 days	150	60 mg/L + 100 µg/L
2	1	-1	-1	1	-1	1	1
3	-1	1	-1	1	1	1	-1
4	1	1	1	-1	-1	1	-1
5	-1	-1	1	-1	1	1	1
6	1	-1	1	1	1	-1	-1
7	1	1	-1	-1	1	-1	1
9	-1	-1	-1	-1	-1	-1	-1
10	-1	1	1	1	-1	-1	1
low level (-1)	48 mg/L	6.7 mg/L	0 mg/L	240 mg/L	5.84 days	150	60 mg/L + 100 µg/L
high level (+1)	958 mg/L	78 mg/L	370 mg/L	3700 mg/L	10 days	3000	120 mg/L + 400 µg/L

The experiments were run for operating times equal to at least two biocompartment HRTs (10 or 20 days, respectively). All tests were performed at a temperature of 23±1 ºC. Samples were taken periodically from the two IEMB compartments as well as from the polluted water and biofeed reservoirs. The samples were used for measuring conductivity, pH and biomass concentration and stored at -20ºC for determination of anions, ammonium and ethanol concentrations.

2.2.2. Anion exchange membrane

The experiments were carried out using an anion-exchange membrane Neosepta ACS from Tokuyama Soda (Japan). This membrane has an ion exchange capacity of 1.42 ± 0.42 meq/g dry

membrane and a thickness of 0.130 ± 0.001 mm [23]. The ACS membrane permeabilities, P_m, at 23ºC to the target anions under study are as follows: $P_{m,NO3-}$ = 3.35·10^{-8} cm^2/s, $P_{m,ClO4-}$ 3.58 x 10^{-8} cm^2/s, $P_{m,H2PO4-}$ 1.23 x 10^{-9} cm^2/s, $P_{m,HPO42-}$ 2.91 x 10^{-12} cm^2/s and $P_{m,SO42-}$ 1.83x10^{-12} cm^2/s [23]. The membrane is classified as a monoanion-permselective membrane since its permeability to anions of higher valence is significantly lower. The membrane permeability to HCO_3^- and total phosphate (represented as PO_4^{3-}) was determined in this study according to the methodology followed in [23].

2.2.3. Analytical methods

Nitrate, phosphate, sulphate and chloride concentrations were determined by an ion exchange chromatography system (Dionex, USA), constituted by an Ionpac AG9 Guard and analytic AS9 columns (4 mm), an Anion Supressor-ULTRA (4mm) and an ED50 electrochemical detector. The mobile phase was 9 mM Na_2CO_3 aqueous solution at 1 mL/min, operating at 23 ºC. Under these conditions, all phosphate present in the sample is measured as PO_4^{3-} due to the high eluent pH (above 13). In the original samples, the amounts of dihydrogenophosphate ($H_2PO_4^-$), hydrogenophosphate (HPO_4^{2-}) and phosphate (PO_4^{3-}), were quantified based on the sample pH according to the pKa values of each acid-base pair: pKa_1 ($H_3PO_4/H_2PO_4^-$) = 2.12; pKa_2 ($H_2PO_4^-/HPO_4^{2-}$) = 7.21 and pKa_3 (HPO_4^{2-}/PO_4^{3-}) = 12.6 [24].

For the ClO_4^- analysis, the same Dionex system was used, with AG16 and AS16 columns, with 1 mL/min flow of 50 mM NaOH aqueous solution as mobile phase. At 30ºC, the limit of ClO_4^- detection was 1 µg/L with the injection of 1 mL of sample. In the biocompartment samples analysis, due to interference of the Cl^- peak with the ClO_4^- peak, a volume of 500 µl was injected and the limit of ClO_4^- detection increased to 2 µg/L.

For the HCO_3^- analysis, the Dionex system was equipped with AG11 and AS11 columns, using a 25 mM NaOH aqueous solution at 1 mL/min at 30ºC. As in the case of phosphate, due to the high pH of the eluent, bicarbonate was measured in the form of CO_3^{2-}, which was then converted into its actual forms in the original samples, using the corresponding pKa values: (H_2CO_3/HCO_3^-) = 6.3; (HCO_3^-/CO_3^{2-}) = 10.3 [23].

Ethanol in the biocompartment and biofeed samples was measured using a HPLC system with an Aminex HPX-87H column (BioRad, USA) and a differential refractometer detector RI-71 (Merck Hitachi, Japan) using a mobile phase of a 0.01N H_2SO_4 aqueous solution at a flow rate of 0.5 mL/min at 30ºC. The ethanol detection limit was 1 mg/L. Ammonium was quantified with a gas-sensitive electrode Orion 95-12 (Thermo, USA), with a detection limit of 1 mg/L.

2.3. Proposed modelling method

2.3.1. Projection to Latent structures (PLS)

The approach followed concerned the identification of relations between the observed membrane fluxes of target counter-ions (anions) and the process operating conditions. The Projection to Latent Structures (PLS) was the adopted non-parametric model that reveals linear relations between the data, by maximizing the covariance between the X matrix (inputs) and the Y (output). This technique combines features from principal component analysis (PCA) and multiple linear regression. Its goal is to predict dependent variables by decomposing iteratively both the X and Y matrices into reduced orthogonal factors called latent variables. Therefore, it differs from traditional multivariate since, with this strategy, redundancy in the input and output data sets are eliminated. Thereby, PLS is considered an excellent predictive modelling technique given that it can handle with collinearity between variables and with noisy and missing data [22].

With this methodology, two equations are obtained (equations 2.1 and 2.2) [25]. The input matrix (X) is decomposed as the product of two different matrix designed scores (T) and loadings (P) that minimizes the residuals (E). In equation 2.2, the product of T and C approximates the output value (Y), where C is the Y-weights matrix and F is the error term. Therefore, the common association is the value of T.

$$X = TP^T + E \quad (2.1)$$

$$Y = TC^T + F \quad (2.2)$$

The loadings matrices columns are the latent variables in which the original data are decomposed. Thus, the score matrix T encloses the new variables obtained from the latent variables. Since the linear PLS model finds a new data arrangement, it is possible to determine and interpret the contribution of the data points and variables to the model. The weights W (T=XW) quantify the relation between X and Y, therefore, it can be used to identify the important variables to the output. Thereby, a multivariate regression model is obtained:

$$Y = XWC^T + F = XB + F \quad (2.3)$$

with regression coefficients given by:

$$B = WC^T \quad (2.4)$$

A large numerical value of B is highly correlated with Y and similar profiles of B-values provide the same contribution to the prediction [22].

2.3.2. Experimental design

The statistical based modelling approach is demanding on the quality, accuracy and variability in data sets. Therefore, the use of an experimental design to define the number and arrangement of experiments to be performed not only allows for decreasing the number of tests but also for generation of data that can be further analyzed by statistical techniques [26]. Consequently, the PLS model benefits with the application of design of experiments since the experimental domain is defined and balance data is ensured.

Based on our previous experience with the IEMB process [11], several factors were identified as mainly affecting the biocompartment performance: the biofeed composition, the driving counter-ion concentration (chloride), the hydraulic retention time in the biocompartment (HRT) and the hydrodynamic conditions in the biocompartment recirculation loop, characterized by the Reynolds number (Re), and the nitrate and perchlorate concentrations in the water to be treated.

The selection of the range of conditions to be studied was based on a previous study [11]. In those experiments, the biofeed was composed by: 1g/L of K_2HPO_4, 0.592 g/L of KH_2PO_4, 0.5 g/L of NaH_2PO_4, 0.233 g/L of NH_4Cl, 0.1 g/L of $MgSO_4.7H_2O$, 5.84 g/L of NaCl and 0.56 g/L of ethanol. The effect of each factor on the flux of a target anion through the membrane was tested using two levels of variation. The biofeed composition (except for the ethanol concentration, which was kept constant) was changed to determine the effect of a given compound on the membrane flux of a target anion. The effect of the biocompartment hydraulic retention time (HRT) was also tested. The effect of hydrodynamic conditions was examined in the biocompartment recirculation loop (Reynolds number set at 150 and at 3000). This parameter can affect the biofilm morphology and consequently, the mass transfer coefficients of the target compounds, as suggested in [2]. The nitrate, perchlorate and chloride concentrations were also varied. These parameters affect the transport rate and may, consequently, influence the biological reactions occurring in the biocompartment. Therefore, it is important to investigate the mass transport at different transport driving forces imposed with a simultaneous variation of the biocompartment conditions.

Since a large number of parameters was studied, it was decided to use a screening experimental design [27]. The Plackett-Burman design is usually preferred for identifying important ingredients in fermentation media development [28], since it allows for examining N-1 variables in N runs with two-level of variation: -1 for the lowest and +1 for the highest value. Table 2.1

summarizes the experiments performed and the respective levels of variation used in the Placket-Burman experimental design. Since the model calibration with the PLS model benefits with the introduction of more data, experiments identified as “1” and “8” were added to the design and were carried out according to previously tested conditions [11]. The experimental design was carried out in a random sequence to guarantee that the statistical analysis was independent of the bioreactor operation “history”.

The impact of each variable on the system performance was estimated as the difference between the mean of the system response for the highest tested setting (+1) and the mean of the response for the lowest setting (-1). A factor is considered to be important if the response variable shift location is significant, independently of the direction of the shift being positive or negative [27].

For the present problem, the X matrix compiles all data of the performed experiments with the physicochemical variables of the IEMB process operation. Considering that PLS is used to capture information from experimental data, it is beneficial to add all the available measurements since the algorithm is able to deal with numerous data to identify the most correlated variables. Thereby, the X columns contain not only the seven variables tested in the design of experiments but also the most relevant physicochemical composition data for the water and for the biocompartment of the IEMB process (discussed in more detail in Section 2.4.3).

2.3.3. Experiments standardisation

Considering that the duration of the experiments and the sampling intervals were not the same for all experiments, it was important to standardise the number of observations for each experiment. This procedure was done by dividing each observation time by the total time duration of the experiment. Therefore, it was guaranteed that each experiment has the same contribution to the model calibration by having the same number of observations.

2.3.4. PLS model synthesis

A flow-chart outlining the procedure for PLS model synthesis is illustrated in Figure 2.2. The starting model structure comprises all predictor variables in the X-matrix (Table 2.2). First, both the inputs (X-matrix) and the outputs (Y-matrix) were scaled to make their distribution in the same range. Considering the lack of knowledge about the contribution of each variable, the X- and Y- variables were scaled using two different techniques: dividing each variable by its

standard deviation to scale it to a unit variance; centering the variables by subtracting their average and dividing by the standard deviation, known as auto-scaling [29].

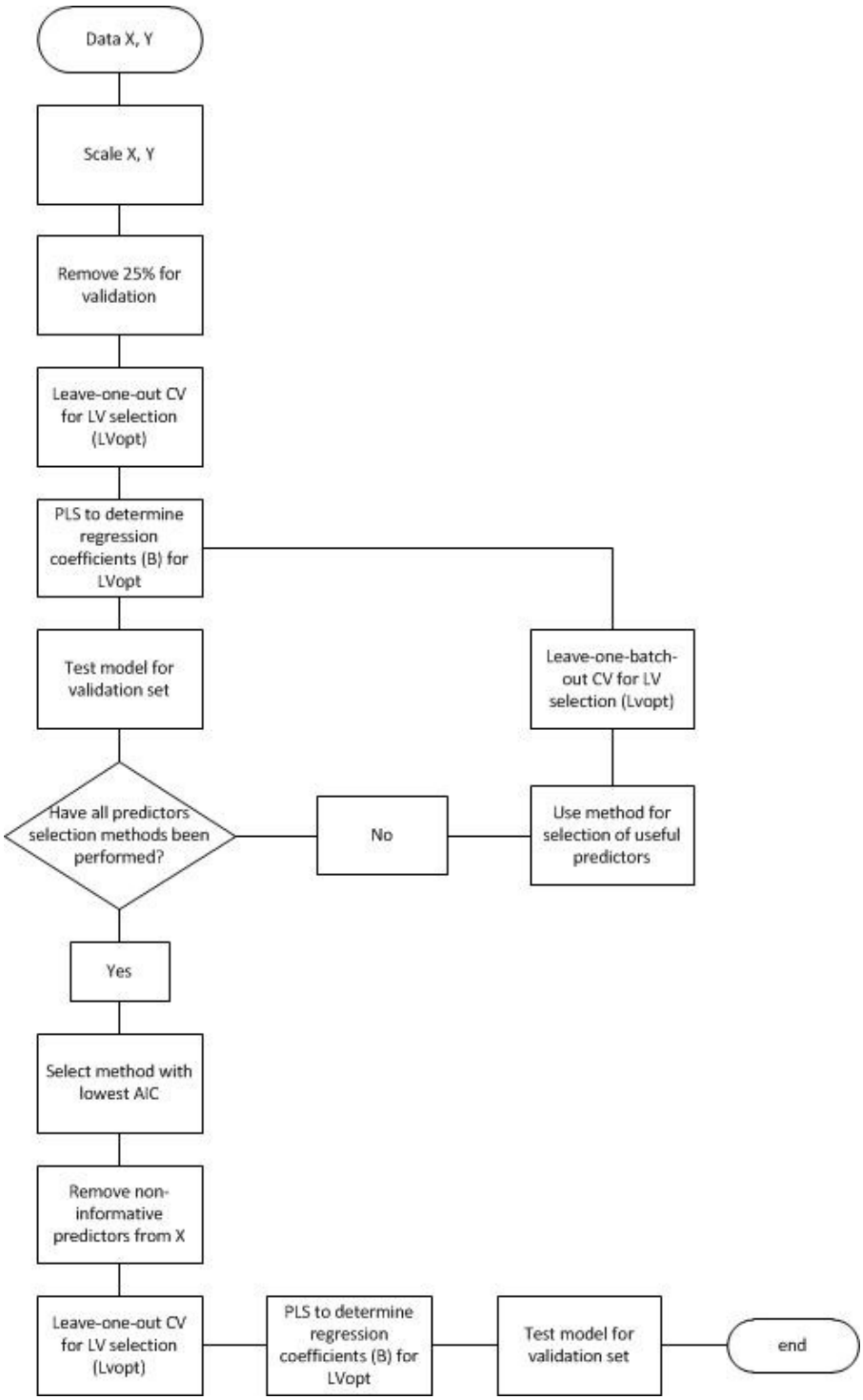

Figure 2.2: Flow-chart outlining the PLS model calibration (X: matrix of inputs; Y: matrix of outputs; CV: cross-validation; LVopt: optimal number of latent variables; AIC: Akaike Information Criterion).

Afterwards, 25 % of the data were randomly removed from the data set in order to be used for validation. Then, leave-one-out cross-validation [30] was applied to the calibration data set to select the optimal number of latent variables (LVopt) and the PLS was performed until LVopt was reached. The routine was implemented on Matlab 2006b [31] using the N-Way toolbox for the PLS calibration [32].

Table 2.2: Input variables used in the initial PLS calibration

Input	Stream/Compartment	Unit
$[NO_3^-]$	Polluted water feed	mM
$[ClO_4^-]$		mM
$[SO_4^{2-}]$		mM
$[Cl^-]$		mM
$[HCO_3^-]$		mM
pH		-
PO_4^{3-} mass flow rate	Biofeed	µmol/h
$H_2PO_4^-$ mass flow rate		µmol/h
HPO_4^{2-} mass flow rate		µmol/h
SO_4^{2-} mass flow rate		µmol/h
Cl^- mass flow rate		µmol/h
NH_4^+ mass flow rate		µmol/h
$[NO_3^-]$	Biocompartment	mM
$[ClO_4^-]$		mM
$[PO_4^{3-}]$		mM
$[H_2PO_4^-]$		mM
$[HPO_4^{2-}]$		mM
$[SO_4^{2-}]$		mM
$[Cl^-]$		mM
$[NH_4^+]$		mM
[Ethanol]		mM
Reynolds number in the recirculation loop		-
Hydraulic retention time		days
pH		-

The resulting model was assessed with the validation data set using the determined regression coefficients. From this point on, the model structure was refined by eliminating redundant predictor variables using 8 different techniques: forward selection [33], backward selection [33], stepwise MLR [33], iterative stepwise elimination (ISE) [34], iterative predictors weighting (IPW) [35], uninformative variables elimination (UVE) [36] and Martens uncertainty test [37] with regression coefficients confidence interval estimated with Jackknife [38] and Bootstrapping [39] resampling techniques. In forward, backward and stepwise MLR, the criteria for incorporation of variables was based on a critical partial F-test with a F value cut-off equal to 4 (α=0.05, 1 variable and more than 100 samples) [39].

The model was then recalibrated using the most informative predictor variables in X. In this PLS modelling, the LVopt was selected with the leave-one-batch-out method in order to decrease the computational time. After all the methods have been performed, the model with the lowest Akaike Information Criterion (AIC) among the 8 models obtained was selected. The X matrix used in the selected model is considered to be optimized since the uninformative predictors were eliminated. Therefore, it is used to recalibrate a PLS model in which the proper number of LV to retain was determined by a leave-one-out cross-validation.

2.3.5. Prediction power criteria

The models obtained were evaluated with different methods in terms of goodness of fitting of the validation set. The initial strategy was to divide the data in two different sets, one for calibration of the model and one for validation to quantify the prediction error. The correlation coefficient (R^2) between the observed output and the predicted value and the Root-mean-square-error-of-prediction (RMSEP) were calculated in order to quantify the prediction capacity of the model [40]. Both methods are based on the model residuals. The RMSEP was used as the criterion in cross-validation to identify the latent variable to be retained, based on the selection of the local minimum RMSEP [37]. Considering the range of concentrations studied (e.g. ClO_4^- concentration was as low as 4 μg/L in some experiments), higher analytical deviations may be expected in these cases. The χ^2 (equation 2.5) is one of the fundamental statistical fit indexes since also the experimental variance is taken into account (σ^2_{exp}) [41]. Since critical values of χ^2 distribution are known, it can be evaluated if the experimental data and the estimated fluxes can be considered statistically similar. This criterion was used to identify the model outliers by applying equation 2.5 to each observation as well as a model measurement of validity when the entire data matrix is considered.

$$\chi^2 = \frac{\Sigma\left(y_{\mathrm{mod}\,el} - y_{\exp}\right)^2}{\sigma^2_{\exp}} \tag{2.5}$$

The Akaike Information Criterion (AIC) [42] was also used since it considers not only the model residuals but also its complexity expressed by the number of parameters (p_m) (equation 2.6).

$$AIC = N\log\left(\frac{\Sigma(y_{\mathrm{mod}\,el} - y_{\exp})^2}{N}\right) + 2p_m \tag{2.6}$$

AIC was important for the selection of the optimal predictor structure since the best model is a compromise between the prediction accuracy and the model complexity. Therefore, it is an essential criterion for comparing statistical models when a different number of parameters are used. The best model should have the lowest possible AIC value.

2.4. Results and discussion

2.4.1. Mechanistic transport model prediction

The mechanistic transport model prediction was evaluated for all experiments performed in order to check its domain of applicability. As expected, the model residuals are above the experimental standard deviation in several experiments (Figure 2.3), which confirms the inability of this model to describe IEMB operating conditions that do not fulfill the model building assumptions. The mechanistic transport model was developed for a trace counter-ion (e.g., ClO_4^-) mass-transfer limited transport, in the presence of a bulk (driving) counter-ion (e.g., Cl^-), at a much higher concentration. In order for chloride to be considered as the major driving counter-ion, the ratio $Cl^-_{biocompartment}$ /$Cl^-_{water\ compartment}$ should be at least over 10 [13]. In experiments 4, 5, 7 and 9, this ratio was intentionally decreased to 5.8-10. However, only in experiments 5 and 7 the mechanistic transport model does not reproduce the experimental results. In those experiments, the driving force was affected not only by a decrease in the chloride concentration in the biofeed but, simultaneously, by a planned increase of nitrate and perchlorate concentrations in the polluted water stream (see Table 2.1). In such experiments, chloride cannot be considered as the major counter-ion present and other anions in the biocompartment (e.g., phosphate, sulphate and bicarbonate), which can also be used as driving counter-ions, may start contributing significantly to the nitrate and perchlorate fluxes from the water to the biocompartment. However, in the mechanistic transport model only the concentration of chloride is considered.

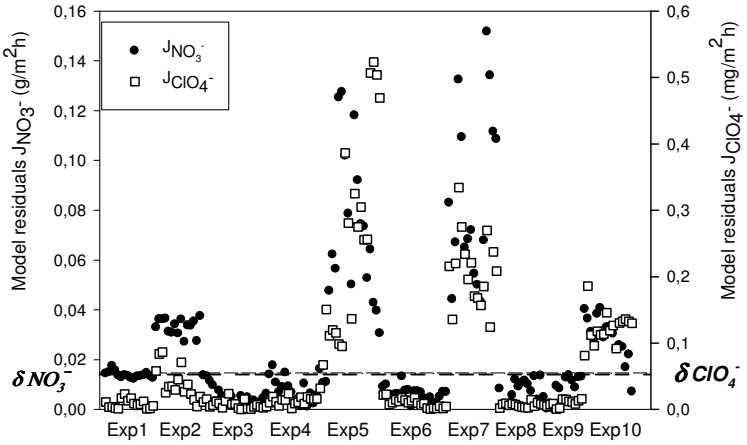

Figure 2.3: Mechanistic transport model prediction residuals for nitrate and perchlorate flux across a Neosepta ACS anion-exchange membrane (δNO_3^-: standard deviation of experimental nitrate flux; δClO_4: standard deviation of experimental perchlorate flux).

In experiment 2, model inaccuracies were also verified, mainly due to inefficient perchlorate removal by the culture. In this case, the effect of the biological reaction on the perchlorate transport cannot be neglected and the mechanistic transport model cannot be correctly applied. On the other hand, nitrate was totally reduced in the biofilm but its membrane flux prediction by the mechanistic model was also inaccurate. Again, an inaccurate flux prediction was observed in experiment 10 although, in this test, chloride is the major anion present and perchlorate was efficiently removed. These results indicate that the transport in membrane-supported biofilm reactors cannot be rigorously described through an one-factor contribution formalism. In fact, the contribution of the biofilm resistance to the transport of target solutes depends on different parameters such as biofilm thickness, density and morphology [2]. Therefore, the effect of the biocompartment conditions on mass transfer should be evaluated as a multivariate combined contribution.

2.4.2. Evaluation of the factors affecting the transport of pollutants

The impact of the variables, used in the Plackett-Burman design, on the nitrate and perchlorate fluxes across the membrane is presented in Figure 2.4. The impact effect of each factor was estimated as the difference between averages of fluxes made at the high level (+1) and at the low level (-1) of that factor. This analysis allowed for identifying the factors that influence the nitrate and perchlorate transport across the membrane and, consequently, have to be taken into account in the model. Some of these factors, such as the target and major driving counter-ion

concentrations, were already considered in the mechanistic transport model. However, the inclusion of additional biocompartment-related information proved to be necessary to predict situations in which the kinetics of the biological reactions is the limiting step.

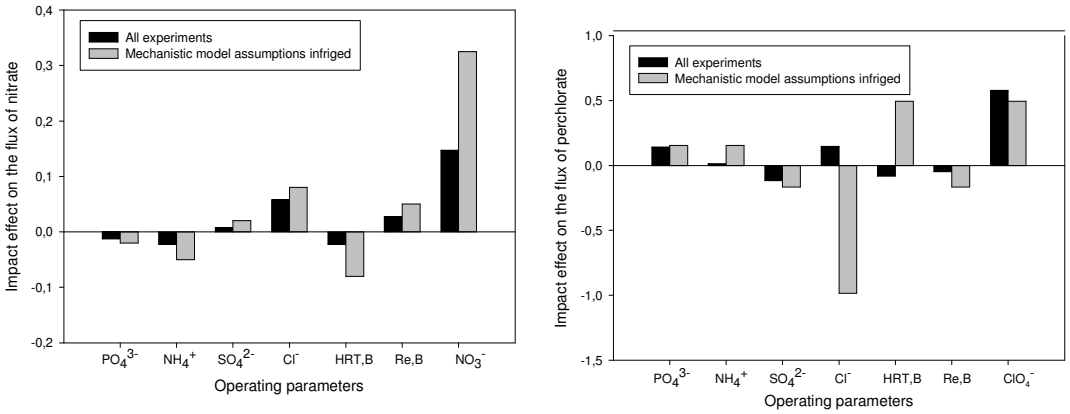

Figure 2.4: Effect of experimental design factors on the flux of nitrate (left) and perchlorate (right) across the membrane. Black bars represent all design experiments and gray bars the ones that do not follow the mechanistic transport model assumptions (experiments 2, 5, 7 and 10 in Table 2.1).

Considering all experiments, it can be observed that the fluxes of nitrate and perchlorate across the membrane were mainly affected by the nitrate concentration in the polluted water stream and by the concentration of chloride in the biofeed. However, the remaining factors cannot be disregarded since they enclose a 30 % contribution to the transport flux, in the case of nitrate, and a 36 % contribution, in the case of perchlorate. Except for the hydrodynamic conditions in the biocompartment, that are taken into account by the mechanistic transport model through the introduction of a boundary layer thickness parameter in this compartment [14], the remaining parameters are not incorporated in the mechanistic transport model. This lack of sufficient information for transport prediction becomes more evident when analyzing the contribution of each variable in the experiments where mechanistic transport model failed (gray bars). Again, the most important contributions to the nitrate and perchlorate fluxes across the membrane come from the nitrate/perchlorate concentration in the polluted water and from the chloride concentration in the biofeed (Figure 2.4). This behavior is in accordance with expectations, since the main deviation from the mechanistic transport model predictions is found for the experiments where low concentrations of chloride were set. The negative effect of chloride on the perchlorate flux evidences that in experiments where lower chloride settings were tested this variable had a stronger contribution to the response.

The HRT in the biological compartment also proved to have an important contribution to the nitrate and perchlorate transport fluxes. Since the biological activity occurs mainly within the biofilm, the HRT in the biocompartment should not have a significant effect on the transport

across the membrane by influencing the rates of nitrate and perchlorate bioreduction. Therefore, this result could most probably be attributed to changes in the ionic composition and, consequently, in the transport driving forces for nitrate and perchlorate transport to the biocompartment. This explanation is supported by the sign of the impact of the HRT when compared to that of chloride (Figure 2.4), since the contributions of these two factors are opposed. In order to maintain a constant mass flow rate, a higher concentration of chloride was fed to the biocompartment at a lower HRT. Consequently, the chloride content in the biocompartment becomes higher and the transport is affected.

These results show the limitation of the mechanistic model to predict counter-ion transport in situations where the biocompartment conditions fall outside the domain of its validity. In such situations, the biocompartment-related parameters have to be considered and incorporated in the modelling. As mentioned previously, the multivariate statistical modelling followed was based on the PLS approach since it has the ability of analyzing data with a high number of collinear variables. The use of an experimental design based on orthogonal matrixes, such as the Plackett-Burman design, allows for analyzing data with a high variability due to the simultaneous change of several factors.

2.4.3. Multivariate PLS regression analysis

A PLS model was obtained using detailed information for the two IEMB compartments, thus giving a total of 24 initial input variables (Table 2.2). Given the capacity of PLS to maximise covariance, it is advantageous to feed the model with all measurements available, because the algorithm is specifically designed to select the most informative inputs and to eliminate redundant information. For that reason, interrelated variables such as the biocompartment HRT and the biofeed mass flow rates to this compartment were also introduced.

The results of the PLS regression analysis for the fluxes of the target anions across the membrane are presented in Table 2.3 and Figure 2.5. These results were obtained by interpolation of the linear model obtained for the validation set. Regarding the two different normalizations applied, the autoscaling method produced better results. The Root-mean-square-error-of-prediction (RMSEP) is acceptable comparing with the experimental standard deviation except for the case of phosphate (σ=0.001), where the PLS model deviates strongly from the experimental data. The phosphate flux prediction is more complex due to distinct membrane permeabilities to the different phosphate species present (see section 2.2.2). Even with the inclusion of the bulk pH as a variable, this information might not be sufficient since the anion-exchange membrane excludes co-ions (cations, including H^+). Therefore, the pH inside the

membrane is probably higher than the bulk pH. On the other hand, the estimation of the phosphate speciation is based on the bulk pH, which may lead to a different partition of the two species (H_2PO4^- and HPO_4^{2-}). This erroneous partition is critical since the membrane used possesses mono-anion perm-selective properties. As a result, the PLS model was not able to find correlations between the operational physicochemical data used and the phosphate transport across the membrane. This is a clear indication that either the inputs are insufficient to describe this transport or that the correlations are non-linear. PLS can be considered as a powerful tool to capture information hidden in the process data for prediction; however, a predictive model can only be obtained when the information used is sufficient to describe the process performance.

The global value of χ^2 allows for concluding about the statistical significance of the model. In order to be considered accurate, the χ^2 value must be lower than the defined value with 95 % confidence. Considering the number of observations for the validation set (252 observations) and the number of parameters (i.e. latent variables) the tabulated value varies from 271.8 and 286.8 for (n-p) degrees of freedom [43]. Since for all anions studied (except for phosphate) the χ^2 was bellow 271.8, the calibrated PLS model can be statistically accepted as a prediction tool for the fluxes of target anions across the membrane in the IEMB process. Even for the case of phosphate, the PLS model gives better results compared to the mechanistic transport model.

Table 2.3: Comparison of the mechanistic and the PLS models flux prediction for target anions (RMSEP: Root-mean-square-error-of-prediction; TNP: Total number of parameters; AIC: Akaike Information Criterion)

Flux	Model	R^2	RMSEP	TNP	χ^2	AIC
$J(NO_3^-)$	Mechanistic	0.80	0.040	1	2091	-700.8
	PLS	0.97	0.012	17	197	-927.4
$J(ClO_4^-)$	Mechanistic	0.95	0.121	1	1228	-459.5
	PLS	0.99	0.047	17	186	-633.8
$J(H_2PO_4^-)$	Mechanistic	0.11	0.052	1	674255	-646.3
	PLS	0.65	0.002	9	1325	-1312.4
$J(HPO_4^{2-})$	Mechanistic	0.08	0.047	1	564190	-665.8
	PLS	0.53	0.002	10	580	-1400.8
$J(SO_4^{2-})$	Mechanistic	0.25	0.028	1	852	-783.9
	PLS	0.83	0.013	9	188	-933.4
$J(HCO_3^-)$	Mechanistic	0.52	0.019	1	878	-869.3
	PLS	0.95	0.007	3	91	-1083.9

On the other hand, the PLS transport model involves more parameters than the mechanistic transport model. Therefore, it is desirable to retain only the important relations between the data and to eliminate data noise. The initial 24 co-ordinate system was reduced to a smaller dimensional 9 co-ordinate system, in the sulphate flux prediction model. Despite the inclusion of more parameters into the PLS model, it is considered more appropriate when comparing the Akaike Information Criterion (AIC) for the PLS and the mechanistic transport model. This

criterion takes into account both a maximum likelihood term and a complexity term in statistical models so, even with an increase in complexity, the PLS model is definitely a better transport predictive tool since a lower value was obtained for each of the anions tested (Figure 2.5). The increase in the model accuracy clearly compensates the inclusion of more parameters into the model.

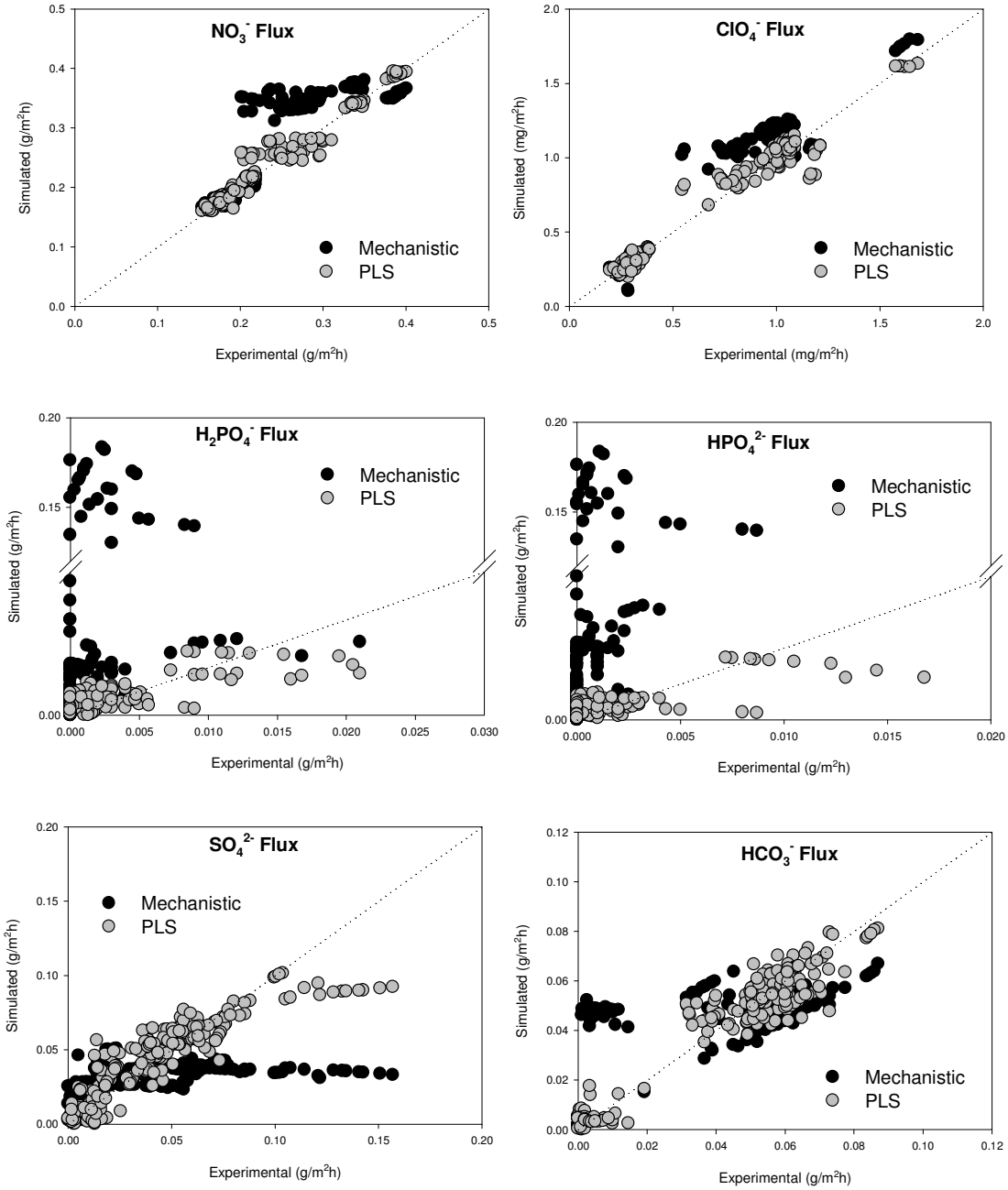

Figure 2.5: Predicted versus experimental flux values of the target anions for the mechanistic model (black dots) and PLS model (gray dots).

The model residuals for the PLS model are illustrated on Figure 2.6. A clear improvement can be observed with an accurate target anion flux prediction for almost all experiments (see Figure 2.3 for comparison). Experiment 5 and 7 were not totally predicted: the average of the residuals in these experiments decreased by 91 % in the case of nitrate and to 95 % in the case of perchlorate. A major progress was observed in experiments 2 and 10 that can be described with the PLS model developed. The use of multivariate calibration avoids the need for more complex formulations and the use of simplifying assumptions, adopted in mechanistic modelling of membrane biofilm reactors (e.g., constant biofilm density, uniform biofilm thickness). Therefore, this modelling approach can be more readily implemented in practice, since the model inputs are easily determined.

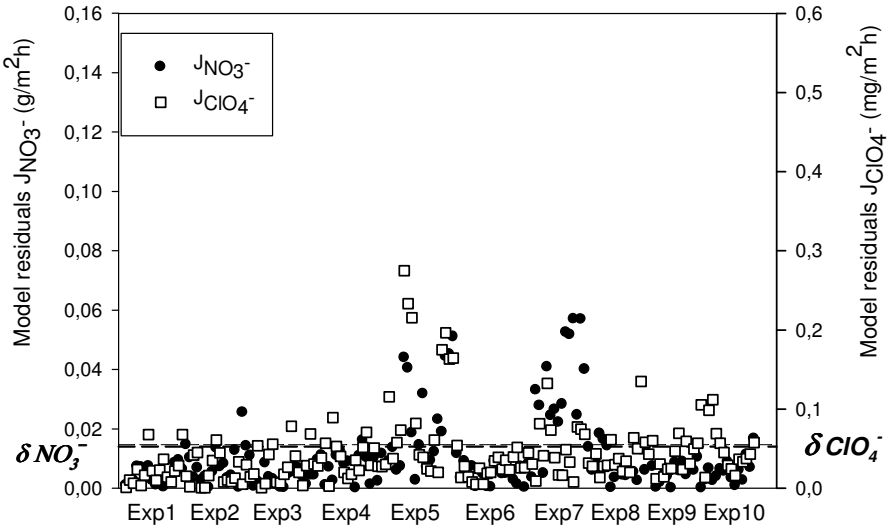

Figure 2.6: PLS model prediction residuals for nitrate and perchlorate flux across a Neosepta ACS anion-exchange membrane (δNO_3^-: standard deviation of nitrate flux; δClO_4^-: standard deviation of perchlorate flux).

2.4.4. Selection of useful predictors

Selection of relevant predictors in multivariate analysis was performed and a clear improvement was observed, especially in terms of reducing the complexity of the model. Table 2.4 summarizes the results for the validation set comparing the PLS model, with all the initial 24 predictors, with the PLS model with a lower number of predictors. Only the method responsible for the best results is presented in column 2 of Table 2.4. It can be observed that the prediction

capacity was maintain for all the models, however a lower number of latent variables (LV) was selected. As a result, a lower AIC value was obtained. This is the key criterion when comparing methods with a different number of parameters. Since the prediction accuracy was maintained, the reduction in the AIC value was mainly related with the decrease in the number of model parameters. The reduction in the number of inputs has also the advantage to reduce the amount of information to feed the model. Consequently, a lower number of analytical measurements will need to be performed.

Table 2.4: Results obtained for PLS model calibrated with the initial 24 inputs with PLS model calibrated with a reduced number of inputs

Flux	Method	No. predictors	LV	Var Y (%)	R^2	RMSEP	AIC
$J(NO_3^-)$	PLS	24	17	97.12	0.97	0.012	-927.4
	Backward selection	19	14	97.12	0.97	0.012	-937.5
$J(ClO_4^-)$	PLS	24	17	98.33	0.99	0.047	-633.8
	MUT-Bootstrapping	21	16	98.32	0.99	0.047	-645.4
$J(H_2PO_4^-)$	PLS	24	9	62.34	0.65	0.002	-1312.4
	MUT-Jackknife	15	8	61.86	0.65	0.002	-1310.0
$J(HPO_4^{2-})$	PLS	24	10	56.22	0.57	0.002	-1400.8
	UVE	11	7	52.65	0.53	0.002	-1396.2
$J(SO_4^{2-})$	PLS	24	9	79.62	0.83	0.013	-933.4
	Backward selection	17	11	79.89	0.83	0.013	-927.2
$J(HCO_3^-)$	PLS	24	18	90.34	0.95	0.006	-1083.9
	IPW	7	3	86.56	0.93	0.007	-1071.2

These improvements are mainly due to the elimination of some predictors that introduced noise into the model. In fact, despite PLS models capture the more relevant variance, the selection of useful predictors techniques should be applied to optimize the model since the variance related with noisy predictors is eliminated. Therefore, the new latent structure concerns the important predictors only and does not give an extra weight to uninformative predictors as the initial PLS. Consequently, the same variance can be captured with a lower number of latent variables. For instance, in the nitrate flux prediction, the same 97% of variance was captured with 14 latent variables instead of using 17 latent variables as in the initial PLS.

The selection methods applied in the present work differed in their criteria for variables inclusion and their applicability was dependent of the target experimental anion flux data. Overall, the results obtained do not favour any particular method for the selection of informative predictors.

In the case of sulphate and bicarbonate fluxes, the reduction of the number of predictors was not beneficial for the transport flux estimation. In the case of sulphate, the number of inputs was reduced but a higher number of latent variables were selected by cross-validation. However, since the accuracy was maintained, it was preferred to use fewer inputs, thus decreasing the number of analyses to be performed. The same criteria was used in the case of bicarbonate: the reduction to only 7 predictors is favourable to the small increase in the prediction model residual, since it is within the experimentally determined standard deviation of 0.01 g/m^2h for the bicarbonate flux.

2.4.5. Analysis of predictors´ contribution to the PLS model

The identification of the important predictors in the PLS model allows for selecting the process variables that most significantly affect the transport of the target anions across the membrane. Figure 2.7 illustrates the principal predictors and their respective contribution to the PLS-based transport model in the IEMB process. Since the PLS model is a linear correlation of the inputs, the values of the coefficients can be weighted as the contribution of a given input in the prediction. Therefore, the relative contribution of each predictor was estimated and represented in Figure 2.7.

In the case of nitrate flux across the membrane, 19 of the initial inputs were selected, indicating that almost all the information introduced in the model is essential for predicting the transport rate of this anion. As anticipated, the most important predictors for the PLS nitrate transport model are related with the driving force for the transport: NO_3^- concentration in the polluted water stream and Cl^- concentration in the biocompartment.

The HRT in the biocompartment was also found to have a significant contribution. This predictor encloses the contribution of chloride in the biofeed, as already discussed, since the concentration of chloride was adjusted to maintain the same mass load to the biocompartment for the two HRT values studied. The first 4 most important predictors (NO_3^- in the polluted water stream, Cl^- concentration and HRT in the biocompartment and Cl^- mass flow rate in the biofeed) contribute as much as 73 % to prediction. The remaining predictors comprise for 27 % of the contribution to the model but the inclusion of these predictors is important, since this information is not accounted for by the mechanistic transport model.

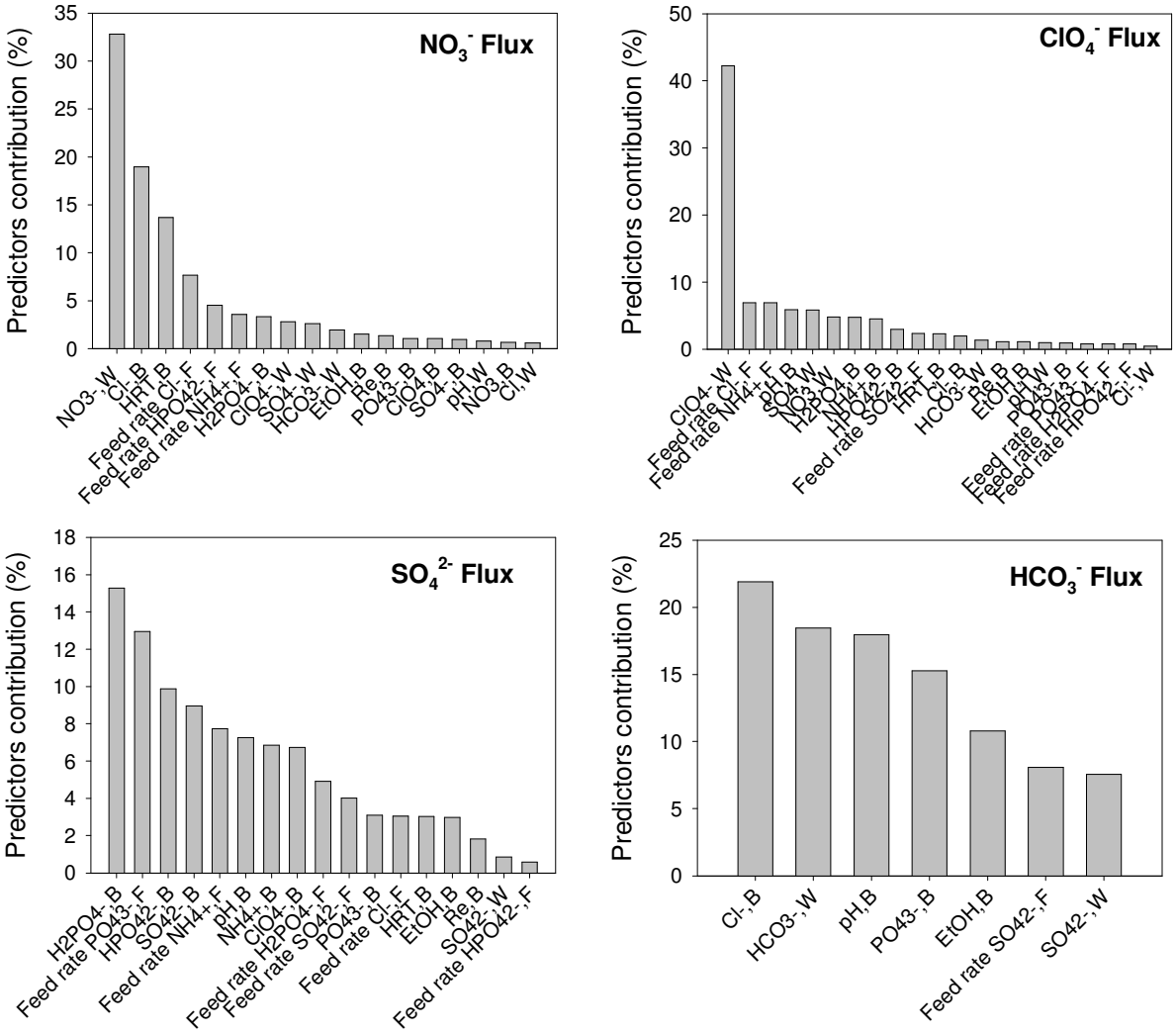

Figure 2.7: Relative contribution of predictors in the PLS model to the flux of the target anions.

For the perchlorate PLS transport model, it was found that its concentration in the polluted water stream is the most important, contributing with 42 % to the model prediction of the perchlorate flux across the membrane. As in the case of nitrate flux, the perchlorate concentration and the major driving counter-ion (chloride) concentration are the two main predictors; however, for perchlorate, its initial concentration in the polluted water is the most important parameter. Since perchlorate is a trace counter-ion, the amount of chloride to be fed to the biocompartment is defined by the amount of nitrate to be transported to the biocompartment. Therefore, for perchlorate transport, the chloride concentration is not limiting the transport since a relative high concentration ratio of driving (chloride) to target (perchlorate) counter-ion is established. The perchlorate transport prediction still needs to include several other inputs from the biofeed and biocompartment, corresponding to 32 % of the weight of all correlation

coefficients. Ammonium mass flow rate to the biocompartment was the third important predictor with a 7 % contribution. Ammonium is required for the microbial activity, since it is used as a nitrogen source for growth. Its limitation was identified as the main cause for the inaccuracy of the mechanistic transport model in experiment 2, in which an incomplete reduction of perchlorate was observed. Therefore, ammonium concentration affects perchlorate reduction in the biocompartment, and, consequently, the perchlorate transport across the membrane.

In the PLS model prediction for sulphate flux, the results indicate that the concentration of phosphate is essential. This was an unexpected result since phosphate was mainly present in the biocompartment and its transport across the membrane is irrelevant in the majority of the experiments. In some cases, it can serve as an additional driving counter-ion (in addition to chloride) for transporting anions from the water to the biocompartment. Transport of sulphate in all experiments occurred from the water to the biocompartment. Probably, since sulphate is not metabolized by the microbial culture, the PLS model main predictors are concentrations of compounds which are less involved in the biological activity (e.g., phosphate).

With respect to the bicarbonate flux estimation, the input matrix was reduced from 24 to 7 variables. This is a clear indication of the importance of applying methods for removal uninformative predictors. Similarly to the results obtained for nitrate and perchlorate, the bicarbonate transport across the membrane is mainly affected by the HCO_3^- concentration in the polluted water and Cl^- concentration in the biocompartment. Ethanol concentration in the biocompartment also proved to be an important variable. This is a rather sensible result since bicarbonate is the major anion that is metabolically produced due to the ethanol oxidation in the biocompartment. Furthermore, due to the formation of bicarbonate, the biocompartment pH value increased during the IEMB operation. Again, this effect was captured by the multivariate analysis identifying the pH in the biocompartment as an important input in the PLS model for this anion.

2.5. Conclusions

PLS-based modelling of transport of counter-ions in an anion-exchange membrane-supported biofilm reactor was successfully performed. The model developed is a clear improvement to previously developed mechanistic modelling, especially for predicting counter-ion transport

under biological reaction rate limited conditions. The biocompartment-related data in such situations contributed with 25-30 % for the prediction of the fluxes of nitrate, perchlorate, phosphate, sulphate and bicarbonate. The use of this modelling approach allowed for capturing the most important process parameters related to the compositions of the polluted water stream and biomedium. Therefore, the model proposed in this study could be considered as a step forward towards modelling of systems combining Donnan dialytic transport with biological reaction.

This strategy may also be advantageous for modelling mass transfer in other types of membrane-supported biofilm reactors since no *a priori* knowledge of the biofilm itself is necessary. The PLS model developed was able not only to infer the process performance, but also to identify the process variables that control the transport of anions. This can be useful for designing operations, in which the most important variables can be varied and process optimization can be achieved.

The model obtained can additionally be incorporated in hybrid structures combining mechanistic knowledge and PLS modelling.

2.6. References

1 Casey, E., Glennon, B., Hamer, G., 1999. Review of membranes aerated biofilm reactors. Resour. Conserv. Recy. 27: 203-215.

2 Shanahan, J.W., Semmens, M.J., 2006. Influence of a nitrifying biofilm on local oxygen fluxes across a micro-porous flat sheet membrane. J. Membr. Sci. 277: 65-74.

3 Lee, K-C., Rittmann, B.E., 2002. Applying a novel autohydrogenotrophic hollow-fiber membrane biofilm reactor for denitrification of drinking water. Water Res. 36 (8): 2040-2052.

4 Brookes, P.R., Livingston, A.G., 1995. Aqueous–aqueous extraction of organic pollutants through tubular silicone rubber membranes. J. Membr. Sci. 104: 119–137.

5 Wolf, G., Almeida, J.S., Reis, M.A.M., Crespo, J.G., 2005. Non-mechanistic modelling of complex biofilm reactors and the role of process operation history. J. Biotechnol. 117: 367-383.

6 Crespo, J.G., Reis, M.A.M., Treatment of aqueous media containing electrically charged compounds. WO Patent. WO 01/40118 A1.

7 Kapoor, A., Viraraghavan, T., 1997. Nitrate removal from drinking water- a review. J.

Environ. Eng. 123: 371-380.

8 Burge, S., Halden, R., 1999. Nitrate and perchlorate removal from groundwater by ion exchange. Lawrence Livermore National Laboratory, Livermore, p. 80.

9 Shrimali, M., Singh, K.P., 2001. New methods of nitrate removal from water. Environ. Pollut. 112: 351-359.

10 Son, A., Lee, J., Chiu, P.C., Kim, C.B., Cha, D.K., 2006. Microbial reduction of perchlorate with zero-valent iron. Water Res. 40: 2027-2032.

11 Matos, C.T., Velizarov, S., Crespo, J.G., Reis, M.A.M., 2006. Simultaneous removal of perchlorate and nitrate from drinking water using the ion exchange membrane bioreactor concept. Water Res. 40: 231-240.

12 Velizarov, S., Reis, M.A., Crespo, J.G., 2002. Ion exchange membrane bioreactor for selective removal of nitrate from drinking water: control of ion fluxes and process performance. Biotechnol. Progr. 18: 296-302.

13 Velizarov, S., Rodrigues, C., Reis, M.A., Crespo, J.G., 2000. Mechanism of charged pollutants removal in an ion exchange membrane bioreactor: drinking water denitrification. Biotechnol. Bioeng. 71: 245-254.

14 Velizarov, S., Reis, M.A., Crespo, J.G., 2003. Removal of trace mono-valent inorganic pollutants in an ion exchange membrane bioreactor: analysis of transport rate in a desnitrification process. J. Membr. Sci. 217: 269-284.

15 Blaedel, W.J., Haupert, T.J., Evenson, M.A., 1969. Mechanism of trace counterion transport through ion-exchange membranes. Anal. Chem. 41(4): 583-590.

16 Miyoshi, H., 1997. Diffusion coefficients of ions through ion-exchange membranes for Donnan dialysis using ions of the same valence. Chem. Eng. Sci. 52(7): 1096-1997.

17 Amang, D.N., Alexandrova, S., Schaetzel, P., 2004. Mass transfer characterization of Donnan dialysis in a bi-ionic chloride-nitrate system. Chem. Eng. J. 99: 69-76.

18 Prado-Rubio, O.A., Møllerhøj, M., Jørgensen, S.B., Jonsson, G., 2010. Modeling Donnan dialysis separation for carboxylic anion recovery. Comput. Chem. Eng. 34: 1567-1579.

19 Schaetzel, P., Favre, E., Auclair, B., Nguyen, Q.T., 1997. Mass-transfer through ion exchange membranes: comparison between the diffusion and the diffusion-convection Stefan-Maxwell equations. Electrochim. Acta 42(16): 2475-2483.

20 Yang, Y., Pintauro, P.N., 2004. Multicomponent space-charge transport model for ion-exchange membranes with variable pore properties. Ind. Eng. Chem. Res. 43: 2957-2965.

21 Nicolella, C., Pavasant, P., Livingston, A.G., 2000. Substrate counterdiffusion and reaction in membrane-attached biofilms: mathematical analysis of rate limiting mechanisms. Chem. Eng. Sci. 55: 1385-1398.

22 Wold, S., Sjöström, M., Eriksson, L., 2001. PLS-regression: a basic tool of chemometrics.

Chemom. Intell. Lab. Syst. 58: 109-130.

23 Matos, C.T., Fortunato, R., Velizarov, S., Reis, M.A.M., Crespo, J.G., 2008. Removal of mono-valent oxyanions from water in an ion exchange membrane bioreactor: Influence of membrane permselectivity. Water Res. 42(6-7): 1785-1795.

24 Pismenskaya, N., Laktionov, E., Nikonenko, V., Attar, A.E., Auclair, B., Pourcelly, G., 2001. Dependence of composition of anion-exchange membranes and their electrical conductivity on concentration of sodium salts of carbonic and phosphoric acids. J. Membr. Sci. 181: 185-197.

25 Brereton, R.G., 2003. Chemometrics: data analysis for the laboratory and chemical plant. John Wiley & Sons, Chichester, p. 489.

26 Kennedy, M., Krouse, D., 1999. Strategies for improving fermentation medium performance: a review. J. Ind. Microbiol. Biotechnol. 23: 456-475.

27 Montgomery, D.C., 2001. Design and analysis of experiments. 5th ed. John Wiley & Sons, Inc, New York, p. 684.

28 Weuster-Botz, D., 2000. Experimental design for fermentation media development: statistical design or global random search?. J. Biosci. Bioeng. 90(5): 473-483.

29 Cela, R., Martinez, E., Carro, A.M., 2000. Supersaturated experimental designs: new approaches to builing and using it. Part I: builing optimal supersaturated design by means of evolutionary algorithms. Chemom. Intell. Lab. Syst. 52: 167-182.

30 Krzanowski, W.J., Kline, P., 1995. Cross-Validation for choosing the number of important components in principal components analysis. Multivar. Behav. Res. 30(2): 149-165.

31 Matlab 2006b, 2006. The Mathworks, Inc., Natick, MA, USA.

32 Andersson, C.A., Bro, R., 2000. The N-way toolbox for MATLAB. Chemom. Intell. Lab. Syst. 52: 1-4.

33 Ryan, T.P., 1997. Modern Regression Methods. John Wiley & Sons, Inc, New York, p. 515.

34 Boggia, R., Forina, M., Fossa, P., Mosti, L., 1997. Chemometric study and validation strategies in the structure-activity relationships of new cardiotonic agents. Quant. Struct-Act. Rel. 16: 201-213.

35 Forina, M., Casolino, C., Millan, C.P., 1999. Iterative predictor weighting (IPW) PLS: a technique for the elimination of useless predictors in regression problems. J. Chemometr. 13: 165-184.

36 Centner, V., Massart, D.L., Noord, O.E., Jong, S., Vandeginste, B.M., Sterna, C., 1996. Elimination of uniformative variables for multivariate calibration. Anal. Chem. 68: 3851-3858.

37 Forina, M., Lanteri, S., Cerrato Oliveros, M.C., 2004. Selection of useful predictors in

multivariate calibration. Anal. Bioanal. Chem. 380: 397-418.

38 Duchesne, C., MacGregor, J.F., 2001. Jackknife and bootstrap methods in the identification of dynamic models. J. Process Contr. 11: 553-564.

39 Faber, N.M., 2002. Uncertainty estimation for multivariate regression coefficients. Chemom. Intell. Lab. Syst. 64: 169-179.

40 Jordan, M.I., Jacobs, R.A., 1994. Hierarchical Mixtures of Experts and the EM Algorithm. Neural Computation. 6: 181-214.

41 Quinn, G.P., Keough, M.J., 2002. Experimental Design and Data Analysis for Biologists. 5th ed. Cambridge University Press, Cambridge, p. 537.

42 Akaike, H., 1974. A new look at the statistical model identification. IEEE Trans. Automat. Contr. 19(6): 716-723.

43 Morrison, D.F., 1990. Multivariate Statistical Methods. 3rd Ed., McGraw-Hill International Editions, Singapore, p. 495.

Chapter

3

Hybrid modelling of counterion mass transfer in a membrane-supported biofilm reactor[2]

Summary

This chapter presents a hybrid mechanistic/statistical model for predicting counter-ion fluxes across an ion-exchange membrane in a membrane-supported biofilm reactor. The model was calibrated with operating data for the removal of nitrate and perchlorate from a simulated contaminated drinking water stream. Two different modelling strategies were tested: a cooperative parallel hybrid model and a competitive mixture-of experts (MOE) structure both joining a mechanistic Donnan-dialytic transport model and a multivariate Projection to Latent Structures (PLS) model. The MOE structure proved to be a better predictive tool since it combines the two hybrid model elements in a mediated network. The PLS model was used to identify the process variables that are responsible for the mechanistic model inaccuracy. The results showed that biocompartment physicochemical data need to be considered in the modelling of the transport of counterions across the membrane, especially in situations in which the target counterion (e.g., perchlorate or nitrate) is metabolically reduced in the biocompartment. By using this strategy, the complex biofilm contribution to the transport was accounted for, without the need of developing mechanistic models built on simplified and/or inaccurate assumptions.

[2] Published on: Biochemical Engineering Journal (2012) 62: 22–33. Reproduced with permission of the copyright owner:
http://www.elsevier.com/wps/find/authorsview.authors/rights

3.1. Introduction

Membrane-attached biofilms (MABs) have been widely used in water and wastewater treatment [1-5]. Since the membrane allows for the physical separation of the microbial culture from a polluted water stream, the biological treatment of toxic organics from wastewater was proved possible using the extractive membrane bioreactor concept [1-3]. MABs have been also successfully combined with gas delivery systems: O_2 to aerobic biofilms and H_2 to anaerobic biofilms, used as electron acceptor or donor, respectively [4-5]. Additionally, biological purification of air by transferring gaseous pollutants through a membrane into a biofilm has been reported [6].

If an electron donor and an electron acceptor diffuse into the membrane-attached biofilm from opposite sides (counter-diffusion), the process modelling differs significantly from the modelling of conventional biofilm reactors with substrates entering into the biofilm from one and the same side (co-diffusion) [1]. In the case of counter-diffusion, the reaction zone could be located in different regions within the biofilm depending on the local concentrations of substrates required for a given reaction [7]. A number of mathematical models applied to membrane-attached biofilms have been developed so far [7-12]. Nicolella *et al* presented a reaction-diffusion model to predict substrate concentration profiles and the biofilm thickness evolution over time in an extractive membrane bioreactor [9]. Several assumptions, such as constant biofilm density, constant diffusivity and uniform biofilm thickness were considered. Even with these simplifications, the biofilm dynamic model developed required numerical solutions of partial differential and integral equations.

The ion exchange membrane bioreactor (IEMB) is a process that combines the transport of target counterions (e.g., nitrate, perchlorate) from contaminated water streams through an anion-exchange membrane to an anoxic membrane-attached biofilm [13]. The transport between the two compartments is governed by the Donnan dialysis principles, thus enhancing the transport of target counterions from the water to the biological compartment by adding an excess of suitable "driving" counterions (e.g., chloride) to this compartment. After transport through the anion-exchange membrane, the ionic pollutants are reduced to innocuous species (such as nitrogen and chloride) by a mixed microbial culture.

The mechanism of transport of ionic pollutants in the IEMB was extensively studied [14-16] and a mechanistic counterion transport model was previously developed [17].

This model was shown to predict accurately the fluxes of counterions across the membrane on the basis of physicochemical and hydrodynamic data, in situations of complete bioreduction of the target counterions in the IEMB biocompartment [14, 17].

The model was developed assuming that the process is mass-transfer limited. The "resistances-in-series" approach was followed considering the sum of the membrane resistance and the diffusion resistances of the two liquid films adjacent to the membrane in the water and biocompartment, respectively. Thereby, the model presupposes non-limiting biological conditions, and neglects possible mass transfer limitations due to the biofilm itself [18]. However, in the initial phase of the process when the biofilm is still not developed, or in situations of nutrient limitation, the rates of the biological reactions may become limiting.

In the previous Chapter, a projection to latent structures (PLS) model was developed to predict the counterion transport during an IEMB operation. This model was shown to have a good prediction potential under both mass-transfer and reaction rate limiting conditions [19]. The model was developed using a Projection to Latent Structures (PLS) technique that captured the underlying relations, assuming that the experimental data contained all the information needed for an adequate process description. Therefore, the use of simplifying assumptions considered in previously developed MABs mechanistic models was avoided. However, the use of purely statistical models ignores any mechanistic knowledge, requires a relatively large amount of experimental data and has a limited extrapolation potential [20].

This Chapter aims at developing a hybrid model, for a membrane-attached biofilm reactor by using statistically-based modelling techniques for capturing underlying information from process operating conditions. The modelling strategy evaluated in the present study was a combined use of mechanistic and statistical models. The working hypothesis was that such a combination might gather the best of both approaches, thus allowing for a certain level of process mechanistic interpretation and, at the same time, for the inclusion of the relevant physicochemical phenomena, which are usually simplified by mechanistic modelling. In this relation, a statistical fraction might account for effects not considered by the mechanistic model, while the mechanistic model could potentially manage the extrapolation of the hybrid model to regions lacking calibration data [21].

The statistical analysis is also important to identify the operation variables that are limiting the mass-transfer of a target counterion across the membrane. This identification is crucial for process optimization and practical implementation. Eventually, the mechanistic formulations might be also improved with the incorporation of the key variables.

3.2. Materials and Methods

3.2.1. Experimental installation and procedure

The IEMB layout is illustrated in Figure 3.1. The membrane module used had two identical rectangular channels in a flat parallel-plate configuration. A Neosepta ACS membrane (Tokuyama Soda, Japan) with 34.5 cm^2 separated water polluted with nitrate and perchlorate from the biomedium, thus organizing two different compartments, a water compartment and a biological compartment, respectively. Polluted water was prepared by supplementing tap water from the Lisbon public distribution network with different concentrations of nitrate and perchlorate, according to the design of experiments described in Table 3.1. The polluted water was continuously fed to the water compartment at 0.18 mL/min to maintain a hydraulic retention time (HRT) of 8 h in this compartment. For maintaining good hydrodynamic conditions, the water was re-circulated at a volumetric flow rate of 1620 mL/min (Reynolds number of 3000).

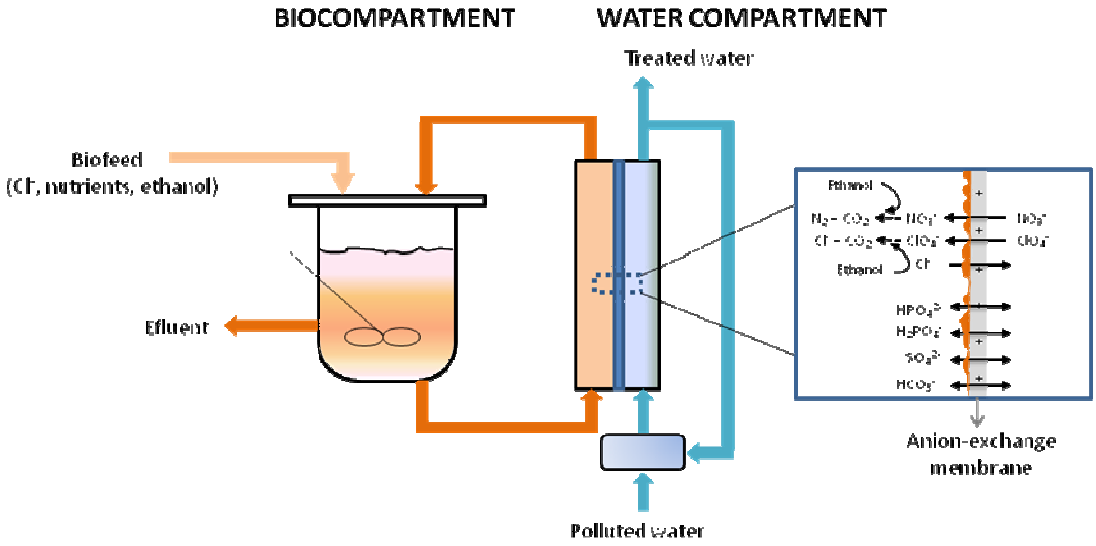

Figure 3.1: Schematic diagram of the experimental set-up and counterion transport mechanism in the ion-exchange membrane bioreactor (IEMB).

A mixed microbial culture was used to reduce nitrate and perchlorate in the biocompartment under anoxic conditions. This culture was enriched from a primary inoculum taken from a municipal wastewater treatment plant [14]. Two different biomedium re-circulation flow rates were used (82 mL/min and 1620 mL/min), corresponding to Reynolds numbers of 150 and 3000, respectively. The total biocompartment volume, including the membrane module channel, the re-circulation loop and the anoxic vessel was 550 mL. The composition of the nutrient

media for the reference experiments was: 1g/L of K_2HPO_4, 0.592 g/L of KH_2PO_4, 0.5 g/L of NaH_2PO_4, 0.233 g/L of NH_4Cl, 0.1 g/L of $MgSO_4.7H_2O$, 5.84 g/L of NaCl and 0.56 g/L of ethanol. In the remaining experiments, the biomedium composition, except for ethanol used as the carbon source and electron donor, was changed according to the experimental design (Table 3.1). The biomedium feeding rate and the recirculation flow rate in the biocompartment were introduced as variables in the experimental design in order to investigate their effects on the fluxes of target counterions across the membrane.

Table 3.1: Operating conditions of the IEMB experiments performed

Exp No.	PO_4^{3-} (mg/L)	NH_4^+ (mg/L)	SO_4^{2-} (mg/L)	Cl^- (mg/L)	$HRT_{Biocomp}$ (days)	$Re_{Biocomp}$ (-)	NO_3^- (mg/L)/ ClO_4^- (µg/L)
1	958	78	40	3700	5.84	3000	60 / 100
2	958	6.7	0	3700	5.84	3000	120 / 200
3	48	78	0	3700	10	3000	60 / 100
4	958	78	370	240	5.84	3000	60 / 100
5	48	6.7	370	240	10	3000	120 / 200
6	958	6.7	370	3700	10	150	60 / 100
7	958	78	0	240	10	150	120 / 200
8	958	78	40	3700	5.84	150	60 / 100
9	48	6.7	0	240	5.84	150	60 / 100
10	48	78	370	3700	5.84	150	120 / 200

All experiments were run at 23 ± 1 ºC with periodic sampling for off-line analyses of conductivity and pH and for analytical determination of the concentrations of anions, ammonium and ethanol.

3.2.2. Analytical methods

Nitrate, phosphate, sulphate and chloride concentrations were determined by an ion exchange chromatography system (Dionex, USA), constituted by an Ionpac AG9 guard and analytic AS9 columns (4 mm), an Anion Supressor-ULTRA (4 mm) and an ED50 electrochemical detector. The analysis was performed at 23 ºC using a 9 mM Na_2CO_3 aqueous solution as the mobile phase at a flow rate of 1 mL/min. Perchlorate concentration was measured at 30 ºC with 50 mM NaOH aqueous solution at a flow rate of 1 mL/min in the same system using AG16 and AS16 columns. The ClO_4^- detection limit was 1 µg/L with the injection of 1 mL of sample. In the biocompartment samples analysis, due to interference of the Cl^- peak with the ClO_4^- peak, 500 µl of sample was injected and, consequently, the limit of detection increased to 2 µg/L of ClO_4^-.

For the bicarbonate analysis, the Dionex system was operated with AG11 and AS11 columns with a 25 mM NaOH aqueous solution at a flow rate of 1mL/min at 30 ºC.

Phosphate and bicarbonate were determined in the form of PO_4^{3-} and CO_3^{2-}, respectively, due to the high eluent pH. The conversion to phosphate and bicarbonate species actually present in the samples was based on the sample pH according to the pKa values of each acid-base pair [22, 23].

Ethanol in the biocompartment and biofeed was determined by HPLC using a mobile phase of 0.01N H_2SO_4 aqueous solution at a flow rate of 0.5 mL/min at 30 ºC with an Aminex HPX-87H column (BioRad, USA) and a differential refractometric detector RI-71. The ethanol detection limit was 1 mg/L.

Ammonium was determined with a gas-sensitive electrode Orion 95-12 (Thermo, USA) with a detection limit of 1 mg/L.

3.2.3. Experimental design

The experiments were designed with a screening Plackett-Burman design [24] in order to obtain data allowing for statistical interpretation through a reduced number of experiments. In the design, seven factors, previously identified as most contributing to the transport of counterions across the membrane [19], were tested at 2 levels of variation. The investigated factors were: phosphate, ammonia, sulphate and chloride concentrations in the biomedium, the hydraulic retention time (HRT) in the biocompartment, the hydrodynamic conditions in the biocompartment recirculation loop, characterized by the Reynolds number (Re), and the concentrations of nitrate and perchlorate in the water compartment. Each factor was tested at two levels of variation based on previously operating conditions [14] as described in Table 3.1. In experiments in which the biocompartment HRT was increased, the concentrations of the nutrients in the biofeed (Table 3.1) were increased correspondingly in order to assure the same mass loads to the biocompartment.

Moreover, two experiments (experiment 1 and 8) were performed according to previously reported conditions [14] under which the mechanistic model was found to accurately predict the fluxes of nitrate and perchlorate across the membrane.

3.3. Mathematical modelling

3.3.1. Mechanistic transport model

The steady-state transport of a trace counterion, *i*, from compartment 1 (water compartment) across the membrane into compartment 2 (biocompartment) can be approximated by a bi-ionic equation (equation 3.1) if a bulk counterion, *bulk*, is present in excess in both compartments [17]. This equation combines the driving force and the resistance (the "resistances-in-series" in the denominator) to mass transfer of a target trace counterion from the water to the biocompartment. In equation 3.1, L is the membrane thickness (m); P_m is the membrane permeability to the target counterion (m^2/h); Q_m is the membrane ion exchange capacity (mmol/m^3 of wet membrane); δ_1 and δ_2 are the thickness (m) of the liquid boundary layers contacting the membrane surface in the water and biocompartment, respectively, and $D_{i,w}$ (m^2/h) is the diffusion coefficient of the target counter ion *i* in water.

$$J_i = \frac{\frac{C_{i,1}}{C_{bulk,1}^Z} - \frac{C_{i,2}}{C_{bulk,2}^Z}}{\frac{L}{P_{m,i}\left(Q_m/a\right)^Z} + \frac{\delta_1}{D_{i,w}C_{bulk,1}^Z} + \frac{\delta_2}{D_{i,w}C_{bulk,2}^Z}} \qquad (3.1)$$

Since the transport in the IEMB process is governed by the Donnan dialysis principles, the flux of a target counterion *i* across the membrane is proportional to the difference between the target counterion (C_i) to driving counterion (C_{bulk}) molar concentration ratios in the two compartments. The parameter Z represents the ratio between the valence of the target counterion and the valence, a, of the major bulk counterion (Cl^- in the case of this study). The thicknesses of the liquid boundary layers at the membrane surfaces in the two channels of the module were estimated using Sherwood number correlations for flat channels [25]. The membrane-related parameters and the P_m values for the studied counterions in the mechanistic transport model were assessed in a previous study [19, 23].

The transport flux of a target counterion across the membrane was calculated using the steady-state mass balance for the water compartment:

$$J_i = \frac{F}{A}\left(C_i^{in} - C_i^{out}\right) \qquad (3.2)$$

In equation 3.2, F is the inlet polluted water flow rate to the water compartment (1.08 x 10^{-5} m^3/h), A is the membrane area (3.45 x 10^{-3} m^2), and C_i is the target counterion concentration in the polluted water (in) and treated water (out), respectively.

3.3.2. Hybrid models

In the present study, two different approaches were tested: 1- a hybrid parallel structure (Figure 3.2a) and 2- a Mixture of Experts structure (MOE) (Figure 3.2b) [26-28]. Both strategies are based on the previously described mechanistic model complemented with a PLS model. However, the PLS contribution, in the parallel structure, can be interpreted as cooperative since the PLS model component forecasts the corrections that are needed to be incorporated in the mechanistic model. On the other hand, in the MOE structure a competitive contribution between the mechanistic and the PLS model is observed since both models individually predict the target counterion flux and their respective contributions are balanced.

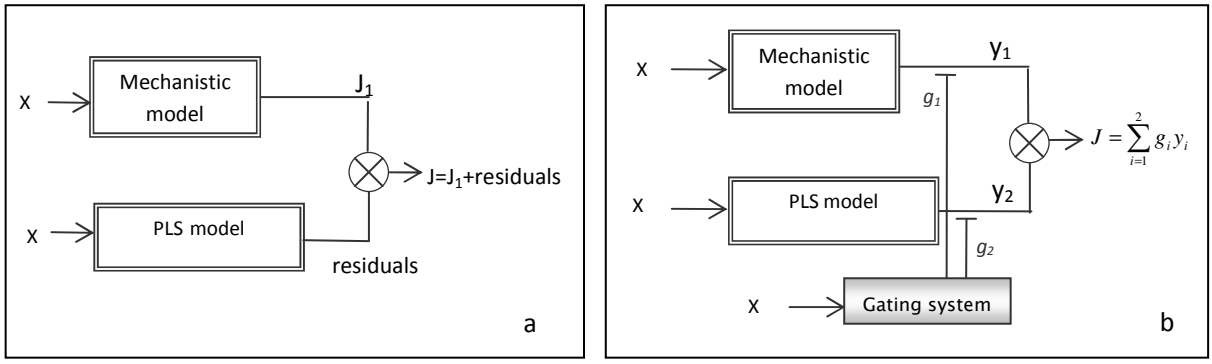

Figure 3.2: Hybrid modelling approaches used: Parallel (a) and Mixture of Experts (b).
(X: matrix of inputs; y: vector of output; J: target counterion flux across the membrane; g: gating equation; Subscripts- 1: mechanistic model, 2- PLS model).

In the hybrid parallel structure, the estimation of a target counterion flux combines the prediction of the previous developed mechanistic model and the PLS model in a single output (Figure 3.2a). The procedure for parallel hybrid calibration followed two steps. First, a target counter-ion flux was estimated using the mechanistic transport model and the residuals were calculated. Then, a PLS regression analysis was used to estimate these residuals as the target output. It has been demonstrated that by using such a structure, a better interpolation and range extrapolation proprieties can be achieved in comparison with mechanistic or statistical models alone [20].

Figure 3.2b illustrates the MOE approach, where the final model is a result of the mediated contribution of the mechanistic and the PLS models. In this structure, the two models predict the counterion mass-transfer across the membrane and the contribution of each model is mediated by a gating system that depends on the operating conditions. The gating system applied was

based on 'softmax' functions (equation 3.3) in which the subscript 1 refers to the mechanistic model contribution [29, 30]. The 'softmax' output is considered a probability choice since its value varies from 0 to 1 [31]. Therefore, if g_1=1 the counter-ion flux prediction is only described by the mechanistic model while when g_1=0 the output is determined by the PLS model. Consequently, the contribution of the PLS model is quantified by the 'softmax' function $g_2 = 1 - g_1$. Since the MOE network comprises two expert systems, the 'sofmax' equation denominator is composed by two terms in the denominator (equation 3.3).

$$g_1 = \frac{e^{\sum_{j=1}^{n} w_j X_j}}{e^{\sum_{j=1}^{n} w_j X_j} + e^{\sum_{k=1}^{n} w_k X_k}} \qquad (3.3)$$

Using this equation, the degree of contribution of each expert model is defined according to the experimental conditions, since the 'softmax' is a non-linear relation between the inputs (X) and theirs weights (w) for all the *n* variables of the PLS model. The same process information is used to feed both the PLS model and the 'softmax' equation. The *w* determination for the optimization of this combinatory problem was based on minimizing the MOE fluxes prediction error, using a modified Levenberg-Marquardt method for estimation.

The PLS model, for both hybrid models, was implemented on Matlab 2006b [32] with the toolbox N-Way [33] using randomly 75 % of the initial data set for calibration. The remaining 25 % were used for predicting the model goodness of fitting (validation set). The number of samples was standardised to have the same contribution to the model calibration, and the data obtained was scaled by subtracting from each of the variables their averages and dividing by their respective standard deviations (auto-scaling).

The PLS model calibration started by computing a X-score matrix T = XW for an appropriate weight matrix W by using the original dimensional input data (X). These weights are estimated so that each of them maximizes simultaneously the covariance between X and T and between Y and T by minimizing the error (noise) term in each equation (E, F): X = TP' + E and Y = TQ' + F, where T and Q are the matrix of X-loadings and Y-loadings, respectively. Once the loadings are computed, the above equations can be combined to obtain a multiple regression model: Y = TQ' + F =XWQ' + F = XB + F, where the PLS regression coefficients, B, equals to WQ. In PLS, dimension of X is reduced since the data set is transformed into another coordinate system, T, which is composed by orthogonal variables [29]. The incorporation of new vector on T occurs as long as it is predictively significant. Therefore, PLS algorithm is specifically designed to deal with noisy, collinear and numerous variables and to eliminate redundant information [29]. Due to this property, it is beneficial to use all available process information to calibrate the

model. Therefore, the PLS model was fed with physicochemical data from the two compartments: the polluted water composition, the biofeed mass flow rate, the biocompartment medium composition, the hydraulic retention time and the Reynolds number in the biocompartment and the pH values in the two compartments (giving a total of 24 input variables, presented in Table 3.2). The remaining operating conditions: membrane area, Reynolds number in the water compartment, and hydraulic retention time in the water compartment were maintained constant in all experiments. The contribution of these factors to the anions transport was previously investigated and correctly taken into account by the mechanistic transport model [17].

Table 3.2: Initial inputs used in PLS model calibration

Input No.	Abbreviation	Stream/Compartment	Compound/Condition
1	NO_3^-,W	Polluted water composition (mmol/m^3)	NO_3^-
2	ClO_4^-, W		ClO_4^-
3	SO_4^{2-}, W		SO_4^{2-}
4	Cl^-,W		Cl^-
5	HCO_3^-,W		HCO_3^-
6	Feed rate PO_4^{3-},F	Biofeed mass flow rate (mmol/h)	PO_4^{3-}
7	Feed rate $H_2PO_4^-$,F		$H_2PO_4^-$
8	Feed rate HPO_4^{2-},F		HPO_4^{2-}
9	Feed rate SO_4^{2-},F		SO_4^{2-}
10	Feed rate Cl^-,F		Cl^-
11	Feed rate NH_4^+,F		NH_4^+
12	NO_3^-,B	Biocompartment medium composition (mmol/m^3)	NO_3^-
13	ClO_4^-, B		ClO_4^-
14	PO_4^{3-},B		PO_4^{3-}
15	$H_2PO_4^-$,B		$H_2PO_4^-$
16	HPO_4^{2-},B		HPO_4^{2-}
17	SO_4^{2-}, B		SO_4^{2-}
18	Cl^-,B		Cl^-
19	NH_4^+,B		NH_4^+
20	EtOH,B		Ethanol
21	Re,B	Operating conditions	Reynolds number in the biocompartment recirculation loop (-)
22	HRT,B		Hydraulic retention time in the biocompartment (days)
23	pH,W		pH of polluted water (-)
24	pH,B		pH of the medium in the biocompartment (-)

The selection on the number of latent variables to use was based on cross-validation [34]. The PLS model was calibrated according to a flowchart described in Chapter 2 (see Figure 2.2). Briefly, the initial PLS model was subjected to several procedures in order to distinguish the

variables that contribute to predict the output from uninformative predictors that only introduce noise. The selection of useful model descriptors was done using 8 different techniques: forward selection [30], backward selection [30], stepwise selection [30], iterative stepwise elimination (ISE) [35], iterative predictors weighting (IPW) [36], uninformative variables elimination (UVE) [37] and Martens uncertainty test [38] with regression coefficients confidence interval estimated with Jackknife [39] and Bootstrapping [40] resampling techniques.

The validation set was compared with the predicted values using different criteria: the correlation coefficient (R^2) and the root-mean-square-error-of-prediction (RMSEP). Both methods are based on the model residuals and quantify the prediction capacity of the model [28].

The model obtained was also evaluated for its lack-of-fit in order to compare its prediction capacity with the experimental variance of the errors (σ^2_{exp}) by the χ^2 statistic [41-42]. Since the error term is supposedly independent and normally distributed, the weighted residuals should approximate a chi-square distribution for n-p degrees of freedom (n: number of observation; p: number of model parameters). Therefore, since the experimental variance of the measurements error is known, the obtained model can be considered statistically fitted if the value of χ^2 is below the critical values of tabulated χ^2 for the model degrees of freedom.

$$\chi^2 = \frac{\sum_{i=1}^{n} \Sigma\left(y_{model} - y\right)^2}{\sigma^2_{exp}} \qquad (3.4)$$

3.4. Results and discussion

3.4.1. IEMB performance and mechanistic model predictions

Before carrying out the design of experiments, the IEMB performance was evaluated for tap water supplemented with nitrate and perchlorate (experiment 1 in Table 3.1) and operated under previously defined conditions [14]. These conditions were demonstrated to guarantee effective bioreduction of nitrate and perchlorate in the biocompartment, since all nutrients were in excess and the process limiting step was the counter-ion mass transport through the membrane. The results obtained in this work were in agreement with the previously obtained data [14]. Under these conditions, the concentrations of nitrate and perchlorate in the treated water (Figure 3.3)

were below the drinking water quality guidelines: 45 mg/L for NO_3^- [43] and 15 µg/L for ClO_4^- [44].

The experimental data obtained were used to validate the mechanistic model (equation 3.1) predictions for transport flux of nitrate, perchlorate, phosphate, sulphate and bicarbonate. These anions are the major species transported through the membrane. The first two anions were initially present in the polluted water, the second two mainly in the biomedium, while bicarbonate was present in both compartments. In previous studies, the biomedium composition was formulated with excess of phosphate in order to prevent nutrient limitation by phosphorous. Therefore, in experiment 1, transport of phosphate from the biological compartment to the water compartment was documented. In order to prevent and/or minimize changes in the ionic composition of the treated water, the control of the fluxes of all counter-ions presents (and not only of nitrate and perchlorate) is mandatory.

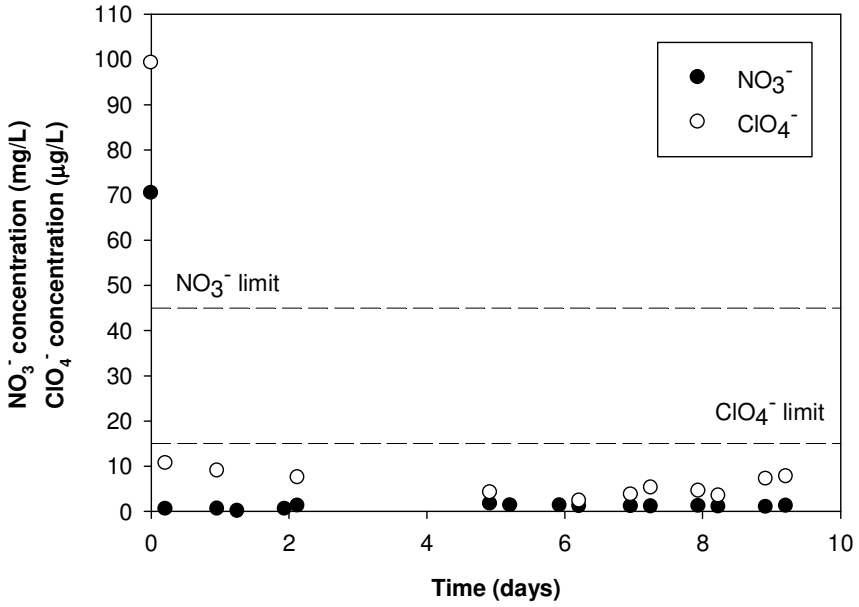

Figure 3.3: Time course of nitrate and perchlorate concentrations in the treated water for a typical IEMB process (experiment 1 in Table 3.1) fed with water polluted with 60 mg/L of NO_3^- and 100 µg/L ClO_4^- .

The accuracy of the mechanistic transport model predictions for experiment 1, performed under standard conditions, was confirmed with a predicted nitrate flux across the membrane of 0.21 g/(m^2h) and an experimentally determined value of 0.22 ± 0.01 g/(m^2h). For perchlorate, the mechanistic model prediction was also accurate since the predicted value of 0.30 mg/(m^2h) corresponded exactly to the experimentally determined value of 0.30 ± 0.05 mg/(m^2h).

The mechanistic model accuracy was afterwards evaluated for all experiments performed. Whenever the residuals rise above the experimental error standard deviation, the model prediction is considered to be not consistent with the values obtained experimentally. As can be seen from the data presented in Figures 3.4a and 3.4b, in 4 of the 10 experiments performed the mechanistic model predictions for the fluxes of nitrate and perchlorate across the membrane were inconsistent. As expected, model inconsistencies coincided mainly with experimental conditions that do not fulfil the building assumptions of the mechanistic transport model (experiments 2, 5, 7 and 10). A relatively low ratio of driving (chloride) to target counter-ion was used in experiments 5 and 7 and an incomplete perchlorate reduction, due to ammonia nutrient limitation, was observed in the biocompartment in experiment 2. However, in experiment 10, the lack of accuracy of the mechanistic model cannot be attributed to these factors, which is an indication that the simplified mechanistic model does not account for all possible parameters and, therefore, its prediction may become unreliable in complex systems.

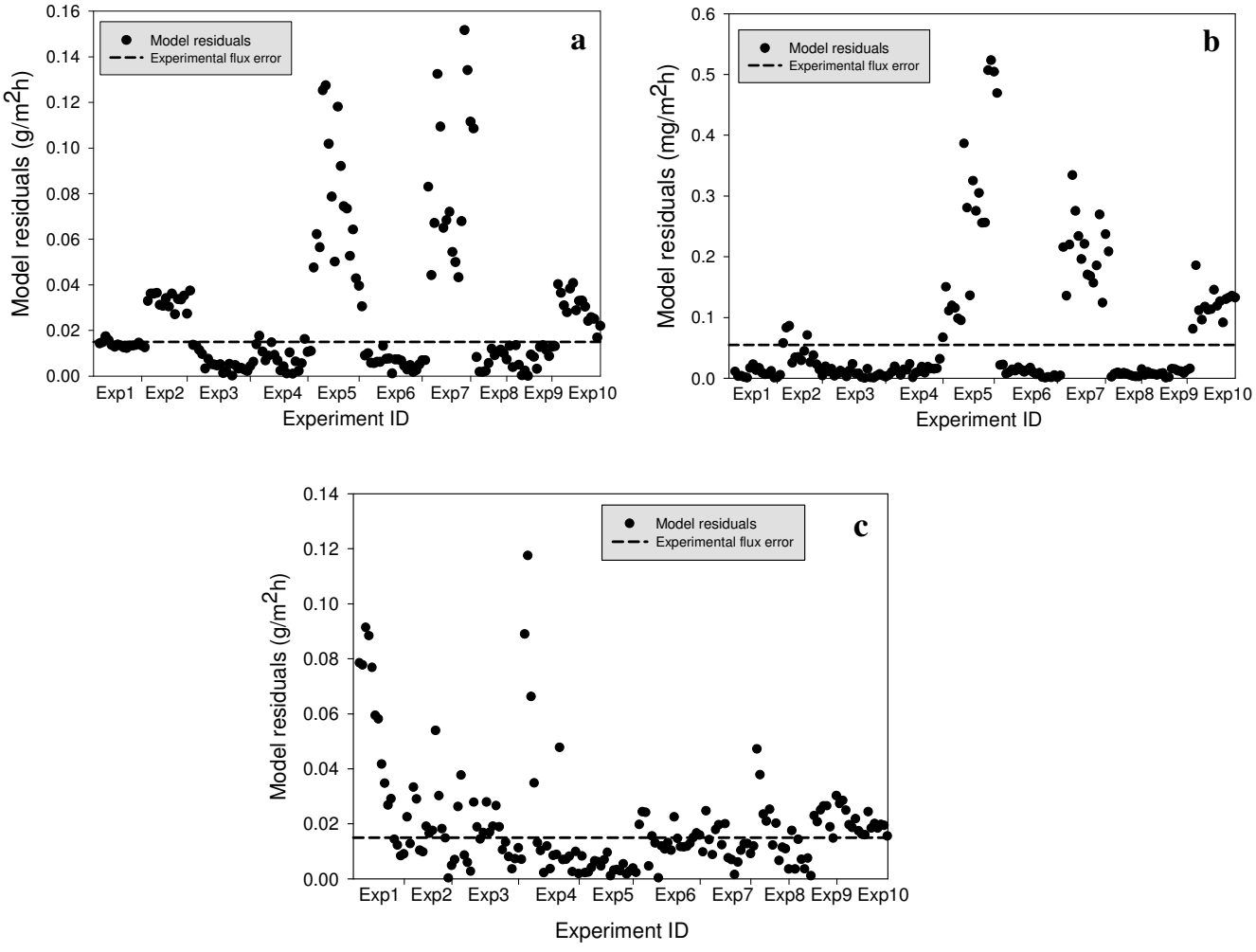

Figure 3.4: Mechanistic model prediction residuals and experimental standard deviation (δ) of the flux error for nitrate (a), perchlorate (b) and sulphate (c) flux across the membrane.

The mechanistic model was not capable of predicting accurately the phosphate, sulphate and bicarbonate fluxes across the membrane (Table 3.3). For the cases of phosphate and bicarbonate, this may probably relate to the pH-dependent character of their speciation in water and/or the co-ion (proton) exclusion from the anion-exchange membrane, resulting in a higher pH inside the membrane compared to the bulk solution pH, thus making impossible a correct estimation of the actual transport driving force defined by equation 3.1 for these anions [19].

In the case of SO_4^{2-}, the mechanistic model inaccuracy cannot be attributed to a particular set of conditions (Figure 3.4c). The SO_4^{2-} mechanistic model prediction mismatch is more significant in the initial phase of each experiment since the mechanistic transport model is applicable under steady-state conditions. This behaviour is not so evident in the NO_3^- and ClO_4^- flux prediction, most probably since the membrane permeability to these anions are about 4 orders of magnitude higher than that of SO_4^{2-} and, consequently, steady-state transport conditions for these anions are much more rapidly established.

Table 3.3: Comparison of different models for prediction of the flux of target anions for the validation set (RMSEP: Root-mean-square-error-of-prediction; TNP: Total number of parameters)

Flux	Model	R^2	RMSEP	TNP	χ^2
$J(NO_3^-)$	Mechanistic	0.80	0.040	1	2091
	Parallel hybrid	0.97	0.012	16	194
	MOE	0.98	0.010	1+14*	139
$J(ClO_4^-)$	Mechanistic	0.95	0.121	1	1228
	Parallel hybrid	0.98	0.057	11	266
	MOE	0.99	0.044	1+16	158
$J(H_2PO_4^-)$	Mechanistic	0.11	0.052	1	674255
	Parallel hybrid	0.02	0.120	22	3623418
	MOE	0.69	0.002	1+8	1206
$J(HPO_4^{2-})$	Mechanistic	0.08	0.047	1	564190
	Parallel hybrid	0.04	0.027	18	181185
	MOE	0.60	0.002	1+7	571
$J(SO_4^{2-})$	Mechanistic	0.25	0.028	1	852
	Parallel hybrid	0.77	0.015	9	250
	MOE	0.84	0.012	1+11	175
$J(HCO_3^-)$	Mechanistic	0.52	0.019	1	878
	Parallel hybrid	0.93	0.007	8	138
	MOE	0.94	0.007	1+3	115

* The MOE structure has 53 estimated parameters (1 from mechanistic model, 14 from the PLS model and 38 from the gating system), but only parameters from the mechanistic and from the PLS model are involved in the input-output regression.

3.4.2. Parallel hybrid model development and assessment

A parallel hybrid model was developed as illustrated in Figure 3.2a. With this structure, the mechanistic and the PLS models outputs were combined in a cooperative way allowing the PLS model to rectify the mechanistic model prediction. Therefore, the deviations of the mechanistic model prediction from the experimental flux data were subjected to a PLS regression analysis in order to establish linear correlations between process informative variables (inputs) and model residuals (target output). In this parallel structure, the PLS model was used to extract information from the mechanistic model residuals.

Table 3.3 compiles the results obtained in terms of goodness of fit for this parallel structure. As can be observed, a clear improvement was obtained with the PLS model, compensating the mechanistic model inaccuracies. Considering that the PLS regression analysis organizes the data into latent variables, a dimensional reduction was observed from initially a 24-dimensional co-ordinate system to a 7-dimensional one (in the case of the HCO_3^- flux modelling). Moreover, since a calibration selection of the informative predictors was performed in the model, the number of model inputs (latent variables) decreased. The selected inputs are indicated in Section 3.4.5.

The root-mean-square-error-of-prediction (RMSEP) is acceptable compared with the experimental standard deviation, except for the case of phosphate (σ=0.001), for which the hybrid model shows a clear deterioration of its prediction capacity. In this particular case, since the hybrid model is more inaccurate than the mechanistic model alone, the residuals used for the PLS calibration obviously included not only process information but also variance introduced by the mechanistic model error. Consequently, the resulting PLS was not able to find a correct correlation between the IEMB operating data and the mechanistic model residuals and the prediction results became unsatisfactory.

On the other hand, the value of χ^2 obtained for the hybrid model is a clear indication of the improvement of the flux prediction compared to the mechanistic model. The value indicated in Table 3.3 corresponds to the sum of χ^2 for all observations and hence for the model to be considered statistically significant the value should be below the tabulated one at 95% confidence. The χ^2 calculation allowed for concluding that the hybrid model can be considered statistically accurate, since it compares its sum of squares with the experimental standard deviation. Considering the number of observations for the validation set, and the number of parameters, the tabulated value varies between 251 and 266, for n-p degrees of freedom [45], where n is the number of observations and p is the number of parameters. The total number of parameters of this hybrid model corresponds to the sum of the parameters from the two models,

one from the mechanistic model (the P_m parameter) and the number of latent variables selected by cross-validation in the PLS model calibration.

Although, the developed hybrid model improved the prediction capacity, it is rather sensitive to a possible mechanistic model discrepancy. When the mechanistic model is inappropriate for prediction (as in the case of phosphate) the parallel hybrid model is also inappropriate. In such situations, the PLS model captures not only the underlying mechanisms from the process data but also the variance introduced by the mechanistic model. In such cases, a different type of hybrid structure needs to be developed.

3.4.3. "Mixture of experts" development and characterization

The mixture of experts (MOE) structure is a distinct modelling approach since, contrary to the previous parallel hybrid approach, the mechanistic and the PLS model have a competitive contribution. In this hybrid approach, the PLS model is weighted. A different contribution of each expert (the mechanistic or the PLS model) is considered in each observation. In the MOE, the PLS model was calibrated to fit target counter-ion flux values across the membrane and not their residuals, as in the case of the parallel hybrid model. Therefore, two independent models for flux prediction are available: a mechanistic and a PLS model and a gating system mediates and weights the contribution of these two experts.

This hierarchical structure combines the best of each model in order to allocate the degree of contribution to capture from each model. It combines linear functions for non-linear regression problems using a gating system, referred to as a "generalized linear" network [28]. The gating system used in the present study was based on a softmax function (equation 3.3) that can be inferred as providing a "soft" division of the input space. This function was calibrated (with the training set of data) in order to maximize the MOE final prediction. Therefore, the analysis of each input weight can be a clear indication of its contribution to each expert. For instance, when modelling the ClO_4^- flux across the membrane, perchlorate concentration in the polluted water is the input with the highest contribution to the gating equation (g_1).

Figure 3.5 illustrates the value of g_1 for the estimation of the fluxes of NO_3^-, ClO_4^- and SO_4^{2-} in all experiments performed. When g_1 is equal to 1, the target counter-ion flux prediction is totally (or 100 %) obtained by the mechanistic model. In Figure 3.5, the mechanistic model residuals are also represented in order to facilitate the identification of the experimental conditions, under which the mechanistic model failed (as discussed in Section 3.4.1).

In the NO_3^- flux prediction, the mechanistic model contribution is insignificant in almost all experiments (Figure 3.5a). Except for the case of experiment 7, the flux prediction is mainly obtained by the PLS model alone (g_1=0). This is a clear indication of the better capacity of the PLS model to predict the NO_3^- flux across the membrane. Furthermore, despite the fact that in experiment 7 the NO_3^- flux was mainly described by the mechanistic model, the MOE structure improved this counterion flux prediction when compared with the parallel hybrid model and also with the PLS model alone (RMSEP=0.012) [19].

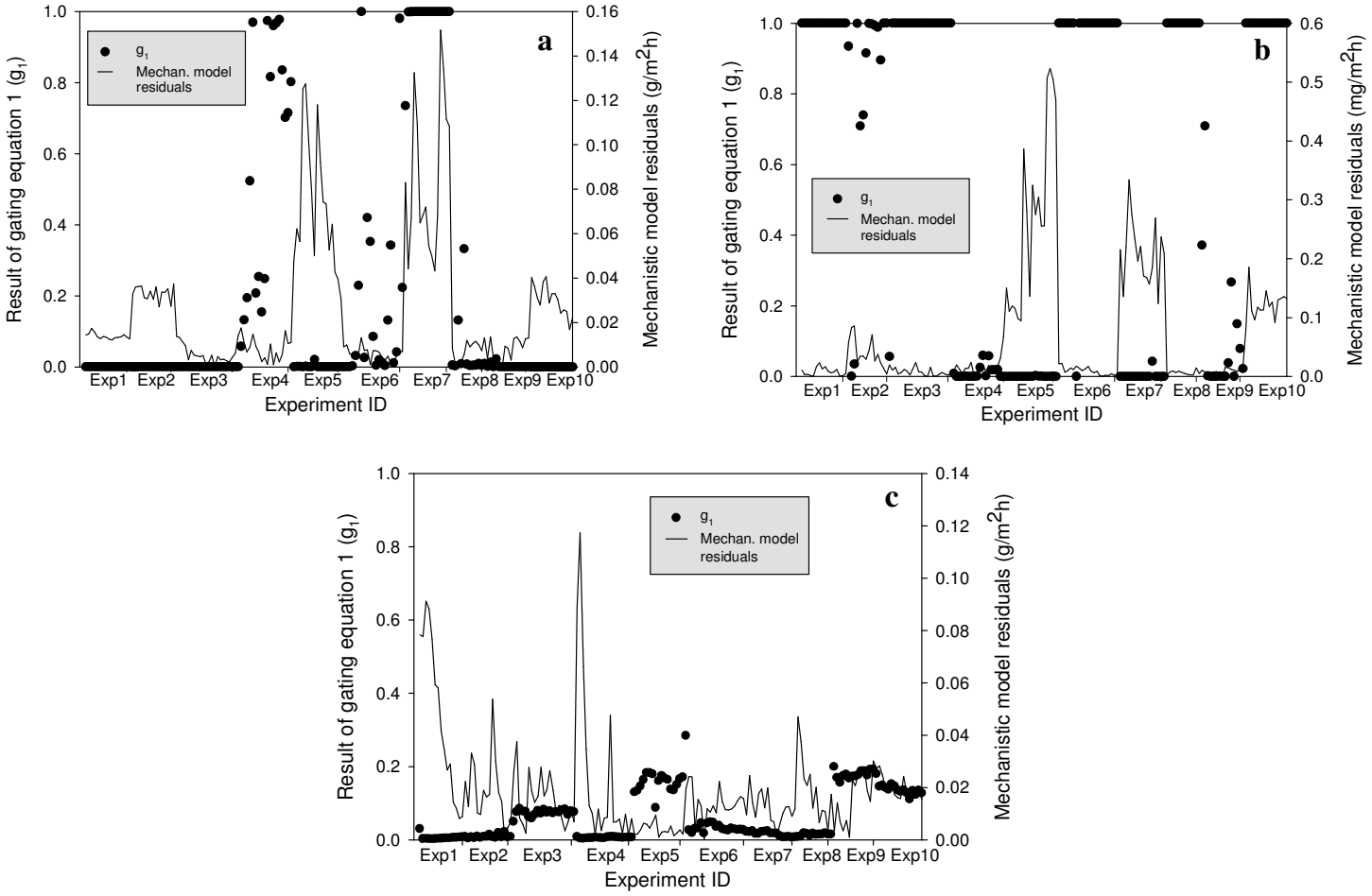

Figure 3.5: Mechanistic model contribution for the MOE structure (g_1) and mechanistic model residuals for NO_3^- (a), ClO_4^- (b) and SO_4^{2-} flux prediction (c).

In respect to the ClO_4^- flux, the experiments that were not captured by the mechanistic model were mainly described by the PLS model. The 100 % mechanistic model contribution to the ClO_4^- flux prediction in the remaining experiments improves the final MOE modelling prediction since the mechanistic model deviations in these experiments are minimal (see Figure 3.4 for comparison). This is not observed for the NO_3^- flux prediction since a considerable

mechanistic model residual is detected in all experiments. Since the mechanistic model was developed for transport of trace counter-ions, it is not surprising that ClO_4^-, which was present in the μg/L concentration range, is the anion that most closely obeys to this condition. The other target counter-ions were all present in the mg/L concentration range and, therefore, higher deviations of their fluxes from the mechanistic model predictions were observed.

In the case of SO_4^{2-} flux, it was not possible to identify specific conditions under which the mechanistic transport model flux prediction is not accurate. As can be observed in Figure 3.5c, the mechanistic model contribution to the global output prediction was at the maximum 20 %. Therefore, the PLS model had the major contribution in the final model since it was able to describe more accurately the SO_4^{2-} flux (R^2 of 0.83, as indicating in Table 2.4 in Chapter 2). Thereby, the PLS model captured the underlying process behaviour directly from process operational data and the balanced combination with the mechanistic model allowed for obtaining a more accurate SO_4^{2-} flux prediction since all available sources of knowledge were incorporated.

3.4.4. Selection of an appropriate hybrid model structure

Different criteria were used for the analysis of the prediction power in order to compare the models (Table 3.3). The MOE proved to be the best model since R^2, RMSEP and χ^2 were improved in comparison with either mechanistic or parallel hybrid models. Figure 3.6 compares the predicted fluxes plotted against the experimental flux values for all counter-ions studied. The dashed line represents an ideal model prediction with a 100 % correlation between the experimental and the estimated flux value. As can be seen, significant improvement is obtained through the MOE when comparing with the mechanistic and the parallel hybrid model prediction. Besides an improved R^2 value, a more accurate model is obtained since the slope of the straight line between experimental and simulated models is closer to 1 for the MOE.

However, even in the MOE, the $H_2PO_4^-$ and HPO_4^{2-} flux predictions were not implemented accurately (χ^2 not significant at the 95% confidence level), indicating that the variables considered were not sufficient to describe phosphate transport across the membrane. As already discussed, the phosphate flux prediction can be more complex due to the pH-dependent speciation of the phosphorus-containing species. Due to co-ion (cation in this case) exclusion by the anion exchange membrane, the measured bulk pH differs from the pH inside the membrane that is not measurable experimentally and, therefore, cannot be used as an operating variable. Nevertheless, the model obtained is a clear improvement compared to the mechanistic model.

For the SO_4^{2-} flux prediction, an increase in the model residuals was detected for values higher than 0.1 g/(m^2h). These values correspond to the initial phase of experiments 1 and 7. Despite the improvement of the prediction obtained with the MOE for this particular situation, a deviation from the experimental SO_4^{2-} flux was found (see Figure 3.6). Most probably, the PLS model was not able to predict these experimental results since they corresponded to only 6 % of all data used for calibration. Under these circumstances, the PLS model did not have enough variance to describe these situations. In any case, an improvement in prediction was obtained when using the MOE structure for fluxes above 0.10 g/m^2h.

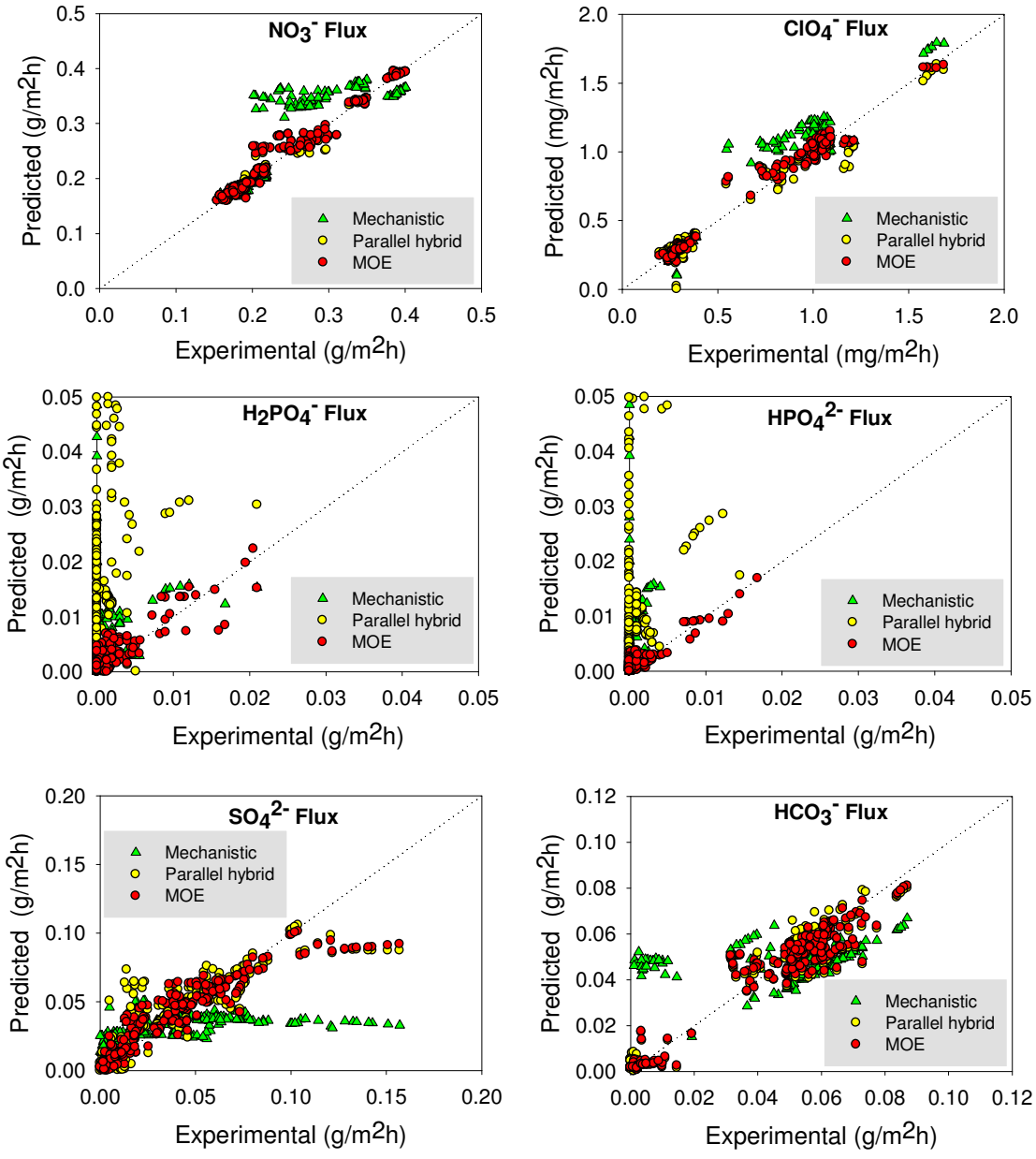

Figure 3.6: Predicted versus experimental flux values for the mechanistic transport model (green triangles), parallel hybrid model (yellow circles) and MOE model (red circles).

3.4.5. Identification of critical process variables not included in the mechanistic model

The use of hybrid models can be helpful not only to increase the model predictive power but also to determine key parameters of a given process. This information can be useful for planning future experiments and for improving mechanistic formulations by identifying the main process variables. Since the PLS model in the parallel hybrid structure was calibrated with the mechanistic transport model residuals, the analysis of the most contributing predictors to that PLS model is an indication of the main variables not accounted for in the mechanistic model.

Since the PLS is a linear model, the regression coefficients can be quantified as the contribution of each predictor to the model. The results, illustrated in Figure 3.7, represent the normalized regression coefficients of the predictors and their respective degree of uncertainty. The regression coefficients are constants in the PLS linear equation that represent the change in the predicted variable (y) as a function of a change in the predictor (x) value. A predictor is considered to be important if its absolute regression coefficient is relatively high and its uncertainty value is as small as possible. The confidence intervals were obtained by the Jackknife resampling technique [39].

The results obtained suggest that the main missing contribution comes from the biocompartment related parameters. This appears logical since the mechanistic transport model cannot predict situations in which the biological reactions kinetics are the limiting step.

In the NO_3^- flux prediction, the major contribution comes from the chloride concentration in the biocompartment. For nitrate, the main deviations of the mechanistic transport model predictions are related with a low chloride concentration in the biocompartment, thus violating the model assumption of chloride as the major bulk counter-ion present in this compartment. Additionally, the hydraulic retention time in the biocompartment (HRT) was also found to have a considerable contribution. This parameter inherently contains the Cl^- effect since its concentration in the biofeed was adjusted to the different HRT in order to maintain the same mass load. Therefore, in the experiments performed at a HRT equal to 10 days, two times higher concentration of Cl^- was used in the biofeed. The contributions of the remaining biocompartment-related parameters are less important for the nitrate transport model.

On contrary, the most important descriptors not accounted for by the mechanistic model in the case of ClO_4^- flux prediction were parameters related with the biological conditions, especially the ammonia concentration (used as nitrogen source) which, in some experiments, became limiting. This limitation was not observed in the NO_3^- bioreduction since NO_3^- can be used as the N source [46]. In the ClO_4^- anion flux prediction, the Cl^- concentration contribution is not as evident as in the NO_3^- model, since ClO_4^- is a trace counter-ion and the driving force for its

transport to the biocompartment is much less sensitive to the Cl^- concentration in this compartment.

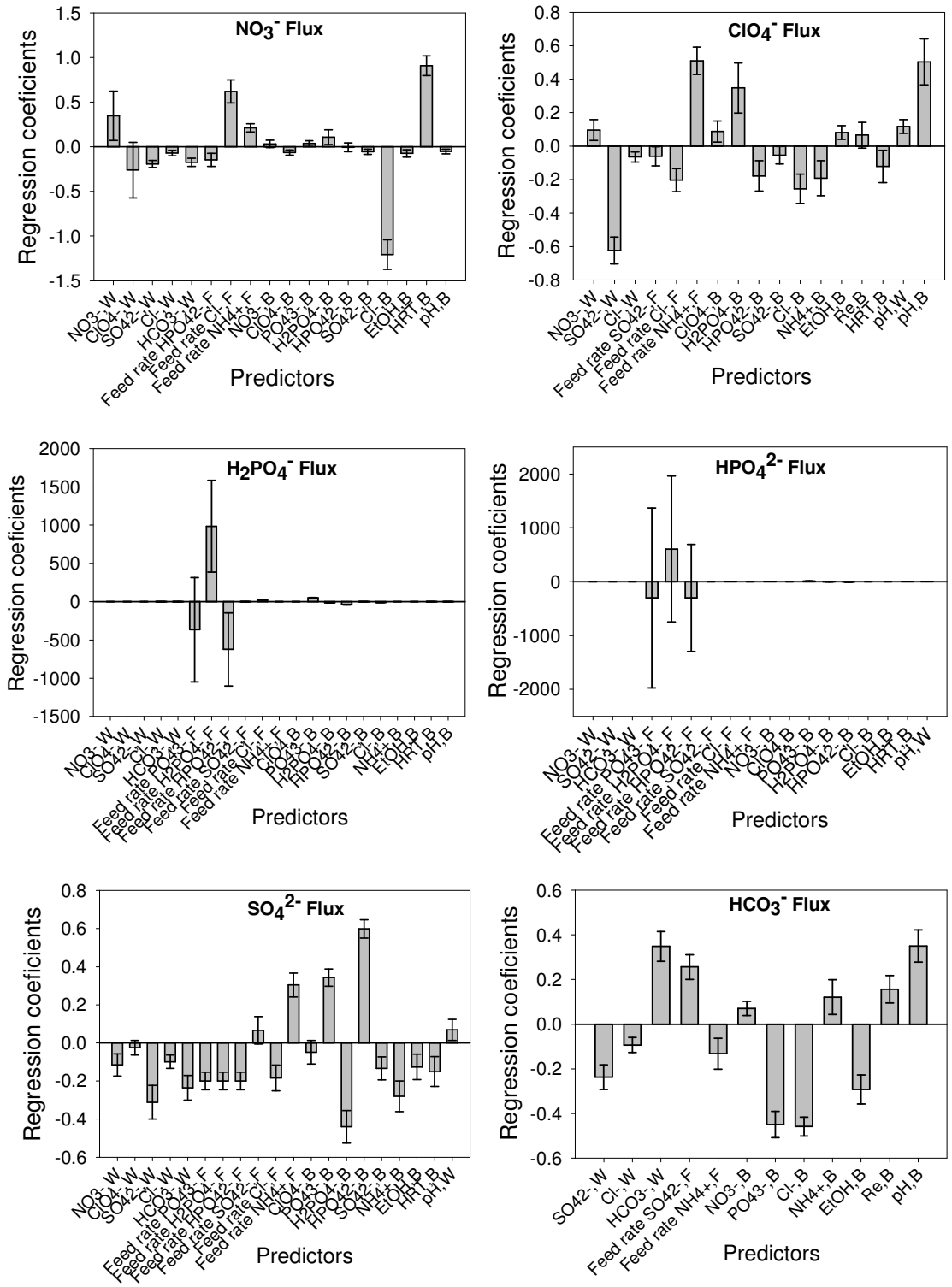

Figure 3.7: PLS regression coefficients in the hybrid model (W: polluted water stream; F: biofeed; B: biocompartment).

The $H_2PO_4^-$ content in the biocompartment and SO_4^{2-} concentration in the polluted water stream were also found to have an important contribution to the PLS model for predicting the ClO_4^- flux across the membrane. Their contributions are not taken into account in the mechanistic model since the driving force term (the nominator of equation 3.1) is calculated considering chloride as the only driving counter-ion. The opposite signs of $H_2PO_4^-$ and SO_4^{2-} regression coefficients is linked to their opposite transport directions through the membrane. Since $H_2PO_4^-$ was initially present only in the biocompartment, it was transported to the water compartment under some of the conditions tested.

The PLS regression coefficient values in the hybrid model for predicting $H_2PO_4^-$ and HPO_4^{2-} membrane fluxes seem to be affected only by the respective concentrations. The mechanistic model was unable to describe correctly the membrane fluxes of phosphate species since their transport was affected by the difference between the pH inside the membrane and the pH values of the two contacting bulk solutions. Given the fact that the PLS model in a parallel hybrid structure was used to correct the mechanistic model residuals, the regression coefficients obtained indicate that the PLS model was also not able to extract valid information from the process data if using such type of a hybrid structure.

In the case of SO_4^{2-}, a considerable amount of information from the process needs to be taken into account by the mechanistic transport model, especially the phosphate species concentration in the biological compartment. These species can be used as driving counter-ions, especially when the chloride concentration in the biocompartment is low. For instance, in experiment 7, in order to maintain the same sulphate flux to the biocompartment, the total phosphorus flux increased 10 times in order to compensate the decrease in the Cl^- flux to the water compartment. This effect was captured by the PLS model and the contribution of the phosphate species to the sulphate flux was emphasized (see Figure 3.7).

The HCO_3^- flux prediction by the mechanistic model requires the incorporation of biocompartment-related inputs as well as information about concentrations of other anions in the polluted water stream. The contribution of biocompartment-related parameters concerned mainly anions that can potentially be used as driving counter-ions for its transport (e.g. Cl^-, $H_2PO_4^-$ and HPO_4^{2-}). The pH in the biocompartment has also an important contribution to the PLS model because it influences the speciation of this anion (HCO_3^- *versus* CO_3^{2-}) for the pH range used in the present study.

3.5. Conclusions

The use of hybrid mechanistic-statistical modelling to describe the counterion transport in an ion-exchange membrane-supported biofilm reactor proved to be adequate for expanding the mechanistic model to situations beyond its building assumptions, such as biological reaction limiting situations.

The statistical analysis of the mechanistic model residuals suggested that the main missing mechanistic information came from biocompartment-related parameters.

The parallel hybrid model allowed for covering a number of process situations outside the domain of applicability of the mechanistic model. In these cases, the PLS model was able to capture the information missing in the mechanistic model from the process operating data. However, for some counterions (e.g., phosphate) the prediction was unsatisfactory, since the mechanistic model error variance was included in the PLS calibration. On the other hand, in the mixture-of-experts (MOE) structure, this limitation was avoided since both models predict the flux of a target counterion in a competitive way. Thereby, this modelling strategy proved to be a better choice, which could be successfully used as a process predictive and optimization tool.

The results obtained can be also applied for a straightforward biomedium design. In that way, the transport of certain undesirable counterions to the water compartment can be either avoided or minimised.

3.6. References

1 Casey, E., Glennon, B., Hamer, G., 1999. Review of membranes aerated biofilm reactors. Resour. Conserv. Recy. 27: 203-215.

2 Freitas dos Santos, L.M, Livingston, A.G., 1995. Novel membrane bioreactor for detoxification of VOC wastewaters: biodegradation of 1,2-dichloroethane. Water Res. 29(1): 179-194.

3 Wolf, G., Almeida, J.S., Reis, M.A.M., Crespo, J.G., 2005. Non-mechanistic modelling of complex biofilm reactors and the role of process operation history. J. Biotechnol. 117: 367-383.

4 Shanahan, J.W., Semmens, M.J., 2006. Influence of a nitrifying biofilm on local oxygen

fluxes across a micro-porous flat sheet membrane. J. Membr. Sci. 277: 65-74.

5 Rittmann, B.E., 2007. The membrane biofilm reactor is a versatile platform for water and wastewater treatment. Environ. Eng. Res. 12(4): 157-175.

6 Bohn, H., 1992. Consider biofiltration for decontaminating gases. Chem. Eng. Prog. 88: 34–40.

7 Pavasant, P., Freitas dos Santos, L.M., Pistikopoulos, E.N., Livingston, A.G., 1996. Prediction of optimal biofilm thickness for membrane-attached biofilms growing in an extractive membrane bioreactor. Biotechnol. Bioeng. 52: 373-386.

8 Juang, R.S., Tsai, S.Y., 2006. Role of membrane-attached biofilm in the biodegradation of phenol and sodium salicylate in microporous membrane bioreactors. J. Membr. Sci. 282: 484-492.

9 Nicolella, C., Pavasant, P., Livingston, A.G., 2000. Substrate counterdiffusion and reaction in membrane-attached biofilms: mathematical analysis of rate limiting mechanisms. Chem. Eng. Sci. 55: 1385-1398.

10 Ye, H., Das, D.B., Triffitt, J.T., Cui, Z., 2006. Modelling nutrient transport in hollow fibre membrane bioreactors for growing three-dimensional bone tissue. J. Membr. Sci. 272: 169-178.

11 Motlagh, A.R.A., Voller, V.R., Semmens, M. J., 2006. Advective flow through membrane-aerated biofilms modelling results. J. Membr. Sci. 273: 143-151.

12 Syron, E., Kelly, H., Casey, E., 2009. Studies on the effect of concentration of a self-inhibitory substrate on biofilm reaction rate under co-diffusion and counter-diffusion configurations, J. Membr. Sci. 335: 76-82.

13 Crespo, J.G., Reis, M.A.M., Treatment of aqueous media containing electrically charged compounds. WO Patent, WO 01/40118 A1.

14 Matos, C.T., Velizarov, S., Crespo, J.G., Reis, M.A., 2006. Simultaneous removal of perchlorate and nitrate from drinking water using the ion exchange membrane bioreactor concept. Water Res. 40: 231-240.

15 Velizarov, S., Reis, M.A., Crespo, J.G., 2002. Ion Exchange membrane Bioreactor for selective removal of nitrate from drinking water: control of ion fluxes and process performance. Biotechnol. Progr. 18: 296-302.

16 Velizarov, S., Rodrigues, C.M., Reis, M.A., Crespo, J.G., 2000. Mechanism of charged pollutants removal in an ion exchange membrane bioreactor: drinking water denitrification. Biotechnol. Bioeng. 71: 245-254.

17 Velizarov, S., Reis, M.A., Crespo, J.G., 2003. Removal of trace mono-valent inorganic pollutants in an ion exchange membrane bioreactor: analysis of transport rate in a denitrification process. J. Membr. Sci. 217: 269-284.

18 Blaedel, W.J., Haupert, T.J., Evenson, M.A., 1969. Mechanism of trace counterion transport through ion-exchange membranes, Anal. Chem. 41(4): 583-590.

19 Ricardo, A.R., Oliveira, R., Velizarov, S., Reis, M.A.M., Crespo, J.G., 2011. Multivariate statistical modelling of mass transfer in a membrane-supported biofilm reactor. Process Biochem. 46 (10): 1981-1992.

20 Duarte, B.P.M., Saraiva, P.M., 2003. Hybrid models combining mechanistic models with adaptative regression splines and local stepwise regression. Ind. Eng. Chem. Res. 42: 99-107.

21 Thompson, M.L., Kramer, M.A., 1994. Modeling chemical processes using prior knowledge and neural networks. AIChE J. 40(8): 1328-1340.

22 Pismenskaya, N., Laktionov, E., Nikonenko, V., Attar, A.E., Auclair, B., Pourcelly, G., 2001. Dependence of composition of anion-exchange membranes and their electrical conductivity on concentration of sodium salts of carbonic and phosphoric acids, J. Membr. Sci. 181: 185-197.

23 Matos, C.T., Velizarov, S., Crespo, J.G., Reis, M.A., 2008. Removal of mono-valent oxyanions from water in an ion exchange membrane bioreactor: Influence of membrane permselectivity. Water Res. 42(6-7): 1785-1795.

24 Montgomery, D.C., 2001. Design and Analysis of Experiments. 5th edition, John Wiley & Sons, Inc., New York, p. 684.

25 Mulder, M., 1996. Basic principles of membrane technology. 2nd edition, Kluwer Academic Publishers, Dordrecht, p. 564.

26 Peres, J., Oliveira, R., Feyo de Azevedo, S., 2001. Knowledge based modular networks for process modelling and control. Comput. Chem. Eng. 25: 783-791.

27 Jacobs, R.A., Jordan, M.I., Barto, A.G., 1991. Task decomposition through competition in a modular connectionist architecture: the what and where vision tasks. Cognitive Sci. 15: 219-250.

28 Jordan, M.I., Jacobs, R.A., 1994. Hierarchical Mixtures of Experts and the EM Algorithm, Neural Comput. 6: 181-214.

29 Wold, S., Sjöström, M., Eriksson, L., 2001. PLS-regression: a basic tool of chemometrics. Chemom. Intell. Lab. Syst. 58: 109-130.

30 Ryan, T. P., 1997. Modern Regression Methods. John Wiley & Sons, Inc., New York, p. 515.

31 Bentz, Y., Merunka, D., 2000. Neural Networks and the Multinomial Logit for Brand Choice Modelling: a Hybrid Approach. J. Forecasting 19: 177-200.

32 Matlab 2006b, 2006. The Mathworks, Inc., Natick, MA, USA.

33 Andersson, C.A., Bro, R., 2000. The N-way toolbox for MATLAB. Chemom. Intell. Lab.

Syst. 52: 1-4.

34 Krzanowski, W.J., Kline, P., 1995. Cross-Validation for choosing the number of important components in principal components analysis. Multivar. Behav. Res. 30(2): 149-165.

35 Boggia, R., Forina, M., Fossa, P., Mosti, L., 1997. Chemometric study and validation strategies in the structure-activity relationships of new cardiotonic agents. Quant. Struct-Act. Rel. 16: 201-213.

36 Forina, M., Casolino, C., Millan, C.P., 1999. Iterative predictor weighting (IPW) PLS: a technique for the elimination of useless predictors in regression problems. J. Chemometr. 13: 165-184.

37 Centner, Z., Massart, D., Noord, O.E., Jong, S., Vandeginste, B.M., Sterna, C., 1996. Elimination of uniformative variables for multivariate calibration. Anal. Chem. 68: 3851-3858.

38 Forina, M., Lanteri, S., Cerrato Oliveros, M.C., Millan, C.P., 2004. Selection of useful predictors in multivariate calibration. Anal. Bioanal. Chem. 380: 397-418.

39 Duchesne, C., MacGregor, J.F., 2001. Jackknife and bootstrap methods in the identification of dynamic models. J. Process Contr. 11: 553-564.

40 Faber, N.M., 2002. Uncertainty estimation for multivariate regression coefficients. Chemom. Intell. Lab. Syst. 64: 169-179.

41 Quinn, G.P, Keough, M.J., 2002. Experimental Design and Data Analysis for Biologists. 5th edition, Cambridge University Press, Cambridge, p. 537.

42 Spiess, A.D., Neumeyer, N., 2010. An evaluation of R^2 as an inadequate measure for nonlinear models in pharmacological and biochemical research: a Monte Carlo approach. BMC Pharmocol. 10(6).

43 US Environmental Protection Agency (USEPA), 2010. National primary drinking water regulations; announcement of the results of EPA's review of existing drinking water standards and request for public comment and/or information on related issues. Federal Register. 75(59): 15500-15572.

44 US Environmental Protection Agency (USEPA), 2011. Drinking water: regulatory determination on perchlorate. Federal Register. 76(29): 7762-7767.

45 Morrison, D.F., 1990. Multivariate Statistical Methods. 3rd edition, McGraw-Hill, New York, p. 495.

46 Gerardi, M.H., 2002. Nitrification and Denitrification in the Activated Sludge Process. John Wiley & Sons, Inc., New York, p. 193.

Chapter

4

Kinetics of nitrate and perchlorate removal and biofilm stratification in ion exchange membrane bioreactor

Summary

The biological degradation of nitrate and perchlorate was investigated in an ion exchange membrane bioreactor (IEMB) using a mixed anoxic microbial culture and ethanol as the carbon source. In this process, a membrane-supported biofilm reduces nitrate and perchlorate delivered through an anion exchange membrane from a polluted water stream, containing 60 mg/L of NO_3^- and 100 µg/L of ClO_4^-. Under ammonia limiting conditions, the perchlorate reduction rate decreased by 10 %, whereas the nitrate reduction rate was unaffected. Though nitrate and perchlorate accumulated in the bioreactor, their concentrations in the treated water (2.8 ± 0.5 mg/L of NO_3^- and 7.0 ± 0.8 µg/L of ClO_4^-, respectively) were always below the drinking water regulatory levels, due to Donnan dialysis control of the ionic transport in the system.

Kinetic parameters determined for the mixed microbial culture in suspension showed that the nitrate reduction rate was 35 times higher than the maximum perchlorate reduction rate. It was found that perchlorate reduction was inhibited by nitrate, since after nitrate depletion perchlorate reduction rate increased by 77 %. The biofilm

developed in the IEMB was cryosectioned and the microbial population was analyzed by fluorescence *in situ* hybridization (FISH). The results obtained seem to indicate that the kinetic advantage of nitrate reduction favored accumulation of denitrifiers near the membrane, whereas per(chlorate) reducing bacteria were mainly positioned at the biofilm outer surface, contacting the biomedium. As a consequence of the biofilm stratification, the reduction of perchlorate and nitrate occur sequentially in space allowing for the removal of both ions in the IEMB.

4.1. Introduction

Perchlorate (ClO_4^-) contamination of surface and ground water is a relevant problem due to its negative impact on human health, particularly on the thyroid gland [1]. The main source of contamination is military facilities, where synthetically manufactured ammonium perchlorate was used as a rocket fuel [2]. The US Environmental Protection Agency (EPA) recommends a maximum of 15 µg/L of ClO_4^- in drinking water sources [3].

The most common technology for perchlorate removal from drinking water is ion exchange [2]. However, the presence of other anions in higher concentrations, e.g., nitrate and sulphate, can reduce the resin binding capacity for perchlorate. Moreover, disposal and/or treatment requirements of the concentrated brine from resin regeneration should be considered.

Biological degradation of perchlorate is a promising treatment alternative to ion exchange, since perchlorate can easily be metabolized by (per)chlorate-reducing bacteria [4]. These organisms, in anoxic conditions, use perchlorate (ClO_4^-) or chlorate (ClO_3^-) as electron acceptors in a reductive pathway with two specialized enzymes: (per)chlorate reductase and chlorite (ClO_2^-) dismutase [4]. The suggested sequence pathway for the first enzyme is $ClO_4^- \rightarrow ClO_3^- \rightarrow ClO_2^-$. Thereafter, chlorite dismutase transforms ClO_2^- into Cl^- and O_2. The biosynthesis of these enzymes was found to be regulated by the presence of perchlorate, oxygen and nitrate [5].

Nitrate (NO_3^-) is often found in water as a co-contaminant of perchlorate since nitrogen is the major element in the production of explosives and, usually, it is present in concentrations 2-5 orders of magnitude higher than those for perchlorate [6]. Nitrate, which is a well-known toxic oxy-anion, is regulated to a drinking water limit of 45 mg/L by the US EPA [7] and 50 mg/L by the European Union [8].

Several biological processes have been applied for bioreduction of nitrate and perchlorate, simultaneously present in drinking water sources and some of them have been already implemented in the field [6, 9-12]. However, the resulting water requires further treatment due to its secondary contamination with microorganisms, culture media components and/or metabolic by-products. Moreover, application of biological treatment directly to drinking water systems is usually not well accepted by the general public [2].

The use of hybrid technologies has shown benefits, especially if biological treatment is combined with membrane processes [13, 14]. In these technologies, a substrate (electron donor or acceptor) diffuses through the membrane and is consumed by an active biofilm formed at the membrane surface contacting the biomedium.

The ion exchange membrane bioreactor (IEMB) is able to physically separate the biomedium from the treated water stream, thus avoiding its secondary contamination [14]. Nitrate and perchlorate, are transported from the water stream through an anion-exchange membrane to a biocompartment, in which they are reduced to innocuous species (nitrogen and chloride, respectively) [15]. During this process, nitrate and perchlorate bioreduction occurs primarily in the biofilm formed at the membrane surface contacting the biocompartment.

In order to optimize the process of simultaneous reduction of these oxy-anions in the IEMB, it is essential to elucidate the effect of nitrate on perchlorate reduction kinetics. The majority of per(chlorate) reducing bacteria identified can use nitrate as an electron acceptor [16]; however, their response vary in the presence of both oxy-anions. Simultaneous as well as sequential reduction, in which perchlorate reduction starts only after depletion of nitrate, has been reported for both pure and mixed microbial cultures [17]. In systems operated with mixed microbial cultures, the identification of the kinetic mechanisms is more difficult, since multiple members of the microbial community can perform denitrification and/or perchlorate reduction. With mixed cultures, Choi and Silverstein observed a simultaneous reduction of the two oxy-anions but with a 30 % decrease in the perchlorate reduction rate in the presence of nitrate in an equimolar concentration [9]. Nevertheless, the presence of nitrate is recommended if the objective is to treat perchlorate in concentrations within the µg/L range, since nitrate can be used as a primary electron acceptor supporting the growth of per(chlorate) reducing bacteria [18].

The main objective of this study is to elucidate the kinetics of nitrate and perchlorate reduction by a mixed microbial culture in the IEMB. Since nitrate was present in the polluted water in a much higher concentration than that of perchlorate, the IEMB process efficiency was mainly limited by the transport of perchlorate and its bio-reduction kinetics. In such situations, perchlorate may accumulate in the biocompartment of the IEMB (as observed in Chapter 2 and

3). Several mechanisms can be responsible for this behavior: 1- inhibition of perchlorate reduction by nitrate, resulting in a sequential consumption of the two oxy-anions; 2- higher reduction rate of nitrate than that of perchlorate; 3- biofilm stratification that favors nitrate over perchlorate consumption. Therefore, this study aims at identifying the mechanisms that regulate the perchlorate reduction rate in the IEMB. First, the effect of nitrate presence on the reduction rate of perchlorate was investigated by determining kinetic parameters for nitrate and perchlorate reduction by the mixed microbial culture. Then, the microbial communities present in both suspended and biofilm cultures were examined using fluorescent in situ hybridization (FISH) with oligonucleotide probes specific for major groups of denitrifiers and per(chlorate) reducing bacteria, in order to find out whether biofilm stratification takes place.

4.2. Material and Methods

4.2.1. Microorganisms and culture medium

A mixed microbial culture was used to operate the IEMB for the treatment of water contaminated with nitrate and perchlorate. Initially, the culture was selected from the primary inoculum of a municipal wastewater treatment plant [15]. Prior to inoculation of the IEMB, the culture was grown for one week in an argon-sparged 500-mL reactor with 60 mg/L of NO_3^- and 100 µg/L of ClO_4^-. During this period, ethanol, used as the electron donor and carbon source, was added initially at 1 g/L and supplemented again to the same level when its concentration dropped to 100 mg/L.

In all experiments, except for the ammonia-limited study, the biomedium composition was: 1 g/L of K_2HPO_4, 0.592 g/L of KH_2PO_4, 0.233 g/L of NH_4Cl, 0.1 g/L of $MgSO_4.7H_2O$, 0.56 g/L ethanol and 5.84 g/L of NaCl. The final pH of the biomedium was adjusted to 7.0 with NaOH.

Since the ionic transport across the membrane in the IEMB is governed by Donnan dialysis principles, chloride (in the form of NaCl) was added to the biocompartment, as a “driving” counterion, to enhance the transport of nitrate and perchlorate from the water compartment to the biocompartment. In the batch kinetic experiments, the same concentration (5.84 g/L of NaCl) was used to simulate the salinity conditions of the IEMB biocompartment.

4.2.2. IEMB experimental setup and operation

The IEMB was operated in a single membrane module, in which the water and the biomedium were recirculated in independent channels physically separated by a Neosepta ACS anion-exchange membrane (Tokuyama Soda, Japan) as illustrated in Figure 4.1. The exposed membrane area was equal to 34.5 cm^2. The water to be treated was recirculated at 1620 mL/min (Reynolds number of 3000 and linear fluid velocity of 0.6 m/s) and polluted water was fed continuously to the water compartment at a flow rate of 0.18 mL/min to guarantee a water flow rate to membrane area ratio of 3.1 L/(m^2.h). These conditions corresponded to a water hydraulic retention time of 8.3 h. Synthetic polluted water was prepared with tap water supplemented with 60 mg/L of nitrate and 100 µg/L of perchlorate, added as their sodium salts. The biocompartment channel was connected to a stirred vessel by an external loop, through which the biomedium was also recirculated with a flow rate of 1620 mL/min. Since water compartment and biocompartment have the same dimensions, the same hydrodynamics conditions were established. The anoxic conditions in the biocompartment were maintained by continuously sparging argon through the head-space of the stirred vessel. The biocompartment was fed with nutrient solution (biofeed), with composition described above, supplemented with ethanol used as a carbon source and electron donor. In the experiment operated under ammonia limiting conditions, the concentration of NH_4Cl in the biofeed was set to 0.04 g/L. The biofeed was fed at 0.8 mL/min, thus providing a biomedium hydraulic retention time of 5.84 days.

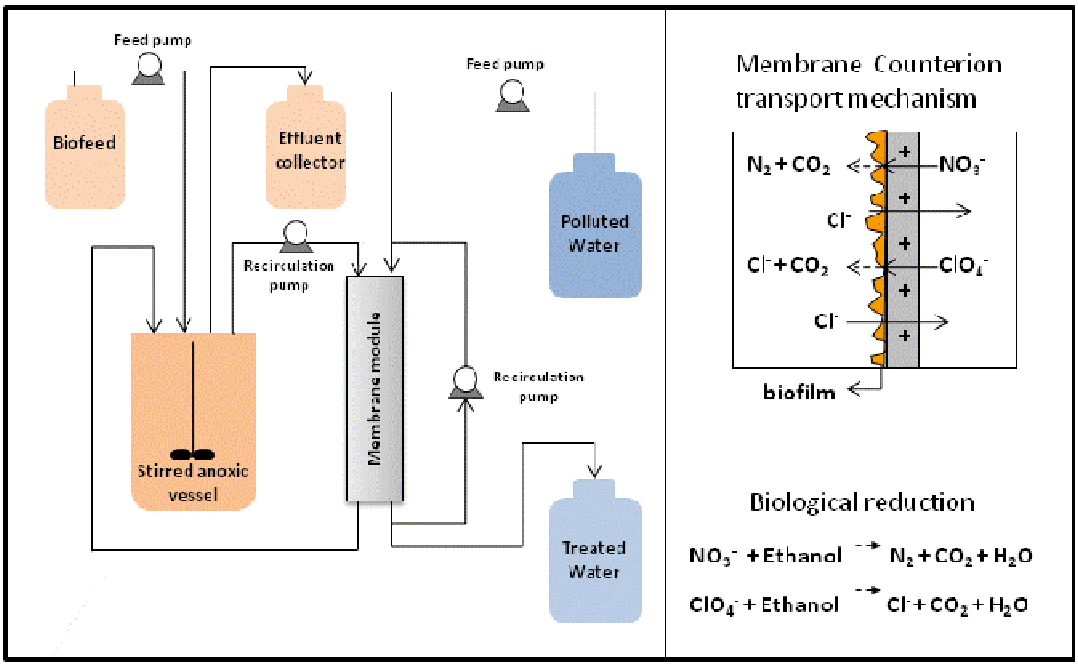

Figure 4.1: Schematic diagram of the experimental set-up and counterion transport mechanism in the ion-exchange membrane bioreactor (IEMB). The membrane has positively charged fixed functional sites allowing for transport of anions.

All experiments were performed at 23±1 ºC in an air-conditioned laboratory.

4.2.3. Nitrate and perchlorate bioreduction of suspended-cell cultures

Nine batch tests were performed using the enriched suspended cells culture (as described in 4.2.1) that was used to inoculate the IEMB. The initial nitrate concentration was kept at 60 mg/L in all tests, whereas the initial perchlorate concentration was varied from 0.4 to 25.5 mg/L. To avoid progressive culture enrichment in per(chlorate) reducing bacteria due to the increment in perchlorate concentration, the experiments were performed randomly.

The culture, stored at 4ºC, was acclimatized for 16 h with 60 mg/L of NO_3^-, 1 mg/L of ClO_4^- and 1 g/L of ethanol in a 500 mL batch reactor fed with the nutrient medium described in section 4.2.1. The cells were harvested after 16 h (all nitrate consumed), by centrifugation at 9800 x g for 9 minutes and resuspended in a fresh nutrient medium to the same initial volume (500 mL). The culture medium was sparged with argon for 20 minutes and then NO_3^-, ClO_4^- and ethanol were added. Anoxic conditions were maintained by argon in the reactor head-space. Samples were taken periodically for pH, nitrate, nitrite, perchlorate, ethanol and optical density (OD_{600nm}) measurements. The optical density was measured with a spectrophotometer (Thermo Spectronic, USA) and converted to concentration of volatile suspended solids (VSS) using a 666 mg/L VSS per OD unit conversion factor determined experimentally (results not shown). This conversion factor was determined by a linear regression between OD_{600nm} and VSS concentration data within the linear OD range (OD_{600nm} between 0.06 and 0.24). The concentration of VSS was determined according to standard methods [19].

4.2.4. Determination of kinetic parameters

The reported reduction rates are the maximal reduction rates, determined by linear regression through the points with maximal rate observed which respond to the initial period of the experiment in nitrate reduction and to the period after nitrate depletion for perchlorate reduction rate calculation. The linear regression was estimated with a minimal of 5-6 experimental values. The inclusion of experimental values stopped when reduction rate declined, i.e. when the slope of the regression curve of substrate concentration (e.g., nitrate, perchlorate) *versus* time decreased.

Kinetic parameters for the mixed culture were calculated assuming a competitive inhibition model for nitrate and perchlorate reduction [20]. For estimation of kinetic parameters, all experimental values were considered. A non-linear regression analysis by least-squares was

used to estimate the following parameters: maximum nitrate and perchlorate reduction rates ($q_{n,max}$, $q_{p,max}$), the half-saturation constants for nitrate and perchlorate (K_n, K_p); the biomass yield on nitrate and perchlorate (Y_n, Y_p) and the endogenous decay rate (b). These parameters were estimated by fitting the results of nine experiments performed at different initial perchlorate concentrations while keeping constant the initial nitrate concentration. Computation was performed on Matlab 2006b (The Mathworks, Inc., USA) using a non-linear least-squares function. The confidence intervals (95% confidence level) for the estimated parameters were calculated assuming that the modeling errors are Gaussian distributed and that the variance is unknown.

4.2.5. Fluorescence in situ hybridization (FISH)

Samples from the exponential growth phase of batch tests were taken for hybridization with specific probes covering major groups of denitrifying bacteria and per(chlorate) reducing bacteria probes as well as three relevant subgroups of the Proteobacteria and a more general probe set for all bacteria (EUBmix).

Biofilm samples were taken to characterize the microbial community composition and to identify possible stratification. For the overall composition analysis, a portion of the biofilm was scrapped from the membrane and resuspended in a fresh nutrient medium using a 200 µL pipette tip for sample homogenization. Biofilm samples for population stratification studies were obtained by carefully cutting (with a scalpel) 0.5 cm x 0.5 cm portions of the biofilm attached to the membrane. The samples were placed in a plastic mold with the same dimensions to guarantee biofilm integrity. All samples were fixed with 4% paraformaldehyde [20]. The biofilm was preserved in a tissue-freezing medium OCT™ (Tissue-Tek, Sakura Finetech) as follows: the fixed sample was immersed in 30 % (w/v) sucrose at 4ºC for 7 hours; the sucrose solution was carefully removed and replaced by a new OCT™:sucrose solution with increasing OCT™ concentration: 1:2 for 9 hours; 1:1 for 8 hours and 100% OCT™ for 14 hours. Finally, the biofilm sample was stored at -20ºC inside the plastic mold in 100% OCT™.

FISH analysis was performed according to Amann [21] using the oligonucleotide probes described in Table 4.1. For biofilm structure analysis, the sample preserved in OCT™ was used. The cryroprotected biofilm was sliced by cryosectioning (Leica CM 30505) with 50 µm thickness. Cryosections were mounted on the wells of Teflon-coated slides, dried for at least 2 hours and coated with a 0.5% (w/v) agarose layer. The same FISH procedure was then followed.

The hybridized cell suspension samples were observed using an epifluorescence microscope (Olympus BX51, Japan) using a 100 x oil objective. The stained cells for each probe were

counted and compared with the total bacteria stained with EUBmix probe for a semi-quantitative analysis. In the hybridization with *Alpha-*, *Beta-* and *Gammaproteobacteria* probes, quantification was performed using at least 20 randomly selected microscopic images obtained with a confocal laser scanning microscope-CLSM (Zeiss LSM 510 Meta, Germany) and analyzed through the software Daime [22]. The confocal laser scanning microscope was also used to examine the cryosectioned biofilm sample.

Table 4.1: Oligonucleotide FISH probes employed in this study

Probe Name	Targeted bacteria	Formamide in the hybridization buffer (%)	Reference
EUBmix (EUB338-I, -II, -III)	All *Bacteria*	0-40	[23]
ALF969	*Alphaproteobacteria*	35	[24]
BET42a	*Betaproteobacteria*	35	[23]
GAM42a	*Gammaproteobacteria*	35	[23]
Dechl2	*Dechloromonas*	30	[23]
Soma1035	*Dechlorosomas*	0	[12]
Azo644	*Azoarcus*	30	[23]
THAU832	*Thauera*	30	[23]
G Rb	*Rhodobacter, Roseobacter*	30	[23]
Pae997	*Pseudomonas*	0	[23]
PAR651	*Paracoccus*	40	[23]

4.2.6. Analytical methods

Prior to analysis, all samples were filtered through a 0.22 µm filter to remove cell debris. Nitrate and nitrite concentrations were measured by an ion exchange chromatography system (Dionex, USA) combining an AS9 analytical and AG9 guard column, an anion self-regenerating suppressor ASRS (4 mm) and an ED50 electrochemical detector. The analysis was performed with a 9 mM Na_2CO_3 aqueous solution as a mobile phase at a flow rate of 1 mL/min and at a temperature of 30ºC. The detection limit when injecting a 100 µL sample was 1 mg/L for nitrate and nitrite. Perchlorate concentration was determined in the same system with an AS16 analytical and AG16 guard column, using a 50 mM NaOH aqueous solution as a mobile phase

at 30ºC at a flow rate of 1 mL/min. Samples taken from the IEMB water compartment were injected using a 1000 µL recirculation loop providing a perchlorate detection limit of 2 µg/L. For samples taken from culture medium, the limit of perchlorate detection was 4 µg/L since 500 µL have to be injected in order to avoid the Cl^- peak interference.

Ethanol was quantified by HPLC using an Aminex HPX-87H column (Biorad, USA) with a 0.1N H_2SO_4 aqueous solution as a mobile phase flowing at 0.5 mL/min and at a temperature of 30ºC. Ethanol was detected (detection limit of 1 mg/L) with a differential refractometric detector RI-71 (Merck-Hitachi, Japan). Ammonium was quantified with a gas-sensitive electrode Orion 95-12 (Thermo, USA) with a detection limit of 1 mg/L.

4.3. Results and discussion

4.3.1. IEMB operation under ammonia limitation

In previous IEMB proof-of-concept studies, the content of nutrients in the biofeed was kept in excess in order to avoid possible microbial growth limitations in the biocompartment [15]. In order to optimize the biofeed composition in this study, the IEMB performance was tested at lower ammonia levels. Two experiments were performed: feeding the biocompartment with ammonia at 9 mg/d (the mass flow rate used previously) [15] and at 0.9 mg/d. Concentrations of perchlorate and nitrate in the polluted water were 100 µg/L and 60 mg/L, respectively. Ethanol was always kept above the limiting conditions.

In the IEMB operated with an ammonia feeding rate of 9 mg/d, ammonia was found to accumulate (34.5 ± 3.2 mg/L) in the biocompartment, as illustrated in Figure 4.2. After the first ten days of operation, due to development of a biofilm on the membrane surface contacting the biocompartment, both nitrate and perchlorate were efficiently removed to concentrations in the biocompartment below the corresponding quantification limits of 1 mg/L of nitrate and 2 µg/L of perchlorate.

When the IEMB biocompartment was fed with 0.9 mg/d of ammonia, the ammonia content in the biocompartment decreased rapidly and after about 10 days no residual ammonia concentration was detected. Under these limiting conditions, the rate of nitrate reduction was practically not affected: 26.3 ± 0.4 mg/L·d experimental *versus* 26.4 mg/L·d expected assuming that all nitrate transported through the membrane was biologically reduced. On the other hand,

perchlorate was not completely reduced and, as a consequence, accumulated in the biocompartment up to 48.3 ± 11.8 µg/L (see Figure 4.2). If all the perchlorate transported through the membrane was consumed, a perchlorate reduction rate of 47.9 µg/L·d would have been expected under steady-state operating conditions. However, a perchlorate reduction rate of 43.2 ± 3.7 µg/L·d (corresponding to a 10 ± 2 % decrease compared to the maximal possible rate) was experimentally obtained.

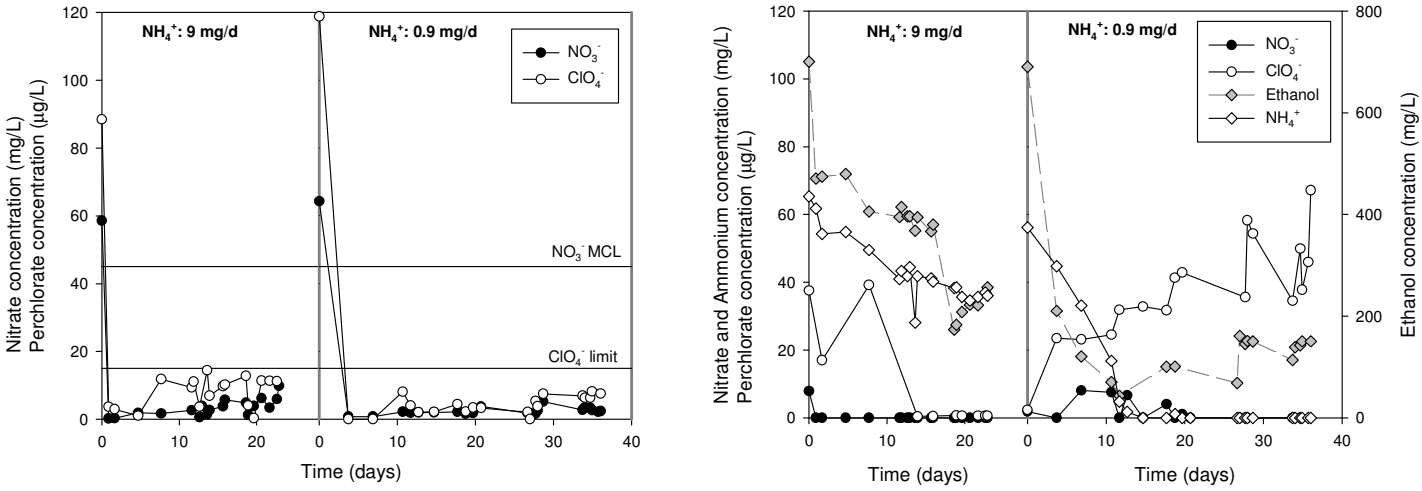

Figure 4.2: IEMB operation at two different ammonia feeding mass flow rates to the biocompartment: water compartment (left) and biocompartment (right). NO_3^- maximum contaminant level (MCL): 45 mg/L [7]; ClO_4^- present regulation: 15 µg/L [3].

It has to be noted however that temporary accumulation of perchlorate in the biocompartment did not affect the quality of the treated water, in which the concentrations of nitrate and perchlorate remained below the EPA guidelines for the entire period of experiment (see Figure 4.2). This is due to the fact that the transport of anions to the biocompartment is governed by the Donnan dialysis principles and is assured by counter transport of chloride from the biocompartment, to the treated water stream. Therefore, if an unexpected disturbance in the ammonia supply occurs the water quality is not affected for at least 30 days.

Nevertheless, it is important to understand the reasons why perchlorate reduction is more affected than nitrate reduction when operating the IEMB under ammonia limitation. A lower decrease on nitrate reduction rate than on perchlorate reduction rate can also be extended to other growth limiting conditions since in a preliminary experiment performed under limiting carbon source (ethanol in this case) addition, perchlorate reduction decreased by 41 ± 13 % while nitrate reduction rate declined only 7 ± 3 % (data not shown). A similar effect was also reported by Choi and Silverstein using a mixed culture for reduction of 16 mg/L nitrate and 1000 µg/L perchlorate in a fixed biofilm reactor [9]. These authors observed that the

consumption of nitrate was less affected than that of perchlorate under acetate limiting conditions, since perchlorate reduction declined by 70 % whereas nitrate reduction only decreased by 20 %. In fact, nitrate was considered as the primary electron acceptor, when both nitrate and perchlorate were present and it was suggested that nitrate should be present to sustain initial growth of per(chlorate) reducing bacteria when the perchlorate concentration is too low [18].

A lower decline in nitrate reduction rate over perchlorate reduction rate observed in the IEMB might be attributed to competition of the microbial cells for the limiting ammonia concentration. In this study, the nitrate concentration in the polluted water was 600 times higher than that of perchlorate and the competition of the microorganisms for ammonia might have been dominated by denitrifiers. The significant difference in concentration between the two electron acceptors, with a consequent impact on their reduction kinetics (competition/inhibition), might have caused community stratification within the biofilm, favoring the growth of denitrifying bacteria and their dominance in the biofilm zone near the membrane surface, where the nitrate concentration is expected to be high.

4.3.2. Influence of nitrate on perchlorate reduction in suspended-cell culture

The influence of nitrate on the reduction rate of perchlorate in suspended-cell cultures was evaluated in batch experiments under ammonia non-limiting microbial growth conditions. These experiments aimed at analyzing the effect of nitrate on perchlorate reduction, when nitrate and perchlorate were present in concentrations of the same order of magnitude. In order to avoid possible influence of biofilm stratification on the anions reduction kinetics, a suspended biomass culture, used to inoculate the IEMB biocompartment, was employed.

The initial concentration of perchlorate varied from 0.4 to 25.5 mg/L while nitrate was kept constant (at 60 mg/L) in all tests. A similar reduction pattern was observed in all the experiments: a low perchlorate reduction rate while nitrate was being reduced, followed by an increase in perchlorate reduction after nitrate and nitrite depletion. As an example, for an initial perchlorate concentration of 20 mg/L a maximal nitrate reduction rate of 14.64 mg NO_3^-/mg VSS·d was observed immediately after inoculation, whereas, during this phase, perchlorate was reduced at 0.006 mg ClO_4^-/mg VSS·d, as illustrated in Figure 4.3. After depletion of nitrate and nitrite, perchlorate reduction rate increased to 0.45 mg ClO_4^-/mg VSS·d.

Inhibition of perchlorate reduction rate by nitrate was observed in all of the tests. After exhaustion of nitrate, the perchlorate reduction rate increased from 0.002 – 0.18 mg ClO_4^-

/mgVSS·d to values between 0.03 – 0.45 mg ClO_4^-/mg VSS·d, depending on the initial concentration of ClO_4^- tested (see Figure 4.4). In the presence of nitrate, the maximum rate of perchlorate reduction was 0.17 mg ClO_4^-/ mg VSS·d, which corresponded only to 38% of its maximal reduction rate (Figure 4.4). The non-inhibited perchlorate reduction rate (i.e. determined after nitrate was depleted) increased with the increase in the initial perchlorate concentration, reaching a maximal value of 0.45 ClO_4^-/mg VSS·d (Figure 4.4).

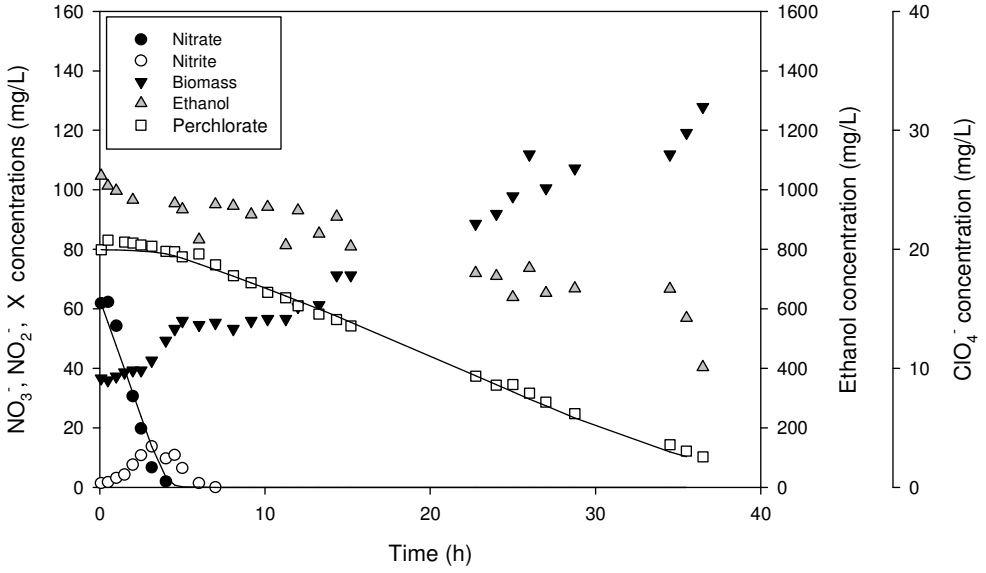

Figure 4.3: A suspended-cell batch test for reduction of 60 mg/L nitrate and 20 mg/L perchlorate. Solid lines represent estimated values using the competitive inhibition model.

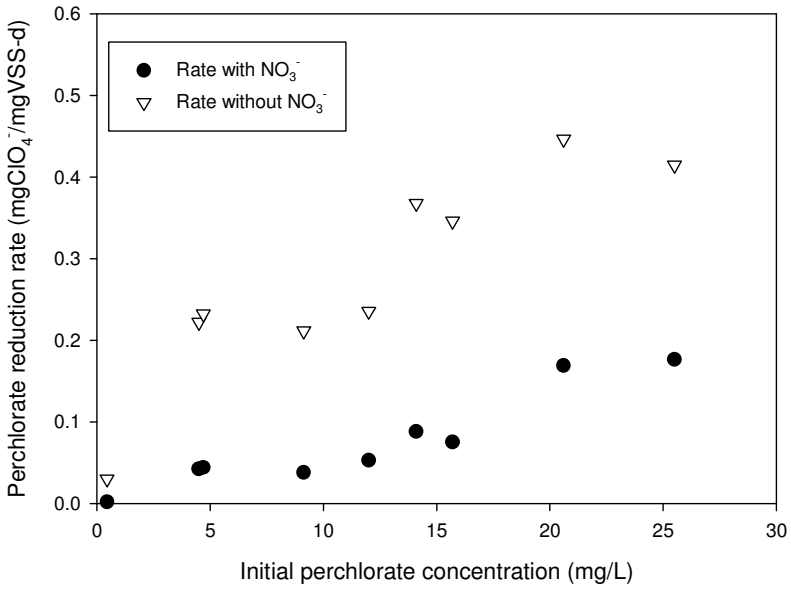

Figure 4.4: Specific perchlorate reduction rate when nitrate is present (full circles) and after nitrate exhaustion (open triangles), determined in batch tests with the suspended-cell culture.

The inhibition of perchlorate reduction by nitrate observed in this study is in agreement with the findings of other studies performed with pure and mixed per(chlorate) reducing cultures [5, 12, 25, 26]. Studying a mixed microbial culture, Gal *et al* observed complete inhibition of perchlorate reduction by nitrate (in concentrations from 29 to 112 mg/L) since perchlorate (with an initial concentration of 70 mg/L) reduction initiated only after complete nitrate reduction [25]. On the other hand, Logan and LaPoint observed a simultaneous reduction of both anions in a packed-bed bioreactor but with a 17 % decrease in the perchlorate reduction rate (initial concentration of 78 µg/L) due to the presence of nitrate (a feed containing 22 mg/L) [26].

While in some pure cultures of per(chlorate) reducing bacteria two distinct inducible enzymatic systems for nitrate and perchlorate reduction were identified [5, 27], other studies showed that perchlorate reductase and nitrate reductase enzymes are able to reduce both anions [17, 28]. Therefore, in the latter case, nitrate may compete with perchlorate for the same enzymes resulting in a lower perchlorate reduction rate.

This competition is even more complex in mixed cultures, since they may be composed of specialized per(chlorate) reducing bacteria and denitrifiers. On the other hand, most of the per(chlorate) reducing bacteria and denitrifying bacteria can use both nitrate and perchlorate as electron acceptors. It could be hypothesized that the community developed in the present study was composed by a low number of perchlorate reducing bacteria and by a high number of denitrifying bacteria able to reduce both nitrate and perchlorate. Following this hypothesis, in the presence of both oxy-anions, the specialized perchlorate reducing bacteria (not inhibited by nitrate) might have been responsible for the low initial reduction perchlorate rate, while after complete nitrate reduction, the majority of the population started to use perchlorate, thus a maximal perchlorate reduction rate was achieved.

Kinetic parameters for nitrate and perchlorate bioreduction were estimated according to the model previously developed by Dudley *et al* for competition between perchlorate and chlorate [20]. It was assumed that the majority of the microbial population was able to reduce both oxyanions. Since a mixed microbial culture was used, the estimated parameters represent average values, lumping the intrinsic kinetic constants for the individual pure strains composing the microbial community.

The kinetic equations for nitrate, perchlorate and biomass, considering the competitive inhibition model [20], can be defined by:

$$\frac{dS_n}{dt} = -q_{n,\max} \frac{S_n}{S_n + K_n\left(1 + {S_p}/{K_p}\right)} X_b \quad (4.1)$$

$$\frac{dS_p}{dt} = -q_{p,\max} \frac{S_p}{S_p + K_p\left(1 + {S_n}/{K_n}\right)} X_b \quad (4.2)$$

$$\frac{dX_b}{dt} = Y_n q_{n,\max} \frac{S_n}{S_n + K_n\left(1 + {S_p}/{K_p}\right)} X_b + Y_p q_{p,\max} \frac{S_p}{S_p + K_p\left(1 + {S_n}/{K_n}\right)} X_b - bX_b \quad (4.3)$$

where S is the substrate concentration, t is the time, q_{max} is the maximum specific substrate utilization rate, K is the half-saturation constant, X_b is the biomass concentration measured as mg VSS/L. Y is the yield coefficient (mg VSS/mg S) and b is the endogenous biomass decay rate (d^{-1}). The subscripts represent nitrate (n) and perchlorate (p), respectively.

The competitive inhibition model describes accurately both the nitrate and perchlorate concentration decay profiles in all experiments (performed at nine different initial perchlorate concentrations). As an example, Figure 4.3 illustrates the estimated concentration profiles by the model (full lines), with squared correlation coefficients (R^2) of 0.98 for nitrate, 0.99 for perchlorate for an experiment with initial concentrations of 60 mg/L of nitrate and 20 mg/L of perchlorate.

Table 4.2 summarizes the average and confidence intervals for the estimated kinetic parameters.

The q_{max} value obtained for the suspended culture was 35-fold higher for nitrate than for perchlorate, due to a clear preference of the mixed culture for nitrate as a primary electron acceptor. Furthermore, the lower value of K_n compared to that of K_p indicates a higher affinity of the culture for nitrate. The K_n value obtained is similar to values reported in the literature, which are typically in the range of 1 mgNO_3^-/L [29].

The value obtained for $q_{n,max}$ by the suspended culture, 10.79 mg NO_3^-/ mg VSS·d, is also within the values reported in the literature: 1.01-12.72 mg NO_3^-/ mg VSS·d [30]. The estimated value of Y_n (0.18 mgVSS/mg NO_3^-) is within the expected range since a theoretical value of 0.64 mg VSS/mg NO_3^- was estimated, using a hypothetical biomass formula ($C_5H_7NO_2$) previously assumed for nitrate and perchlorate reduction [31]. The Y_p parameter obtained, 3.64 mg VSS/mg ClO_4^-, is above the theoretical value of 0.54 mg VSS/mg ClO_4^-. Nevertheless, even

higher yields (2.6-12 mg VSS/mg ClO_4^-) have been also reported in previous works for perchlorate reduction [32].

Table 4.2: Nitrate and perchlorate kinetic parameters and biomass yields for enriched suspended-cell culture when both electron acceptors are simultaneously present (average values from 9 different experiments)

Parameter	Unit	Average	Confidence interval $_{95\%}$
Nitrate			
$q_{n,max}$	mg NO_3^-/(mg VSS.d)	10.79	2.09
K_n	mg NO_3^-/L	1.05	1.86
Y_n	mg VSS/mg NO_3^-	0.18	0.05
Perchlorate			
$q_{p,max}$	mg ClO_4^-/(mg VSS.d)	0.30	0.06
K_p	mg ClO_4^-/L	4.97	3.14
Y_p	mg VSS/mg ClO_4^-	3.64	1.04
b	1/d	0.008	0.008

The estimated $q_{p,max}$ value of 0.30 mg ClO_4^-/mg VSS·d, is lower than the values obtained for pure cultures, which are ranging from 1.68 to 24 mg ClO_4^-/mg VSS·d [20, 33, 34] and is slightly lower than the value 0.49 mg ClO_4^-/mg VSS·d for the mixed culture characterized by Wang *et al* using acetate as the electron donor and carbon source and perchlorate as the sole electron acceptor [32]. To the best of my knowledge, no kinetic constants have been reported so far for per(chlorate) reducing bacteria using ethanol as the electron donor.

For the IEMB operation tested, the mass rate entering the biocompartment at steady state was 8.4 mg/m^2·d of ClO_4^- corresponding to a volumetric rate of 48.3 µg/L·d. For a biocompartment hydraulic retention time of 5.84 days, assuming no perchlorate reduction, the maximal concentration in the bulk of the biocompartment would be as high as 280 µg/L. Since the value of K_p was found to be equal to 4.97 mg ClO_4^-/L, the perchlorate reduction rate was kinetically limited during the IEMB operation given that the local perchlorate concentrations within the biofilm would be in the range of µg/L. On the other hand, the nitrate concentration in the biocompartment was expected to be in the mg/L range since the volumetric rate of nitrate supplied to this compartment was equal to 26.4 mg/L·d (mass rate of 4.6 g/m^2·d). Therefore, it

is likely that nitrate was not limiting within the biofilm since the estimated K_n value was equal to 1.05 mg NO_3^-/L. This result may explain the difference between nitrate and perchlorate reduction efficiency achieved in the IEMB operated under limiting conditions (ammonia limitation). Indeed, given that the hydrodynamic situation in the biocompartment is favorable (Reynolds number of 3000), it is unlikely that transport of ammonia through the biofilm is mass transfer limited. In this situation, the biokinetics would be the process limiting step and then perchlorate would preferentially accumulate in the IEMB biocompartment.

4.3.3. FISH analysis of microbial community composition

Samples from the enriched suspended-cells culture used as inoculum for the IEMB, biocompartment suspended cells from the IEMB and biofilm from the IEMB were screened with both general and specific probes for major groups of denitrifiers and per(chlorate) reducing bacteria. It was observed that the enriched suspended-cell culture was majorly composed of *Gammaproteobacteria*, followed by *Alphaproteobacteria* (Table 4.3). This culture contained only 4 % of *Betaproteobacteria*, the bacterial group that includes the genera *Dechlorosomas* and *Dechloromonas*, which comprise most of the per(clorate) reducing bacteria found in perchloratate treatment reactors [4]. After 3 months of IEMB operation, the *Betaproteobacteria* in the biofilm increased to 44 % of the bacterial population, although the same was not observed in the suspended cells taken from the IEMB biocompartment, which shifted to a dominance of the *Alphaproteobacteria* (50 %). The latter includes the genera *Rhodobacter*, *Roseobacter* and *Paracoccus*, which have been reported to comprise some species that are able to reduce perchlorate [35-37]. Therefore, it is not surprising that this subgroup of Proteobacteria was enriched in the suspended biomass, since part of the perchlorate may cross the biofilm and be available for these cells, such as observed in ammonia limiting conditions (Figure 4.3). Additionaly, this could also resulted from detachment of the biofilm surface that is enriched in per(chlorate) reducing bacteria, if a sequential consumption of nitrate and perchlorate is assumed. An enrichment in *Alpha-* and *Gammaproteobacteria* was previously observed in a membrane biofilm reactor for the treatment of a high-salinity brine containing nitrate and perchlorate [38].

In the IEMB biocompartment suspended cells, the *Alfa-*, *Beta-* and *Gammaproteobacteria* did not cover the totality of the EUBmix-targeted bacteria (88 %, see Table 4.3). Nevertheless, other bacteria *phyla* contain a limited number of organisms able to reduce nitrate and/or perchlorate. *Wolinella* is an identified *Epsilonproteobacteria* able to use both electron acceptors, however, its characteristic morphology was not observed in this study. Despite the very specific conditions that the cultures were subjected to, where no other electron acceptors rather than

nitrate and perchlorate were provided, it is also possible that some of the bacteria present both in the biofilm and in the suspension may not be able to reduce nitrate or perchlorate. Indeed, bacteria not identified for perchlorate removal were observed in a biofilm reactor together with per(chlorate) reducing bacteria [12]. Those cells could be using oxygen that is produced in the perchlorate reducing pathway [4].

Table 4.3. FISH quantification of the three most relevant groups of *Proteobacteria* in the suspended-cells culture used in batch tests, the biofilm and the IEMB biocompartment suspended culture. Abundance is given in respect to total bacteria (EUBmix-targeted). SEM = standard error of the mean. Congruency between the population and general probes, as per the software Daime

	Enriched susp. culture			Biofilm			Biocompartment susp. culture		
Proteobacteria group	Abundance (%)	SEM (%)	Congruency (%)	Abundance (%)	SEM (%)	Congruency (%)	Abundance (%)	SEM (%)	Congruency (%)
Alpha	29	3	100	20	2	100	50	3	99
Beta	4	0.2	99	44	3	99	6.1	0.7	99
Gamma	70	2	99	34	3	98	32	2	97

The FISH semi-quantitave results for the specific probles are summarized in Table 4.4. In the same table, the classification for each group of organisms as denitrifiers or per(chlorate) reducing bacteria is indicated. The suspended-cell culture used as inoculum for the IEMB and for the batch tests had a higher number of denitrifying organisms than per(chlorate) reducing bacteria, mainly *Rhodobacter* and/or *Roseobacter* bacteria, which are not able to reduce perchlorate (only chlorate) [36, 37]. *Dechloromonas* was not detected by FISH and *Dechlorosomas* represented only a reduced number of organisms.

This result supports the assumption of two populations reducing perchlorate in sequence: first only specialized per(chlorate) reducing bacteria and after nitrate depletion both per(chlorate) reducing bacteria and some denitrifiers contributing for perchlorate reduction. This hypothesis explains the low perchlorate consumption rate observed in the first phase (while nitrate was still available, Figure 4.3) since only a small number of *Dechlorosomas* was detected.

After prolonged IEMB operation, an enrichment of denitrifiers was observed both in the biocompartment suspended cells and in the biofilm. Not only the existing G Rb-targeted bacteria increased in abundance, but also there was a proliferation of *Paracoccus*, *Azoarcus* and *Thauer*a. Interestingly, the G Rb oligonucleotide probe also targets other members of the *Rhobacterales* order, including many species of the *Paracoccus* genus (such as *Paracoccus*

denitrificans). Thus, the simultaneous increase in PAR651-targeted and G Rb-targeted bacteria in these samples (Table 4.4) can be majorly attributed to a proliferation of *Paracoccus*. *Paracoccus* and *Azoarcus* are described as denitrifiers, although they are also able to reduce perchlorate when both electron acceptors are present [35, 37].

Table 4.4: Summary of FISH results using specific probes for per(chlorate) reducing bacteria and denitrifying bacteria for the suspended-cell culture used as inoculum, the IEMB biofilm and the suspended culture in the IEMB biocompartment

Probe	Organism	Sample			Classification	
		Enriched susp. cultures	Biofilm	Biocompartment susp. culture	Denitrifiers[37]	Per(chlorate) reducing bacteria [4]
Azo644	*Azoarcus*	+	+	++	✓	
Dechl2	*Dechloromonas*	-	+	+		✓
Soma1035	*Dechlorosomas*	+	-	+		✓
PAR651	*Paracoccus*	-	+	+++	✓	
Pae997	*Pseudomonas*	-	-	-	✓	✓
G Rb	*Rhodobacter*	++	+	+++	✓	
G Rb	*Roseobacter*				✓	
THAU832	*Thauera*	-	+	++	✓	

(−) Less than 1%; (+) few; (++) some; (+++) abundant; n/a: not available

Within those organisms that can grow on perchlorate, an increase in *Dechloromonas* was observed in both the IEMB biocompartment and the biofilm, with a simultaneous decline in *Dechlorosomas* in the latter. This phenomenon was also detected for perchlorate contaminated groundwater biofilm reactors [12, 18] and could be related with the selective advantage of *Dechloromonas* to grow simultaneously on both substrates without nitrate inhibition [12]. The lower value of K_p for *Dechloromonas* can also potentiate selection of this organism in media with low concentration of perchlorate [34]. Moreover, in *Dechlorosomas*, perchlorate reduction is inhibited by the presence of nitrate [12]. This explains the detection of *Dechlorosomas* in the

biocompartment suspended culture and not in the biofilm, where nitrate was present in higher concentrations.

FISH analysis was also carried out for *Pseudomonas*, another group of important denitrifiers using ethanol as electron donor, but this group was not detected in this study.

4.3.4. Biofilm stratification analysis by FISH

The spatial distribution of major bacterial groups comprising denitrifiers and per(chlorate) reducing bacteria was investigated through a FISH analysis of cryosectioned biofilm samples. Figure 4.5 depicts a longitudinal cut of the biofilm where it is clear that *Dechloromonas* is most abundant at the biofilm surface, whereas the denitrifying *Thauera* prevail closer to the membrane. This result was confirmed through FISH analysis of transversal cuts of the biofilm (Figure 4.6a and b). G Rb-targeted bacteria (*Rhodobacter*, *Roseobacter* and some *Paracoccus*) could also be found in higher numbers closer to the membrane, where *Azoarcus* seemed less abundant (Figure 4.6c, d and e). However, stratification of these denitrifiers was not as clear as for the *Thauera*, possibly due to their ability to use either nitrate or perchlorate as electron acceptor [36, 37].

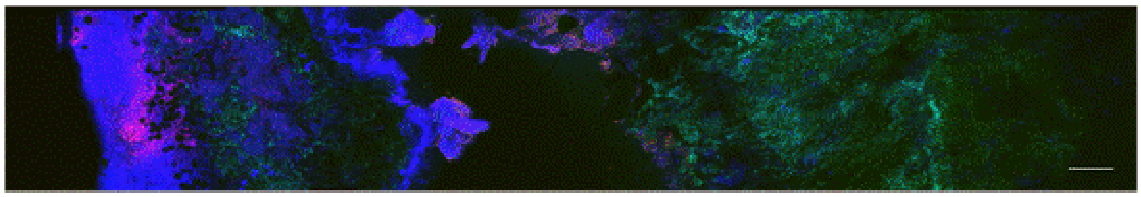

Figure 4.5: FISH micrograph of a longitudinal cut of the biofilm hybridized with Cy3-labelled Dechl2 (in magenta) and FitC-labelled Thau832 (in cyan), with Cy5-labelled EUBmix (blue). The membrane is on the right side. Bar = 50 µm

In the IEMB, nitrate and perchlorate are supplied through the anion-exchange membrane. Therefore, it is not surprising that microorganisms that use nitrate as electron acceptor thrive in the deeper parts of the biofilm, closer to the membrane. In particular *Thauera*, which was not described as being capable to reduce perchlorate, is likely to be only able to grow where nitrate is present in higher concentrations. In fact, *Thauera* seems to have a high growth rate since it represents the major group of bacteria found in granules in a high-nitrate rate denitrifying reactor [39]. So, these denitrifiers are likely to have been pioneers in the biofilm colonization on the membrane surface.

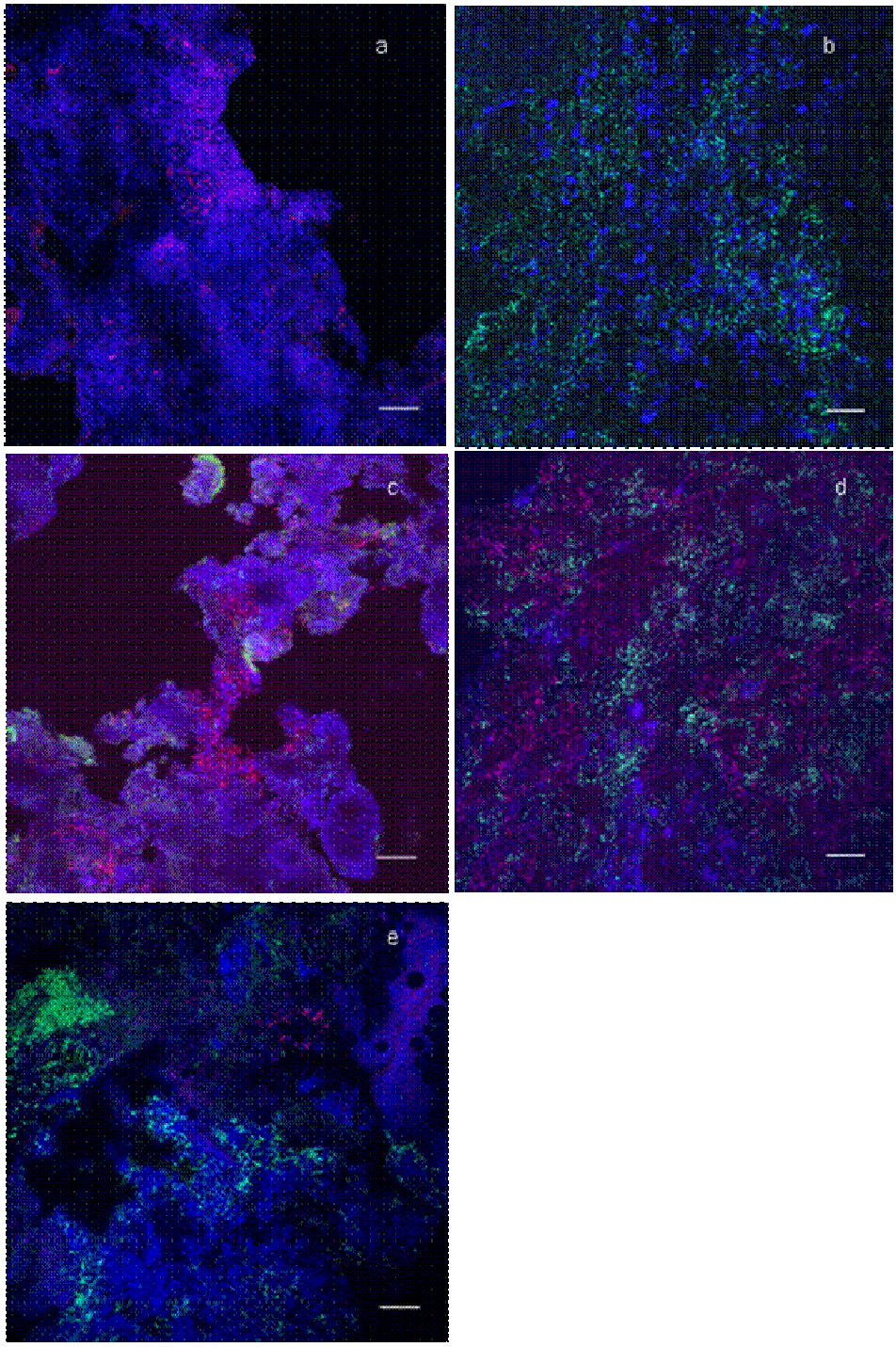

Figure 4.6: FISH micrographs of transversal cuts of the biofilm at (from the surface): a) 350 µm; b) 550 µm; c) 250 µm; d) 650 µm; e) 850 µm. Specific probes where, a and b) Dechl2 (Cy3, in magenta) and Thau832 (FitC, in cyan); c, d and e) Azo644 (Cy3) and GRb (FitC). In all images, Cy5-labelled EUBmix (blue) was used as general probe. Bar = 20 µm.

Perchlorate was present in the polluted water in a very low concentration, thus it is likely to have lower impact on microbial selection than nitrate. Furthermore, all the per(chlorate) reducing bacteria groups screened (including *Dechloromonas* and *Dechlorosomas*) have strains

that are also able to use nitrate [12]. *Dechloromonas* has lower growth rates on nitrate than the other organisms investigated in this study, but it has higher affinity to perchlorate [34]. This explains why *Dechloromonas* were not detected in deeper parts of the biofilm, where they were overgrown by faster growing denitrifiers, but thrived at the biofilm surface, where the concentration of nitrate was not high enough to promote competitive growth on nitrate, and perchlorate was the primary substrate.

These results give strong evidences that bioreduction inside the biofilm is also sequential as observed for suspended cultures, with nitrate being consumed immediately after crossing the membrane, whereas perchlorate is consumed mainly in the biofilm zone contacting the biomedium, where the concentration of nitrate is lower. Therefore, under growth limiting conditions, the perchlorate degradation rate is more affected since the nutrients are used primarily for nitrate reduction, as discussed in section 4.3.1. This biofilm organization was potentiated by the much higher membrane mass transfer rate of nitrate over perchlorate (higher driving force for transport through the membrane), which favoured the growth of denitrifiers over per(chlorate) reducing bacteria at the membrane surface. Under non-limiting conditions, neither nitrate nor perchlorate were detected in the bulk of the biocompartment (see Figure 4.2). This is an important advantage of the IEMB process relatively to the cell suspension systems, since due to the biofilm stratification the reduction of nitrate and perchlorate occur sequentially in space, thus allowing the perchlorate reducing bacteria perform at its maximum reduction rate for such perchlorate concentration. Indeed, the inhibitory effect of nitrate on perchlorate reduction observed in suspended culture experiments was avoided.

4.4. Conclusions

This research showed that bioreduction of nitrate and perchlorate in the IEMB occurred spatially sequentially in the mixed culture biofilm, using nitrate as the primary electron acceptor. This conclusion can be withdrawn since:

- Operation of the IEMB under ammonia limiting conditions resulted in decreased perchlorate reduction rate whereas nitrate reduction was unaffected.
- Nitrate inhibited perchlorate reduction, since maximum perchlorate reduction rate, 0.45 mg ClO_4^-/mg VSS·d, only occurred after nitrate depletion. In the presence of nitrate, a maximum perchlorate reduction rate of 0.18 mg ClO_4^-/mgVSS·d was observed.

- Kinetic parameters estimated with a competitive inhibition model showed a 35-fold higher value of q_{max} for nitrate than for perchlorate. The lower K_n (1.05 mg/L) compared to K_p (4.97 mg/L) value also indicate a higher affinity for nitrate of the culture in suspension.
- FISH analysis showed a proliferation of denitrifiers, such as *Paracoccus*, *Azoarcus* and *Thauera*, in the IEMB. During enrichment, an increase in *Dechloromonas*, a per(chlorate) reducing organism that is not inhibited by nitrate, was observed.
- FISH analysis of cryosections of biofim samples showed that *Dechloromonas* is more abundant at the biofilm outer surface, whereas the denitrifying *Thauera* prevail closer to the membrane. Stratification of organisms that can grow on both nitrate and perchlorate (*Rhodobacter, Roseobacter, Paracoccus*) also seemed to occur in a higher number closer to the membrane.

It can be concluded that the IEMB developed nitrate-controlled biofilm stratification. Thus, denitifiers prevailed closer to the membrane (higher nitrate concentration) due to their kinetic advantage, whereas perchlorate reducers were mainly located near the biofilm surface (non-inhibiting nitrate concentration). Due to this biofilm stratification, the IEMB presents an advantage in comparison to a bioremediation process using a suspended biomass. In IEMB, reduction of nitrate and perchlorate is likely to occur sequential in space, allowing for perchlorate reduction to occur at its maximum rate since inhibition by nitrate is avoided. As a consequence, nitrate and perchlorate were completed removed in the IEMB despite they were present in a different range of concentrations (mg/L for nitrate and µg/L for perchlorate).

4.5. References

1 Greer, M.A., Goodman, G., Pleus, R.C., Greer, S.E., 2002. Health effects assessment for environmental perchlorate contamination: the dose response for inhibition of thyroidal radioiodine uptake in humans. Environ. Health Perspect. 110 (9): 927-937.

2 Srinivasan, R., Sorial, G.A., 2009. Treatment of perchlorate in drinking water: a critical review. Sep. Pur. Techn. 69: 7-21.

3 US Environmental Protection Agency (USEPA), 2011. Drinking water: regulatory determination on perchlorate, Federal Register. 76(29): 7762-7767.

4 Coates, J., Achenbach, L.A., 2004. Microbial perchlorate reduction: rocket-fuelled metabolism. Nature Reviews Microb. 2: 569-580.

5 Chaudhuri, S.K., O'Connor, S.M., Gustavson, R.L., Achenbach, L.A., Coates, J.D., 2002.

Environmental factors that control microbial perchlorate reduction. Appl. Environ. Microbiol. 68: 4425-4430.

6 Van Ginkel, S.W., Ahn, C.H., Badruzzaman, M., Roberts, D.J., Lehman, S.G., Adham, S.S., Rittmann, B.E., 2008. Kinetics of nitrate and perchlorate reduction in ion-exchange brine using the membrane biofilm reactor (MBfR). Water Res. 42: 4197-4205.

7 US Environmental Protection Agency (USEPA), 2010. National primary drinking water regulations; announcement of the results of EPA's review of existing drinking water standards and request for public comment and/or information on related issues, Federal Register. 75(59): 15500-15572.

8 European Community (EC), 1980. Council directive of 15 July 1980 relating to the quality of water intended for human consumption. Off. J. Eur. Commun. 23 (L229): 11.

9 Choi, H., Silverstein, J., 2008. Inhibition of perchlorate reduction by nitrate in a fixed biofilm reactor. J. Hazard. Mat. 159: 440-445.

10 Hatzinger, P.B., 2005. Perchlorate biodegradation for water treatment. Environ. Sci. Tecnol. 39: 239A–247A.

11 Xiao, Y., Roberts, D.J., Zuo, G., Badruzzaman, M., Lehman, G.S., 2010. Characterization of microbial populations in pilot-scale fluidized-bed reactors treating perchlorate- and nitrate-laden brine. Water Res. 44: 4029-4036.

12 Zhang, H., Logan, B.E., Regan, J.M., Achenbach, L.A., Bruns M.A., 2005. Molecular assessment of inoculated and indigenous bacteria in biofilms from a pilot-scale perchlorate-reducing bioreactor. Microbial Ecol. 49: 388-398.

13 Nerenberg, R., Rittmann, B.E., Gillogly, T.E., Lehman, G.E., Adham S.S., 2003. Perchlorate reducing using a hollow-fiber membrane biofilm reactor: kinetics, microbial ecology and pilot-scale studies. Proceedings on the seventh International in situ and on-site Bioremediation Symposium, Orlando, Florida, USA

14 Velizarov, S., Rodrigues, C.M., Reis, A.M., Crespo, J.G., 2001. Mechanism of charged pollutants removal in an ion exchange membrane bioreactor: drinking water denitrification. Biotechnol. Bioeng. 71 (4): 245–254.

15 Matos, C.T., Velizarov, S., Crespo, J.G., Reis, M.A.M., 2006. Simultaneous removal of perchlorate and nitrate from drinking water using the ion exchange membrane bioreactor concept. Water Res. 40: 231-240.

16 Nozawa-Inoue, M., Scow, K.M., Rolston D.E., 2005. Reduction of perchlorate and nitrate by microbial communities in vadose soil. Appl. Environ. Microbiol. 71: 3928-3934.

17 Bardiya, N., Bae, J., 2011. Dissimilatory perchlorate reduction: a review. Microbiol. Res. 166(4): 237-254.

18 Nerenberg, R., Kawagoshi, Y., Rittmann, B.E., 2008. Microbial ecology of a perchlorate-

reducing hydrogen-based membrane biofilm reactor. Water Res. 42: 1151-1159.

19 American Public Health Association, American Water Works Association & Water Pollution Control Federation (APHA, AWWA & WPCF), 1995. Standard methods for the examination of water and wastewater, A.D. Eaton, L.S. Clesceri, A.E. Greenberg, (Eds.), Standard Methods for the Examination of Water and Wastewater, Port City Press, Baltimore.

20 Dudley, M., Salamone, A., Nerenberg, R., 2008. Kinetics of a chlorate-accumulating perchlorate-reducing bacterium. Water Res. 42: 2403-2410.

21 Amann, R.I., 1995. Molecular microbial ecology manual, Kluwer Academic Publications, Dordrecht, pp. 1–15.

22 Daims, H., Lücker, S., Wagner, M., 2006. Daime, a novel image analysis program for microbial ecology and biofilm research. Environ. Microbiol. 8: 200-213.

23 Loy, A., Maixner, F., Wagner, M., Horn, M., 2007. ProbeBase—an online resource for rRNA-targeted oligonucleotide probes: new features. Nucleic Acids Res. 35: D800–D804.

24 Oehmen, A., Zeng, R.J., Saunders, A.M., Blackall, L.L., Keller, J., Yuan, Z.G., 2006. Anaerobic and aerobic metabolism of glycogen accumulating organisms selected with propionate as the sole carbon source. Microbiology 152: 2767–2778.

25 Gal, H., Ronen, Z., Weisbrod, N., Dahan, O., Ronit, N., 2008. Perchlorate biodegradation in contaminated soils and the deep unsaturated zone. Soil Biol. Biochem. 40: 1751-1757.

26 Logan, B.E., LaPoint, D., 2002. Treatment of perchlorate- and nitrate-contaminated groundwater in an autotrophic, gas phase, packed-bed bioreactor. Water Res. 26: 2647-3653.

27 Xu, J., Trinble, J.J., Steinberg, L., Logan, B.E., 2004. Chlorate and nitrate reduction pathways are separately induced in the perchlorate-reducing bacterium *Dechlorosoma* sp. KJ and the chlorate-respiring bacterium *Pseudomonas* sp. PDA. Water Res. 38: 673-680.

28 Giblin, T., Frankenberger, W.T., 2001. Perchlorate and nitrate reductase activity in the perchlorate-respiring bacterium *perclace*. Microbiol. Res. 156: 311-315.

29 Halling-Sørensen, B.H., Jørgensen, S.E., 1993. The removal of nitrogen compounds from wastewater. Elsevier, Amsterdam, p. 443.

30 Rabah, F.K., Dahad, M.F., Zhang, T.C., 2007. Estimation of the intrinsic maximum substrate utilization rate using batch reactors with denitrifying biofilm: a proposed methodology. Water Environ. Res. 79 (8): 887-892.

31 Farhan, Y.H., Hatzinger, P.B., 2009. Modeling the biodegradation kinetics of perchlorate in the presence of oxygen and nitrate as competing electron acceptors. Biorem. J. 13(2): 65-78.

32 Wang, C., Lippincott, L., Meng, X., 2008. Kinetics of biological perchlorate reduction and

pH effect. J. Hazard. Mat. 153: 663-669.

33 Logan, B.E., Zhang, H., Mulvaney, P., Milner, M.G., Head, I.M., Unz, R.F., 2001. Kinetics of perchlorate- and chlorate-respiring bacteria. Appl. Environ. Microbiol. 67: 2499-2506.

34 Nerenberg, R., Kawagoshi, Y., Rittman, B.E., 2006. Kinetics of a hydrogen-oxidizing, perchlorate-reducing bacterium. Water Res. 40: 3290-3296.

35 Okeke, B.C., Giblin, T., Frankenberger Jr, W.T., 2002. Reduction of perchlorate and nitrate by salt tolerant bacteria. Environ. Pollut. 118: 357-363.

36 Roldán, M.D., Reyes, F., Moreno-Vivián, C., Castillo, F., 1994. Chlorate and nitrate reduction in the phototrophic bacteria *Rhodobacter capsulatus* and *Rhodobacter sphaeroides*. Curr. Microbiol. 29 (4): 241-245.

37 Shapleigh, J.P., 2006. The denitrifying prokaryotes. In: The prokaryotes: an evolving electronic resource for the microbiological community, M. Dworkin (Eds.), 3rd edition, ed. online.

38 Ahn, C.H., Oh, H., Ki, D., Van Ginkel, S.W., Rittmann, B.E., Park, J., 2009. Bacterial biofilm-community selection during autohydrogenotrophic reduction of nitrate and perchlorate in ion-exchange brine. Appl. Microbiol. Biotechnol. 81: 1169-1177.

39 Etchebehere, C., Tiedje, J., 2005. Presence of two different active nirS nitrite reductase genes in a denitrifying *thauera* sp. from a high-nitrate-removal-rate reactor. Appl. Environ. Microbiol. 71(9): 5642–5645.

Chapter

5

Up-scaling of membrane-supported biofilm reactors: the Ion-Exchange Membrane Bioreactor case-study

Summary

The Ion Exchange Membrane Bioreactor (IEMB) is a particular case of a membrane-supported biofilm reactor, in which oxy-anions, used as electron acceptors by an anoxic mixed microbial culture, are removed from polluted water through an anion-exchange membrane. The opposite side of this membrane is used for biofilm development, contacting a separate compartment (biocompartment), to which chloride counter-ions are fed as "driving" counter-ions. The applicability of a plate-and-frame IEMB module configuration, consisting of a series of anion-exchange membranes, for the treatment of drinking water simultaneously contaminated with nitrate and perchlorate, was evaluated during long-term process operations of up to 3 months. The process performance was evaluated and systematically characterized by HPLC, Scanning electron microscopy and 2D-fluorescence spectroscopy. On-line monitoring by 2D-fluorescence spectra of the membrane surface proved adequate for early detection of fouling formation. Permeation of carbon source across the membrane to the treated water stream was avoided by a dedicated start-up procedure involving a gradual increase of ethanol feeding to the IEMB biocompartment. It was demonstrated that the biocompartment pH does not influence significantly the nitrate reduction but must be controlled in order to guarantee a complete perchlorate removal. pH control in the biocompartment was also necessary to avoid precipitation of struvite on the

membrane surface, which ads membrane scaling and decreases the availability of nutrients for the biofilm. It was found out that the amount of Cl^- required in the process could be supplied by the pH-regulating agent (HCl), thus completely utilizing this chemical as a source of both H^+ and Cl^- for pH adjustment and as "driving" anions for the counter transport of nitrate and perchlorate to the biocompartment, respectively. Under these conditions, the IEMB process was successfully operated maintaining the nitrate and perchlorate concentrations in the treated water below their recommended levels for drinking water supplies.

5.1. Introduction

Membrane attached biofilm reactors (MABs) gather the unique feature of combining mass-transfer of target solutes across a membrane with biological reactions carried out by a biofilm that is naturally-formed on the membrane surface. They are used in water treatment to supply dissolved gases directly to a biofilm growing on the outer surface of a hollow-fiber or a flat membrane [1-2]. Since gas (oxygen or hydrogen) transfer occurs by diffusion through the membrane, higher gas-transfer efficiency than that of air bubbling is obtained, which results in a reduction in the energy demands [1]. In addition, treatment of toxic volatile compounds becomes feasible since the counter-diffusion of oxygen and organics across the biofilm, prevents gas stripping of the volatile compounds, which may occur in processes utilizing air bubbling [3].

In the Ion Exchange Membrane Bioreactor (IEMB), ionic pollutants which diffuse through an ion-exchange membrane, are biologically degraded by a biofilm formed at the outer membrane surface contacting a separate compartment, to which a carbon source and other required nutrients are fed [4]. The IEMB concept has been so far validated for the removal of toxic ions such as nitrate, perchlorate, bromate and ionic mercury [5]. The possibility of simultaneous removal of nitrate and perchlorate from contaminated water streams was also proved [6]. In the IEMB, the physical separation of the water and the biological streams by a dense ion-exchange membrane [4-5] allows to avoid direct contact between the treated water stream and the microbial culture. Therefore, secondary contamination of the treated water by microbial cells, metabolic by-products and residual nutrients is avoided [6]. It was recognized that for a successful IEMB operation, the membrane has to gather two important characteristics: a low resistance to the transport of the target charged compound(s) and a high resistance to transport of the carbon source from the biological compartment to the treated water compartment.

However, these proof-of-concept studies were performed using a laboratory-scale module, in which a single flat membrane was separating two identical rectangular flow channels, a configuration that did not require inclusion of spacers and which cannot be applied in large-scale membrane operations. Among the commercially available membrane module arrangements: plate-and-frame, spiral-wound and hollow-fiber [7], only plate-and-frame modules are presently used with ion-exchange membranes for Donnan dialysis or electrodialysis process operations. Therefore, considering a possible large-scale application of the IEMB process, the performance of a plate-and-frame module configuration with a number of anion-exchange membranes must be investigated. This design allows also to better address situations expected to occur in real operation facilities such as membrane fouling since a plate-and-frame membrane arrangement necessarily requires the use of spacers for physical separation of the membranes and for providing adequate hydrodynamic conditions inside the module channels. However, the presence of spacers may also lead to accumulation of particles and to accelerated membrane fouling problems and/or scaling [8].

The key aspect that has to be considered when up-scaling the IEMB process in a plate-and-frame membrane arrangement is the guarantee of a sufficiently high ratio of membrane area per biological compartment liquid volume (A/V_b). This is due to the fact that the reduction of nitrate and perchlorate takes place within the biofilm growing on the membrane surface contacting the biological compartment. Therefore, the up-scaling of biomass content is achieved by increasing the membrane area and not the biological compartment volume, as in suspended cell cultivation processes. The main advantage of maintaining relatively small liquid volume of the biological compartment (a high A/V_b ratio) is the minimization of the system footprint and associated capital costs.

However, such up-scaling strategy leads to serious implications for the IEMB operation that need to be investigated. The increase in specific membrane surface area leads to higher mass transport rates of the anions present in the water to be treated to the biocompartment. Consequently, the amount of nutrients required as well as the metabolic products of the biofilm is increased. In the IEMB, nutrients have to be fed in excess to the biocompartment to assure that the reduction rates of nitrate and perchlorate depend only from their mass-transfer rates across the membrane. On the other hand, it is important to avoid high concentrations of nutrients (especially of the carbon source) in order to prevent their possible permeation into the treated water compartment. This is particularly critical during the process start-up period, when the membrane biofilm is still not developed. Therefore, dedicated control of the carbon source addition in the start-up period may become necessary in order to avoid situations of its excess or limitation for the growth of the biofilm.

Another implication of up-scaling the process is the accumulation of higher levels of metabolic by-products. This accumulation may lead to inhibition of nitrate and/or perchlorate reduction, which would decrease the IEMB process efficiency.

Therefore, the aim of this study was to evaluate the impact of up-scaling on IEMB performance and to define adequate conditions and strategies for successful process operation.

5.2. Materials and Methods

5.2.1. IEMB experimental setup and operation

The IEMB process was operated using a modified electrodyalysis module, EDR-Z-Mini (Mega, Czech Republic) equipped with 12 Neosepta ACS anion-exchange membranes (Tokuyama Soda, Japan). In this adapted module, the modification concerns the use of only anion-exchange membranes and an increase of the channels height to 4 mm (instead of the commonly used 0.8 mm) for the concentrate compartment (used as a biological compartment in the case of the IEMB process) in order to allow for biofilm development in this compartment. The biocompartment channels were connected by a recirculation loop to a stirred anoxic vessel, to which fresh biofeed was continuously added (see Figure 5.1). In the biocompartment channels, the biomedium was re-circulated at 97.2 L/h (equivalent to a linear fluid velocity of 0.17 m/s). In the diluate channels, the treated water was re-circulated through an external vessel at 44.4 L/h (linear fluid velocity of 0.41 m/s). In the two terminal compartments of the module, deionised water was re-circulated at a flow rate of 30 L/h (linear fluid velocity of 0.26 m/s).

The water compartment was continuously fed with tap water supplemented with 60 mg/L of NO_3^- and 100 µg/L of ClO_4^- in the form of their sodium salts at 0.22 L/h to guarantee a treated water throughput of 3.1 L/(m^2h). This value proved to be suitable for the treatment of water contaminated with 60 mg/L nitrate and 100 µg/L of perchlorate in a previous proof-of-concept study performed in a single membrane module [6]. Before entering the system, the water was filtered through a 5 µm. The biocompartment total circuit volume (bioreactor, membrane channels and tubing) was equal to 0.7 L and anoxic conditions were maintained in this compartment by passing argon through the vessel head-space. The hydraulic residence time in the biocompartment was maintained at 5.84 days by continuous feeding of a fresh biofeed containing 1 g/L K_2HPO_4, 0.6 g/L KH_2PO_4, 0.1 g/L $MgSO_4$ and 5.86 g/L NaCl with a pH value pre-adjusted to 7.0. The bioreduction of nitrate and perchlorate was performed by a mixed microbial culture enriched from a primary inoculum taken from a municipal wastewater treatment plant [6]. The biocompartment pH was not controlled, except when mentioned, using

1M HCl solution to control the pH at 7.0. Nitrogen source was added in the form of NH_4Cl at 0.738 g/L, to maintain the same C/N ratio as in the single membrane module. Ethanol, used as the carbon source and electron donor, was initially set to 0.8 g/L in the biofeed and its feeding protocol was adjusted according to each experiment objective (see section 5.3).

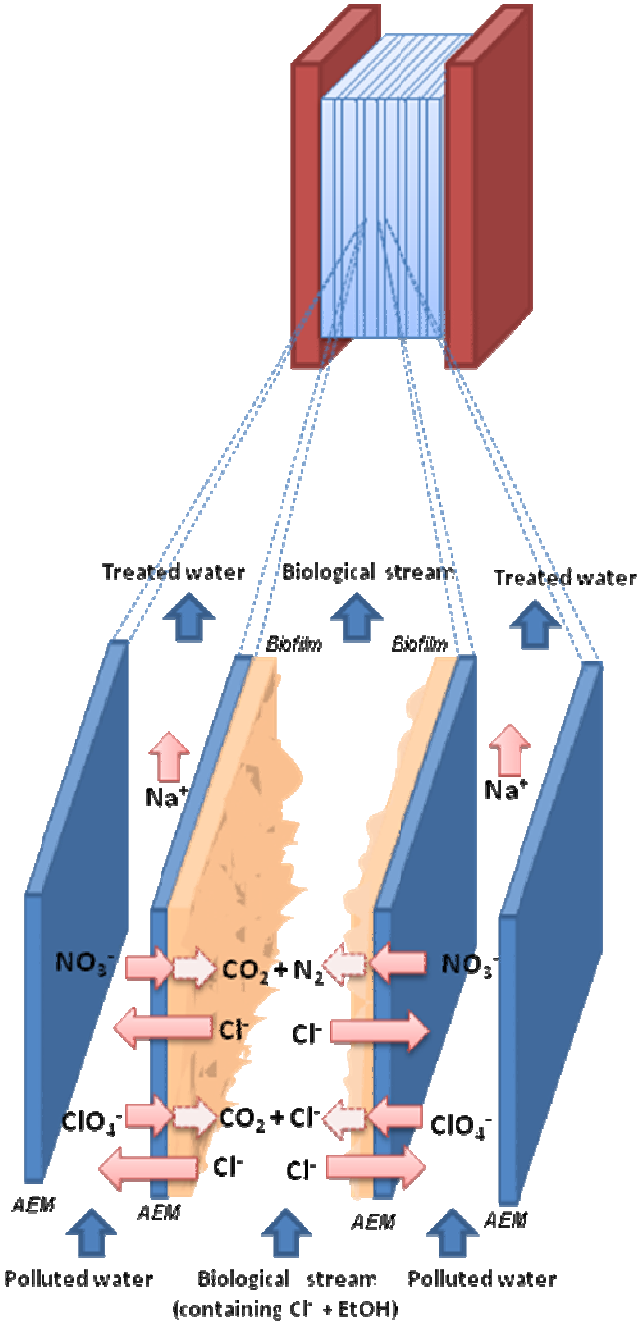

Figure 5.1: Schematic representation of counter-ion transport and nitrate and perchlorate bioreduction in the plate-and-frame membrane module composed of a series of anion exchange membrane (AEM). For simplicity reasons, only 4 membranes are illustrated and spacers located between the membrane are not presented.

Polluted water, treated water, biofeed and biocompartment outlet streams were monitored, for at least 2 months, through periodical sampling for nitrate, perchlorate, phosphate, sulphate, ammonia, magnesium, ethanol and cell concentration measurements. All experiments were performed at 23 ± 1 ºC.

5.2.2. Donnan dialysis experiments

Donnan dialysis experiments were carried out under the same conditions of the IEMB (but without adding microbial culture and ethanol to the biocompartment). These experiments were performed in order to investigate possible fouling caused only by natural organic matter present in the water.

Two different modules were used: the plate-and-frame module (as already described in section 5.2.1) and a single membrane module without spacers. The single membrane module had two identical rectangular channels separated by an anion exchange membrane sample with an area of 34.5 cm^2. This module was made of Plexiglas with a window located in the center of the channel for introducing a fluorescence probe. This window is made of quartz and is located 3 mm away from the membrane surface (a distance equal to the channel height). In this module operation, to maintain the same water flow rate per unit of membrane area (F/A) ratio as in the plate-and-frame module, polluted water was fed at 0.2 mL/min to the water compartment.

5.2.3. On-line fluorescence monitoring

2D-fluorescence spectra of membrane surface were obtained with a Varian Cary Eclipse fluorescence spectrophotometer (Varian, USA) equipped with excitation and emission mono-chromators. This technique was used to characterize membrane fouling in the current study since it was described previously to be able to monitor fouling formation in both drinking water and wastewater treatment membrane processes [9-11]. The use of excitation-emission matrices (EEMs) captures information about the presence of multiple fouling agents typically present in water systems as natural organic matter (NOM). Compared with other NOM characterization techniques, fluorescence analysis is rapid and has high sensitivity [10]. Moreover, it is capable of capturing the specific fluorescence features of protein and humic-like substances in the same matrix.

A fluorescence optical fibre bundle probe with 294 randomized optical fibres (147 excitation and 147 emission) each with a length of 2 m and a diameter of 200 µm was used. Fluorescence spectra were generated in a synchronous mode in the range of 250 to 700 nm for excitation and

260 to 710 nm for emission wavelengths. The excitation wavelength had a 10 nm increment step. A scan speed of 3000 nm/min was used with an excitation slit of 5 nm and an emission slit of 10 nm.

5.2.4. Scanning electron microscopy images

Scanning electron microscopy (SEM) images were captured for the membrane operated in the IEMB before and after pH control (see section 5.3.2). Membrane squares of 1 x 1 cm size were cut and instantaneously frozen in liquid nitrogen (-196 ºC) to preserve biofilm structure and stored at 25 ºC in a dark room from 24 h to several weeks. Before analysis, samples were sputter-coated with gold-palladium and examined with a scanning electron microscope (JSM 7001F, JEOL, Japan) with an accelerating voltage of 15 kV.

5.2.5. Analytical techniques

Before analysis, the samples were centrifuged and filtered through a 0.22 µm filter to remove suspended particles. Nitrate, phosphate and sulphate concentrations were measured using a Dionex system (Dionex, USA) composed by an AG9 guard column, an AS9 analytical column (4 mm), an ASRS suppressor and an ED50 electrochemical detector. The analysis was performed at 30 ºC using a 9 mM Na_2CO_3 aqueous solution at 1 mL/min as mobile phase. Perchlorate was determined using the same system with AG16 and AS16 columns with 1 mL/min 50 mM NaOH aqueous solution as mobile phase. Chloride present in the biocompartment samples was removed prior to perchlorate analysis by passing the sample through an OnGuard II Ag/H Cartridge (Dionex, USA) to avoid overlapping with the perchlorate chromatographic peak.

Magnesium was determined by an Inductively Coupled Plasma-Atomic Emission Spectrophotometer (Ultima, Horiba Jobin-Yvon, France). Ammonium concentration was measured using a potentiometric sensor Orion 95-12 (Thermo Electron Corporation, USA). Ethanol was determined by HPLC using an Aminex HPX-87H column (Biorad, USA) and a differential refractometric detector RI-71 (Merck-Hitachi, Japan). An aqueous solution of 0.1N H_2SO_4 at 0.5 mL/min was used as mobile phase.

5.3 Results and discussion

5.3.1 Impact of start-up conditions on IEMB process performance

An experiment was first performed using the plate-and-frame membrane module for the treatment of tap water contaminated with 60 mg/L nitrate and 100 μg/L of perchlorate. This experiment was carried out under biocompartment operating conditions (biofeed composition and recirculation flow rate and HRT), which were identical to the ones used in a previous study performed with a single membrane module [6]. During the first 6 days of operation, both nitrate and perchlorate accumulated in the biocompartment due to carbon source limitation (ethanol concentration in the biofeed of 0.85 g/L) (see Figure 5.2). This was due to the use of an increased membrane area/reactor volume, which leads to higher mass transport rates of nitrate and perchlorate, requiring higher carbon source levels to be reduced. To avoid this problem, after 6 days of operation, the ethanol concentration in the biofeed was increased to 4.9 g/L (corresponding to an ethanol mass flow rate of 0.5 mmol/h). This value was estimated assuming that the nitrate reduction requires ethanol in stoichiometric amounts (according to equation 5.1, [12]) and for a nitrate flux across the membrane of 0.2 g/(m^2·h) (determined experimentally in the single membrane module for the same F/A ratio) [6].

$$2\ NO_3^- + 5\ C_2H_5OH + 2\ H^+ \rightarrow N_2 + 6\ H_2O + 5\ C_2H_4O \qquad (5.1)$$

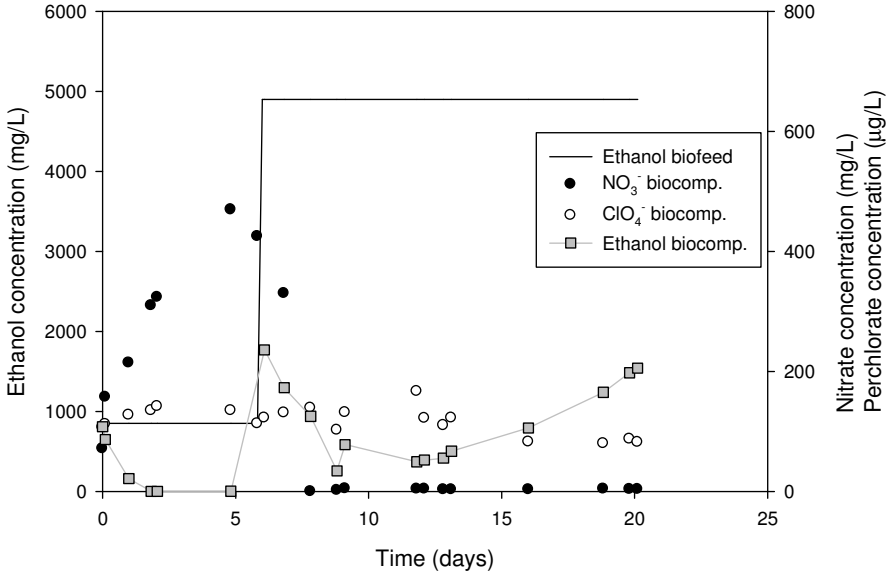

Figure 5.2: Time course of ethanol concentration in the biofeed and nitrate, perchlorate and ethanol concentration in the bulk of the biocompartment of an IEMB operated with a single increase in the ethanol content in the biofeed.

The ethanol demand is dominated mainly by the amounts required for nitrate reduction since perchlorate is present in the water in a 600 times lower concentration than that of nitrate. The increase in mass flow rate of ethanol fed to the biocompartment to 0.5 mmol/h proved to be adequate for complete removal of nitrate (see Figure 5.2), while perchlorate, was detected in the bulk of the biocompartment due to reasons, which will be addressed in section 5.3.2. However, this increased ethanol mass flow rate led to ethanol permeation into the water compartment (detected ethanol concentrations higher than 1 mg/L). As a result of carbon source availability, the water side channels were rapidly clogged due to biomass growth. This observation demonstrated that, during the IEMB start up period, the feeding rate of ethanol should be increased gradually in order to avoid its excess in the bulk of the biocompartment and its transport to the water compartment.

A stepwise ethanol feeding strategy was therefore tested in an IEMB experiment by setting initially the ethanol concentration in the biofed to 0.8 g/L and increasing it by 20-25 % every 4-5 days until day 22 of operation (see Figure 5.3a). On day 22, the ethanol concentration in the biofeed was increased to 2.7 g/L. No further increase in the ethanol level in the biofeed was performed, since nitrate was found to be completely removed with this ethanol concentration.

As it can be observed (Figure 5.3b), during the first 22 days of operation, the ethanol concentration in the biocompartment never raised above 6.5 mg/L and during the majority of this period, ethanol was below its detection limit (1 mg/L by the HPLC analysis used). This period of limited ethanol affected nitrate and perchlorate bioreduction rates and, consequently, both anions accumulated in the biocompartment up to values of 500 mg/L of NO_3^- and 430 μg/L for ClO_4^-, respectively. The accumulation of NO_3^- and ClO_4^- in the biocompartment led to a decrease in the driving forces for their transport from the water compartment and, during this period, the levels of both pollutants in the treated water raised above the drinking water limits (45 mg/L for NO_3^- and 15 μg/L for ClO_4^-, as defined by the US EPA) [13,14] as illustrated in Figure 5.3c.

After day 22, the ethanol concentration in the biocompartment increased to values above 50 mg/L and nitrate and perchlorate biocompartment volumetric removal rates increased from 12.1 mg NO_3^-/L·day to 28.5 mg NO_3^-/L·day and 0.34 mg ClO_4^-/L·day to 0.43 mg ClO_4^-/L·day, respectively. As a consequence of this increased nitrate removal rate, the nitrate concentration in the biocompartment dropped to undetectable levels (detection limit of 1 mg/L). This led to a corresponding decrease in the nitrate level in the treated water to 7 mg/L (much below the maximal nitrate value allowed). However, the perchlorate level in the treated water remained above 15 μg/L since a residual concentration of 200 μg/L in the biocompartment was still documented. Therefore the perchlorate reduction rate was obviously limited by other factors than ethanol limitation (as discussed in section 5.3.2).

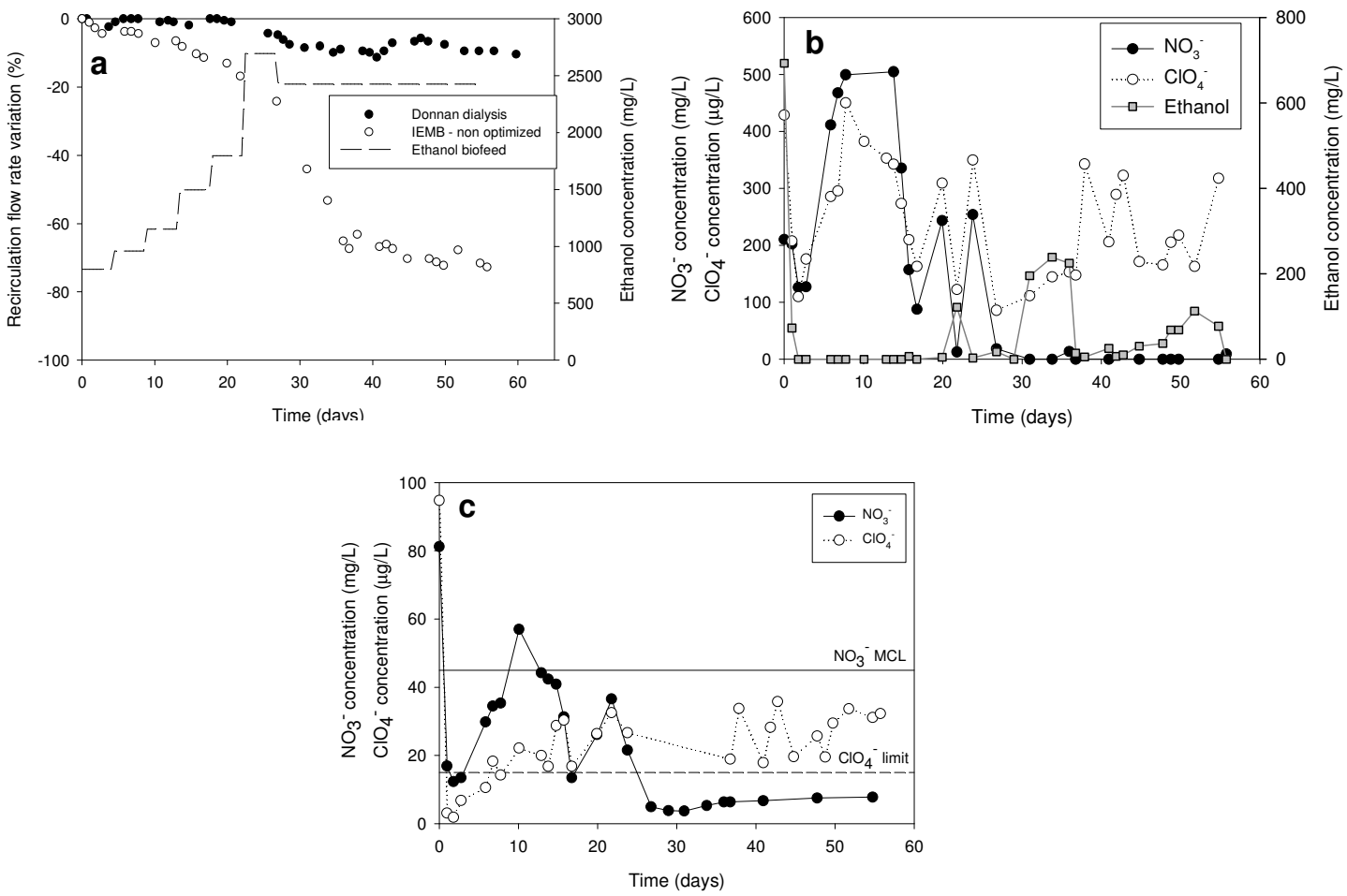

Figure 5.3: Time course of water compartment recirculation flow rate decrease in Donnan dialysis and IEMB operation with a gradual increase in ethanol content in the biofeed (a); nitrate, perchlorate, ethanol concentrations in the biocompartment (b); and nitrate and perchlorate concentrations in the treated water (c) of the plate-and-frame IEMB module.

Furthermore, the ethanol feeding protocol proved to be inadequate to avoid ethanol permeation to the water compartment, in which a significant reduction of the recirculation water flow rate was observed (see Figure 5.3a), due to increased pressure drop in this compartment. At the end of the experiment, the water was recirculating at a flow rate of 12.0 L/h instead of the initial 44.4 L/h. This reduction was a consequence of the increased resistance caused by deposit of materials in the water channels, as confirmed by visual observation when opening the membrane module after the end of the experiment. Despite the fact that ethanol was not detected in the water compartment (detection limit of 1 mg/L by HPLC), it might have diffused through the membrane to the water compartment, thus serving as a carbon source to support microbial cells growth on the membrane surface contacting the water compartment. Indeed, the significant decrease in the recirculation water flow rate observed at day 22 matches well with the increase

in ethanol biofeed concentration from 1.8 g/L to 2.7 g/L performed at that day (see Figure 5.3a). It may be concluded, therefore, that even though the Neosepta ACS membrane used has a very low ethanol diffusion coefficient of 1.8 x 10^{-8} cm^2/s [15], which is 3 orders of magnitude lower than the ethanol diffusion coefficient in water (1.28 x 10^{-5} cm^2/s at 20ºC), ethanol can permeate through this membrane during the process start-up period, when the membrane-supported biofilm is still not developed.

Additionally, fouling in the water compartment can be partially associated with the natural organic matter (NOM) typically present in drinking water sources [16]. Therefore, a Donnan dialysis experiment (without microbial cells and ethanol in the biocompartment) was performed to determine the NOM contribution to the recirculation flow decrease caused by deposit of foulants present in the water stream. Under these conditions, the recirculation flow rate in the water compartment dropped by 10 % after 28 days of operation and then remained stable for the next 30 days (see Figure 5.3a). Given that the composition of water was the same in both experiments, this result supports the conclusion that in the IEMB operation, the water compartment fouling was mainly caused by ethanol transport through the membrane to the treated water.

5.3.1.1. Membrane fouling characterization by fluorescence spectroscopy

The fouling material attached to the membrane surfaces contacting the water and biocompartment channels at the end of previously described IEMB operation was characterized by a 2D-fluorescence spectroscopy. Changes in the fluorescence signal have been used to follow membrane fouling as reported by several authors [10-11, 17]. In the present study, the membrane surface of an unused membrane was analyzed and compared to a membrane taken from the module after the IEMB operation, in order to find out if fouling formation could be detected at early state. Figure 5.4a illustrates a 2D-fluoresce spectrum of the Neosepta ACS membrane before operation (unused membrane). A broad peak in the Ex/Em region of 320-400/400-450 can be observed. This spectrum was used as a membrane fingerprint and subsequent fouling formation was evaluated by the change in the fluorescence signal. After the IEMB operation, the peak observed in the Ex/Em 320-400/400-450 region decreased on both membrane surfaces (see Figures 5.4b and 5.4c). Furthermore, in the case of the membrane surface contacting the biocompartment, a peak in the Ex/Em 280/320-350 nm region was observed. This is the region of Emission/Excitation of proteins [11], which is typical in the presence of a biological material. Indeed, the membrane surface contacting the biocompartment was covered by a biofilm (approximately 1 mm thick). For both surfaces, the peaks observed in the Ex/Em 320-400/400-450 region decreased in comparison with that for the unused membrane. The fouling layers should have obstructed the excitation light and therefore the

membrane characteristic peak signal. These results prove that 2D-fluorescence spectroscopy was able to detect changes on the membrane surface and to monitor fouling formation.

a) Unused membrane

b) Fouled membrane: water compartment

c) Membrane with biofilm: biocompartment

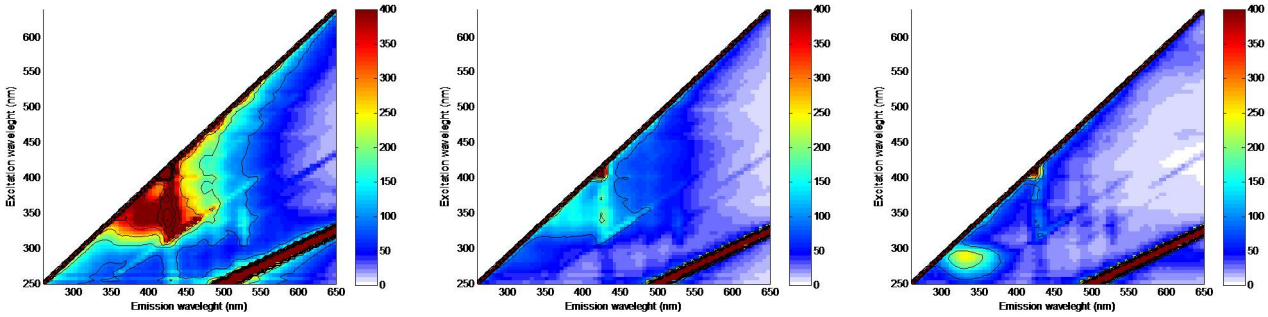

Figure 5.4: Fluorescence spectra of unused membrane surface (a), membrane surface contacting the water compartment (b) and membrane surface contacting the biocompartment (c) after 56 days of an IEMB operation.

The potential of 2D-fluorescence spectroscopy to detect fouling due to compounds present in the water to be treated (the same water used in the previous experiments) was also evaluated. For this, a Donnan dialysis experiment was performed in a dedicated single membrane module, in which no ethanol was added to the receiving compartment. This module possessed a special window for a fluorescence probe insertion, in order to acquire 2D-fluorescence spectra on-line during a long-term operation. A gradual decrease of the peak in the Ex/Em 280/320-350 nm region during the operation time was observed (Figure 5.5). After 4 days of operation, it was possible to detect changes in the 2D-fluorescence spectrum. The peak signal intensity in the Ex/Em 280/320-350 nm region was decreasing until 30 days of operation. After this period, no considerable difference was observed in the fluorescence map until the end of operation. It is interesting to compare this result with the results obtained for the Donnan dialyisis experiment performed in the plate-and-frame module (see Figure 5.3a), in which the recirculation water flow rate decreased until day 28 and then also remained constant until the end of the experiment. Thus, both observations, obtained through rather distinct ways, support the same conclusion of fouling approaching a steady-state after about a month of process operation.

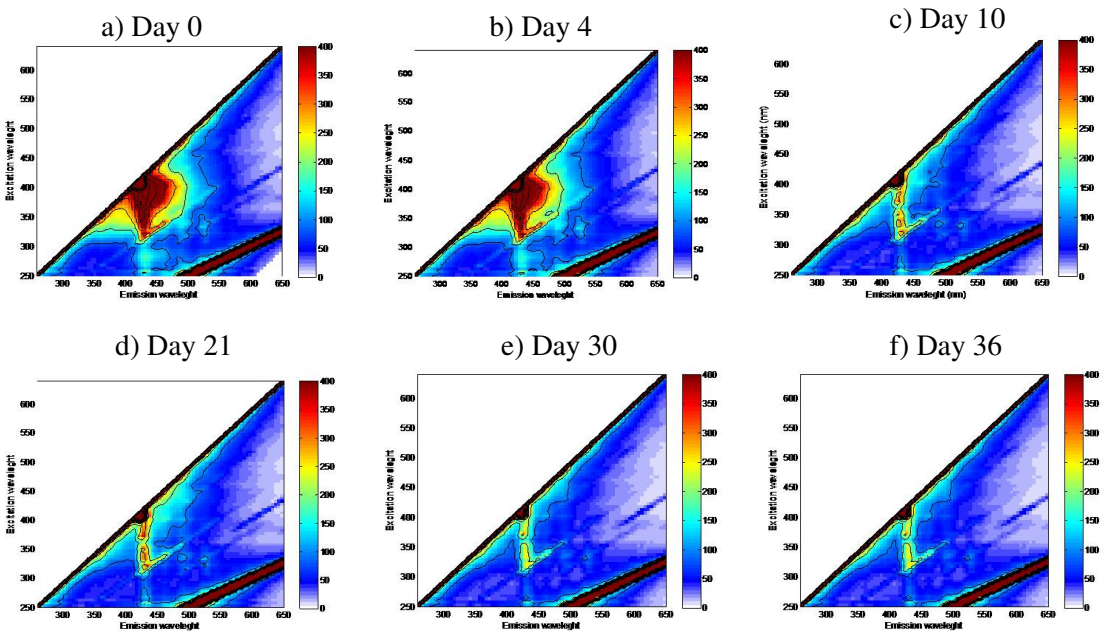

Figure 5.5: Fluorescence spectra of membrane surface contacting the water compartment during Donnan dialysis: at the start of the experiment (a) and after 4 (b), 10 (c), 21 (d), 30 (e) and 36 days (f) of operation.

5.3.1.2. Strategy for ethanol feeding to the IEMB biocompartment

In order to avoid ethanol permeation to the water compartment, a dedicated ethanol feeding strategy proved to be necessary during the process start-up period, when the biofilm is still not developed. As a controlling parameter, the redox potential in the biocompartment was used. This parameter was previously used with success by Nam *et al* to control carbon source addition to an anoxic reactor for nitrogen removal [18].

Ethanol was initially fed at 0.1 mmol/h (corresponding to an ethanol concentration in the biofeed of 1 g/L) and increased by 10 % every 6-7 days until a value of 0.2 mmol/h was reached (1.8 g/L in biofeed). This stepwise increase was defined by the variation of the redox potential: whenever the variation was positive ($\Delta(redox) > 0$, in which $\Delta(redox) = redox_{t+\Delta t} - redox_t$), the ethanol concentration in biofeed was increased. Thereby, in situations of ethanol limitation, the rate of perchlorate and nitrate reduction decreased and consequently the redox potential increased. With this ethanol feeding strategy, no significant reduction of the recirculation flow rate in the water compartment was observed as illustrated in Figure 5.6. In fact, the decrease in recirculating flow rate in the IEMB process followed almost the same profile observed for an operation without any ethanol addition (Donnan dialysis). Considering that ethanol permeation potentiated biofouling formation, as shown in Figure 5.3, this result suggests that no ethanol has permeated through the membrane. After 35 days of operation, the recirculation flow rate value reached a plateau and remained constant for other 20 days. Thus, the IEMB process was

operated for two months without any detectable fouling formation caused by ethanol permeation.

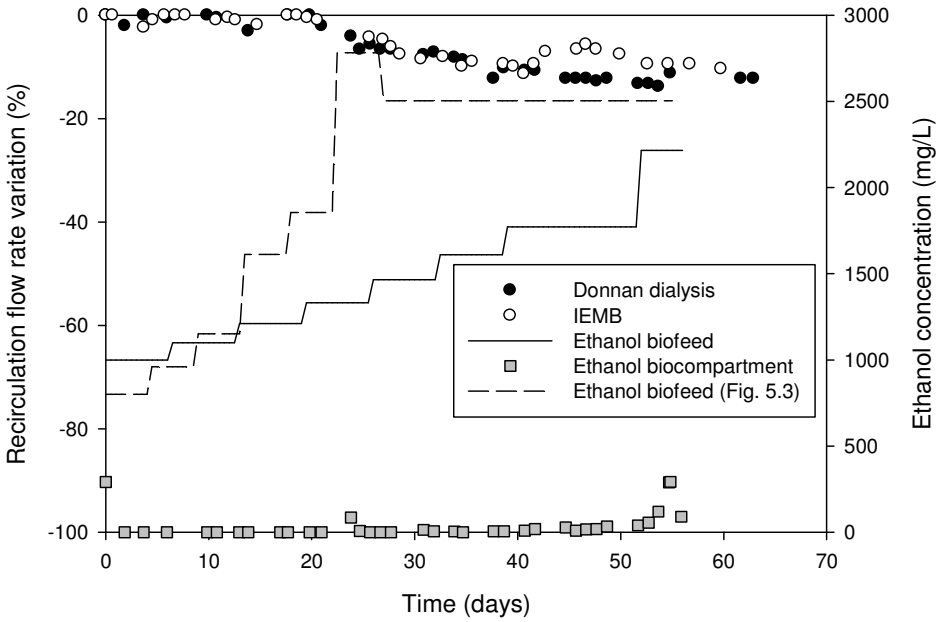

Figure 5.6: Flow rate decrease in the water compartment recirculation loop and ethanol concentration in the biofeed and in the IEMB biocompartment. To facilitate the comparison, the recirculation flow rate decrease under Donnan dialysis operating conditions and with the IEMB ethanol feeding protocol followed previously (see Figure 5.3a) are also presented.

This stepwise increase of the ethanol feeding rate was essential only during the process start-up period. After this period, the biofilm acted as an additional reactive barrier minimizing ethanol permeation since the process performance remained stable even with an ethanol level of 300 mg/L in the bulk of the biocompartment (Figure 5.6). At day 50, the ethanol concentration in the biofeed was increased by additional 25 %, again without any detectable effect on the water recirculation flow rate (Figure 5.6). Therefore, after the biofilm formation, strict control of the rate of addition of ethanol is no longer necessary.

This strategy was also appropriate to avoid ethanol limitation for the reduction of nitrate by the microbial cells. Nitrate accumulation was only detected in the first 10 days of operation, reaching a maximum of 280 mg/L (see Figure 5.7a). After this period, nitrate started to be reduced and, after 17 days of operation, the nitrate concentration in the treated water was already below the maximum contaminant limit allowed for drinking water sources, as illustrated by Figure 5.7b. However, perchlorate still accumulated in the biocompartment bulk, even though ethanol was available in the biocompartment. This indicates that the perchlorate reduction was inhibited by other factors and not by carbon source limitation.

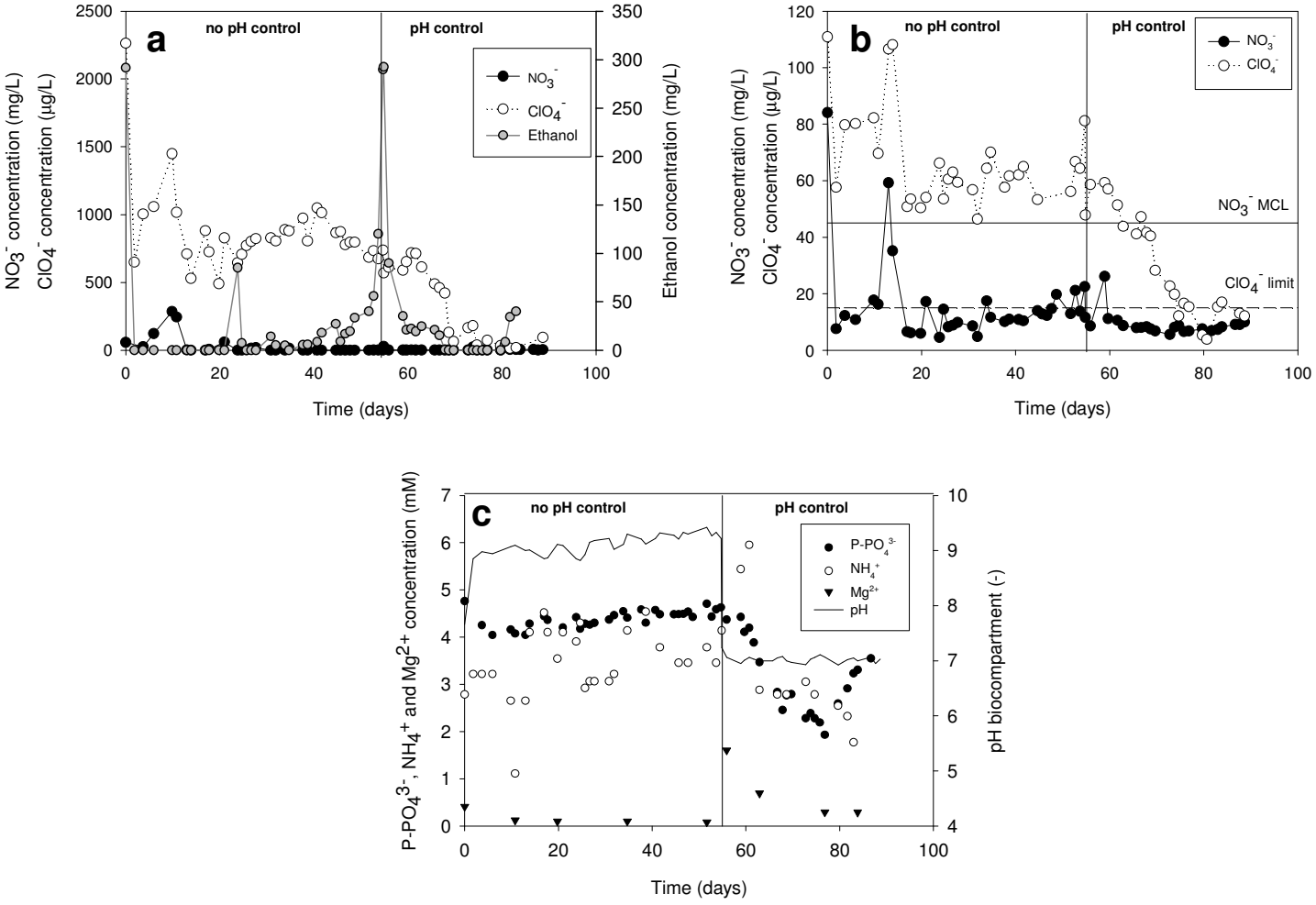

Figure 5.7: Time course of concentrations of nitrate, perchlorate and ethanol in the biocompartment (a), nitrate and perchlorate in the treated water (b) and phosphorus as phosphate, ammonium and magnesium in the biocompartment, as well as pH in the biocompartment (c). Control of the biocompartment pH (at pH=7) was started after 55 days of operation.

5.3.2. Effect of biocompartment parameters on perchlorate removal

The up-scaling design (high A/V_b ratio) might cause accumulation of inhibiting metabolic by-products since a higher number of perchlorate and nitrate reducing bacteria are present in the same biocompartment volume. Indeed, it was found out that the biocompartment pH reached a value of 9.5. This value could be inhibitory for perchlorate reduction since previous studies have shown that bacteria can reduce perchlorate within the pH range between 5 and 9 [19]. Moreover, Wu *et al*. observed a 90% decrease in the perchlorate reduction rate at pH 9 when comparing with the perchlorate reduction rate at pH 7-8 [20]. The higher pH value in the plate-and-frame module compared to that in the previously used single membrane module (pH 8) [21] was a consequence of the biocompartment design, leading to a higher ratio of membrane area

per biocompartment liquid volume. Due to the higher mass transport rates of nitrate and perchlorate per biocompartment volume: 16.1 mg NO_3^-/h and 19.1 µg ClO_4^-/h compared to 0.7 mg NO_3^-/h and 1.0 µg ClO_4^-/h in the single membrane module, [21], the concentration of metabolically produced bicarbonate increased, thus leading to higher pH values in the biocompartment. This higher pH may affect the perchlorate reduction rate by two ways: 1) direct effect on the perchlorate reducing activity of the microbial cells; 2) indirect impact due to precipitation of some nutrients. Indeed, it is known that at high pH values, phosphorus, magnesium and ammonia can precipitate in the form of struvite, a mineral which minimal solubility occurs at pH 9 [22]. Besides a possible decrease of the amount of soluble nutrients needed for biological activity, struvite formation may also lead to membrane scaling and therefore to an increase of the diffusional resistance to nitrate and perchlorate transport to the biocompartment.

To confirm that the inhibition of perchlorate reduction was caused by the high biocompartment pH, a pH control at 7 (by adding HCl), which is considered optimal for both nitrate and perchlorate reduction [19, 23] was started at day 55. Moreover, at this pH value, struvite precipitation is expected to be minimal [22]. During the period without pH control, perchlorate accumulated to 700 µg/L in the biocompartment under a non-limiting ethanol concentration, whereas nitrate was consumed to undetectable values (see Figure 5.7a). After starting the biocompartment pH control, the perchlorate reduction rate increased from 0.30 mg ClO_4^-/L·day to 0.63 mg ClO_4^-/L·day. With this rate, the concentration of perchlorate in the biocompartment decreased to 13 µg/L and, as a consequence, the rate of perchlorate transport across the membrane was enhanced due to the increase of the driving force for perchlorate transport. As a result, both nitrate and perchlorate concentrations decreased to below the respective recommended levels for drinking water, as illustrated by Figure 5.7b.

With the decrease of the biocompartment pH, an immediate increase in the soluble magnesium concentration from 0.08 mM (2.0 mg/L) to 1.6 mM (39 mg/L) was observed, as illustrated in Figure 5.7c. Since magnesium was fed to the biocompartment at a biofeed concentration of 10 mg/L in the form of $MgSO_4$, this increase in the concentration of soluble magnesium can be attributed to dissolution of magnesium stored in the form of struvite. The same behavior was observed for the concentration of ammonium in the bulk of the biocompartment: an increase from 4.14 µM (74.7 mg/L) to 5.95 µM (107.3 mg/L). Regarding phosphate, the struvite dissolution did not contribute for a significant increase in its soluble concentration since only a maximum of 3% (0.3 mM) of phosphate fed to the biocompartment was expected to precipitate. This value was estimated considering that struvite is formed in stoichiometric molar amounts from the three ions: magnesium, ammonium and phosphate [24] and assuming that all magnesium consumed (0.3 mM), was for struvite precipitation. This assumption is

straightforward since magnesium cations due to their positive charge are not transported through the anion exchange membrane.

Struvite dissolution was also confirmed by visual observation of the membrane surface contacting the biocompartment. The presence of crystals of precipitate formed was documented by scanning electron microscopy (SEM) images, as illustrated in Figure 5.8. No precipitate can be observed on the membrane surface when the process was operated with pH control at 7.

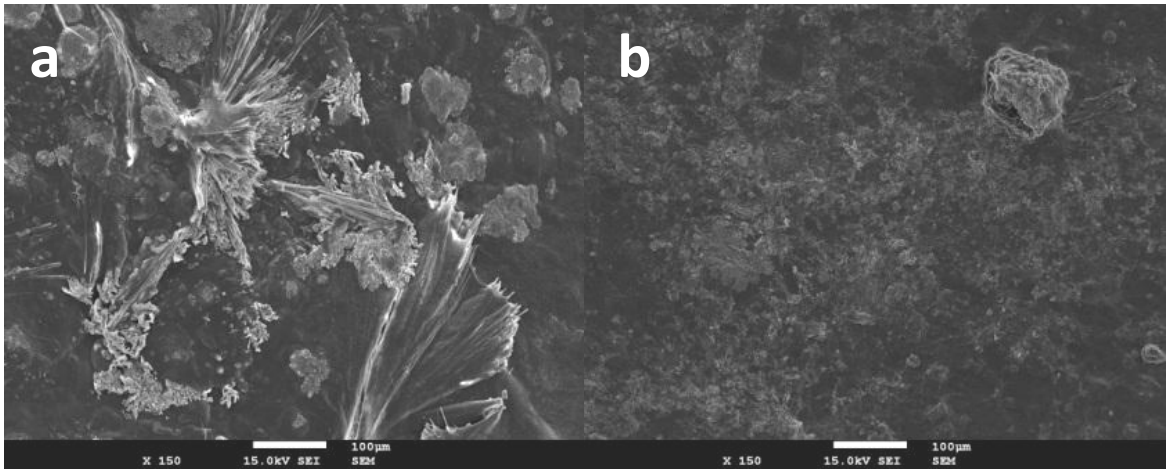

Figure 5.8: Scanning electron microscope images of the membrane surface contacting the biocompartment before (a) and after (b) pH control.

It is worth noting that the use of HCl as a pH regulating agent not only allowed maintaining the desired pH value but, at the same time, Cl^- can be used as the driving counter-ion for the transport of nitrate and perchlorate to the biocompartment. In fact, for pH regulation, 9.3 mmol/day of Cl^- were fed in the form of HCl, which corresponds to almost all the chloride that was added in the form of NaCl (11.5 mmol/day). Therefore, the amount of Cl^- required in the process can be supplied by HCl as pH-regulating agent, thus completely utilizing this reagent and avoiding addition of NaCl as a source of driving Cl^- counter-ions.

5.4. Conclusions

The IEMB process was successfully up-scaled and operated using a plate-and-frame membrane module for the simultaneous removal of nitrate and perchlorate from contaminated drinking water streams. Based on the results obtained in this study, the following main conclusions can be drawn:

- A dedicated ethanol feeding strategy, involving a stepwise increase of its concentration in the biofeed must be performed during the process start-up period, in order to avoid ethanol permeation into the treated water stream. This is particularly critical during the start-up period, since the microbial biofilm on the membrane surface contacting the IEMB biocompartment is still not developed.
- 2D-fluorescence spectroscopy proved to be an adequate and sensitive non-invasive technique for detecting and on-line monitoring possible fouling formation on the membrane surface contacting the treated water stream.
- The biocompartment pH does not significantly influence nitrate reduction, but must be controlled at pH=7 in order to assure complete perchlorate removal. pH control is also necessary to avoid process operation under alkaline conditions, favoring struvite precipitation on the membrane surface. Such precipitation is undesirable because of membrane scaling and decreased availability of nutrients for the biofilm.
- The use of HCl as a pH-regulating agent allows for the simultaneous delivery of H^+ for pH adjustment and Cl^- driving counter-ions for enhanced counter-transport of nitrate and perchlorate to the biofilm, thus completely utilizing this reagent and avoiding the necessity of adding NaCl to the biocompartment.

5.5. References

1 Rittmann, B. E., 2007. The membrane biofilm reactor is a versatile platform for water and wastewater treatment. Environ. Eng. Res. 12 (4): 157-175.

2 Shanahan, J.W., Semmens, M.J., 2006. Influence of a nitrifying biofilm on local oxygen fluxes across a micro-porous flat sheet membrane. J. Membr. Sci. 277: 65-74.

3 Freitas dos Santos, L.M., Livingston, A.G. , 1995. Novel membrane bioreactor for detoxification of VOC wastewaters: biodegradation of 1,2-dichloroethane. Water Res. , 29 (1): 179-194.

4 Velizarov, S., Rodrigues, C.M., Reis, M.A., Crespo, J.G., 2000/2001. Mechanism of charged pollutants removal in an ion exchange membrane bioreactor: drinking water denitrification. Biotechnol. Bioeng. 71 (4), 245-254.

5 Velizarov, S., Reis, M.A., Crespo, J.G., 2011. The Ion-Exchange Membrane Bioreactor: developments and perspectives in drinking water treatment. In Water Purification and Management, J. Coca-Prados, G. Gutiérrez-Cervelló (Eds.). Nato Science for Peace and Security Series C: Environmental Security. Springer, pp. 119-145.

6 Matos, C.T., Velizarov, S., Crespo, J.G., Reis, M.A. , 2006. Simultaneous Removal of Perchlorate and Nitrate from Drinking Water using the Ion Exchange Membrane Bioreactor Concept. Water Res. 40: 231-240.

7 Baker, R.W., 2004. Membrane Technology and Applications. 2nd Edition. John Wiley & Sons, Ltd, Chinchester, p. 538.

8 Song, L., Toy, K.G., 2011. Advanced Membrane Fouling Characterization in Full-Scale Reverse Osmosis Processes. In Membrane and Desalination Technologies, L. K. Wang, J. P. Chen, Y.-T. Hung, & N. K. Shammas (Eds.). Humana Press, London, pp. 101-134.

9 Her, N., Amy, G., McKnight, D., Sohn, J., Yoon, Y., 2003. Characterization of DOM as a function of MW by fluorescence EEM and HPLC-SEC using UVA, DOC, and fluorescence detection. Water Res. 37: 4295-4303.

10 Henderson, R.K., Baker, A., Murphy, K.P., Hambly, A., Stuetz, R.M., Khan, S.J., 2009. Fluorescence as a potential monitoring tool for recycled water systems: A review. Water Res. 43: 863-881.

11 Galinha, C.F., Carvalho, G., Portugal, C.A., Guglielmi, G., Reis, M.A., Crespo, J.G., 2011. Two-dimensional fluorescence as a fingerprinting tool for monitoring wastewater treatment systems. Chem. Technol. Biotechnol. 86: 985-992.

12 Comeau, Y., 2008. Microbial metabolism. In Biological wastewater treatment: principles, modelling and design, M. Henze, M. van Loosdrecht, G. Ekama, D. Brdjanovic (Eds.). IWA Publising, London, pp. 9-32.

13 US Environmental Protection Agency (USEPA), 2010. National primary drinking water regulations. Federal Register 75(59): 15500-15572.

14 US Environmental Protection Agency (USEPA), 2011. Drinking Water: Regulatory Determination on Perchlorate. Federal Register 76 (29): 7762-7767.

15 Fonseca, A.D., Crespo, J.G., Almeida, J.S., Reis, A.M., 2000. Drinking water denitrification using a novel ion-exchange membrane bioreactor. Environ. Sci. Technol. 34 (8): 1557-1562.

16 Porcelli, N., Judd, S., 2010. Chemical cleaning of potable water membranes: A review. Sep. Pur. Technol. 71: 137-143.

17 Wang, Z., Wu, Z., Tang, S., 2009. Extracellular polymetic substances (EPS) properties and their effects on membrane fouling in a submerged membrane bioreactor. Water Res. 43: 2504-2512.

18 Nam, H.U., Kim, Y.O., Lee, J.H., Hur, S.H., Park, T.J., 2004. Automatic control of external carbon source addition for nitrogen removal in sewage with low C/N ratios. Water Sci. Technol. 49 (5-6): 245-249.

19 Wang, C., Lippincott, L., Meng, X., 2008. Kinetics of biological perchlorate reduction and

pH effect. J. Hazard Mater. 153 (1-2): 663-669.

20 Wu, D., He, P., Xu, X., Zhou, M., Zhang, Z., Houda, Z., 2008. The effect of various reaction parameters on bioremediation of perchlorate-contaminated water. J. Hazard Mater. 150: 419-423.

21 Ricardo, A.R., Oliveira, R., Svetlozar, V., Reis, M.A., Crespo, J.G., 2011. Multivarite Statistical Modelling of Mass Transfer in a Membrane-Supported Biofilm Reactor. Process Biochem. 46: 1981-1992.

22 Doyle, J.D., Parsons, S.A., 2002. Struvite formation, control and recovery. Water Res. 36: 3925-3940.

23 Wong, C.H., Barton, G.W., Barford, J.P., 2003. The nitrogen cycle and its application in wastewater treatment. In The handbook of water and wastewater microbiology, D. Mara, N. Horan (Eds.). Elsevier, London, pp. 427-439.

24 Rahamn, M.S., Ellis, N., Mavinic, D.S., 2008. Effects of various process parameters on struvite precipitation kinetics and subsequent determination of rate constants. Water Sci. Technol. 57 (5): 647-654.

Chapter

6

Final overview and suggestions for future work

6.1. Final Overview

The contamination of drinking water resources with inorganic ionic pollutants, such as perchlorate and nitrate, represents a serious problem for human health. Therefore, it is imperative to develop technologies that allow for their complete removal from contaminated water streams. The ion exchange membrane bioreactor (IEMB) proved to be a suitable process for complete elimination of nitrate and perchlorate from the environment by combining their transport across monovalent perm-selective anion-exchange membranes with simultaneous bio-transformation to innocuous compounds (nitrogen and chloride, respectively). In the studies performed in the frame of this PhD project, the IEMB process was experimentally investigated, mathematically modeled, and validated in an industrially relevant type of membrane module configuration.

The statistic and hybrid (mechanistic-statistic) counter-ion mass transport models developed allowed to predict the flux of the counter-ions that can permeate through the membrane over a broad range of process operating conditions, including biological reaction rate-limiting situations. These models are a step forward compared to a previously steady-state mechanistic model, applicable only to counter-ion mass-transfer limiting situations. The use of statistically-based modeling approaches showed that, under specific conditions (e.g., nutrient limitation and/or unfavorable pH in the IEMB biocompartment), physicochemical and hydrodynamic

parameters associated with the biocompartment operation become important input variables, controlling the transport of a target counter-ion (anion) across the membrane and, therefore, must be accounted for. Therefore, accurate models for predicting nitrate, perchlorate, sulfate and bicarbonate were developed without the need of accessing complex and time-dependent biofilm parameters such as thickness, density, morphology, etc.

Within the modeling strategies followed, the more accurate model was obtained by combining the mechanistic model with a projection to latent structures (PLS) model in a mixture of experts (MOE) structure. This structure merges the two models in a way allowing the use of the mechanistic model in situations within its range of validity, while partially involving or completely switching to the statistical component in situations where the biocompartment conditions limit the transport of target anion(s) across the membrane.

One of the main challenges for an efficient simultaneous removal of nitrate and perchlorate is the fact that they are commonly present in contaminated drinking water sources in rather different concentration ranges (nitrate in mg/L and perchlorate in µg/L). Nevertheless, the IEMB process proved to be capable of removing both oxy-anions to concentrations below the maximum recommended levels in drinking water accompanied by their simultaneous degradation by a mixed membrane-attached anoxic microbial biofilm. Moreover, different controlling mechanisms were identified for nitrate and perchlorate bioreduction in the IEMB.

The IEMB process efficiency for nitrate removal was mainly controlled by its mass-transport rate to the biocompartment, while the perchlorate removal within the µg/L concentration range was much more sensitive to biological-reaction related kinetic parameters. Due to the kinetic advantage of nitrate reduction, denitrifiers were pioneers in the biofilm formation and were located near the membrane surface, whereas perchlorate reducing bacteria were displaced to the biofilm outer surface, contacting the biomedium. It was demonstrated that in the presence of nitrate, perchlorate reduction rate was diminished by 62 %. Therefore, due to the biofilm stratification, perchlorate reduction occurred at its maximum rate, since inhibition by nitrate was avoided. The operation of the IEMB with a biofilm, allowing for sequential reduction of nitrate and perchlorate in space, is beneficial when compared with suspended-cell systems, since it provides the opportunity for distinct microbial species to grow under adequate conditions by creating different micro-environments within the biofilm. This biofilm stratification is also important to avoid secondary contamination of the treated water by excess of carbon source (ethanol). Due to the biofilm stratification, a gradient in the reduction rate is expected, with the maximum rate for nitrate more likely to occur closer to the membrane. Thereby, since the carbon source and the two electron acceptors (nitrate and perchlorate) enter the biofilm in a counter-diffusion mode, the presence of denitrifiers closer to the membrane surface may be

advantageous as a reaction zone providing an additional barrier to the transport of carbon source to the treated water.

This work also demonstrated the feasibility of the IEMB to be operated in a plate-and-frame configuration. The up-scaling of the process from a single membrane to a plate-and-frame module with a number of membranes and spacers allowed for evaluating its impact on the IEMB process efficiency. The feasibility of a plate-and-frame IEMB module configuration for the simultaneous treatment of drinking water contaminated with nitrate and perchlorate was validated during long-term process operations of up to 3 months. Permeation of carbon source across the membrane to the treated water stream was avoided by a dedicated start-up procedure involving a gradual increase of ethanol feeding to the IEMB biocompartment.

It was demonstrated that the biocompartment pH does not influence significantly the nitrate reduction but must be controlled in order to guarantee a complete perchlorate removal. pH control in the biocompartment was also necessary to avoid precipitation of struvite on the membrane surface, which led to membrane scaling and a decreased availability of nutrients for the biofilm. It was found out that the amount of Cl^- required in the process could be supplied by the pH-regulating agent (HCl), thus completely utilizing this chemical as a source of both H^+ and Cl^- for pH adjustment and as "driving" anions for the counter transport of nitrate and perchlorate to the biocompartment, respectively. Under these conditions, the IEMB process was successfully operated maintaining the nitrate and perchlorate concentrations in the treated water below their recommended levels for drinking water supplies.

6.2. Suggestions for future research

The results obtained in the frame of this PhD project were a step forward in both mathematical modeling and validation of the IEMB process for the simultaneous removal of polluting oxy-anions such as nitrate and perchlorate from contaminated drinking water streams. Aiming at a possible industrial application of the IEMB process, the following recommendations for future work can be proposed.

The hybrid mechanistic-statistical mathematical model developed allowed for predicting the flux of target anions based on data related to both polluted water composition and biocompartment medium and operating conditions. However, some of the model predictors

concern biocompartment variables, which are dependent upon the flux(es) of target anion(s) across the membrane. Therefore, an alternative modelling approach could be the use of hybrid modelling structures, which involve appropriate mass balance equations. In the dynamic material balance of the biological compartment, a statistically based model (such as PLS) could be used to identify the biological reaction kinetics. This model could then be combined with the model developed in this work, for a global IEMB predictive tool. Furthermore, this model could be used to support the integrated optimization of operational parameters of the two IEMB compartments.

A global predictive model may be used to design a proper biofeed composition. In fact, the biofeed composition in terms of nutrients was always kept in excess to avoid biological limitation. However, in Chapter 2 transport of phosphate from the biocompartment to the treated water stream was detected. The optimization of nutrients concentration is important not only to prevent changes in the water composition but also to minimize the operating costs associated with the nutrients supplementation. The use of such a global IEMB model would allow developing process operations, in which the cells metabolic needs are accounted for.

In chapter 5, the IEMB process feasibility in a plate-and-frame configuration was proven. In this configuration, the hydrodynamic conditions in the water compartment were guaranteed by dedicated spacers. It was previously demonstrated that the fluid dynamics in the water compartment controls the liquid boundary layer thickness in this compartment that has a significant impact on the resistance to transport of the target counter-ions [1]. Therefore, the role of spacers for mass transfer enhancement is of major importance. In this relation, the design of appropriate spacers to be used in the water channels is essential to assure a low mass transfer resistance at a low pressure drop. For this propose, the use of computational fluid dynamics (CFD) may facilitate the simulation and design of the most appropriate spacer configuration. This modelling technique proved to be suitable for spacers design, since it was able to predict accurately flow and concentration distributions in spacer-filled channels [2, 3].

At this moment, the high cost of ion-exchange membranes is a significant limitation. The fact that these membranes are industrially produced only with a flat geometry (for electrodialysis processes), limits the compactness of the membrane reactor and the control of the fluid dynamic conditions in the water compartment (as the controlling resistance is most frequently located in the boundary layer at the membrane/water interface). Therefore, the development and investigation of the performance of ion-exchange membranes with hollow-fibre geometry will make possible the design of IEMB systems more compact and with an easier and more efficient control of the water fluid dynamics, by circulating the treated water stream inside the lumen of the fibres.

Further research is also needed for designing the IEMB application for the treatment of water streams containing high perchlorate concentrations. This is due to the fact that the amount of water to the treated is defined by the very low perchlorate concentration to be achieved - the current regulation requires the perchlorate concentration in the treated water to be below 15 μg/L. When dealing with perchlorate concentrated water streams, the water throughput could be enhanced by applying different IEMB process schemes, such as, for example, using more than one IEMB modules, organized in series or in parallel mode. Furthermore, it should be studied how each module would best operate: a) with water single-pass or with water recirculation and b) the appropriate hydrodynamic regime - plug-flow, or complete stirring. To support this evaluation, it is desirable to develop a differential mathematical model able to predict axial concentration profiles of the target anions in the water compartment of the membrane module.

Additionally, the feasibility of the IEMB concept for applications not solely related to drinking water treatment must be investigated. The treatment of concentrated ion-exchange brine solutions is one of the possibilities. Other potential applications of the IEMB concept for the removal (or recovery) of target ions (anions or cations depending on the case) could be develop for culture media, or for selective desalination of pharmaceutical and/or liquid food products for special applications, e.g. those used in baby diets.

6.3. References

1 Velizarov, S., Reis, M.A., Crespo, J.G., 2003. Removal of trace mono-valent inorganic pollutants in an ion exchange membrane bioreactor: analysis of transport rate in a denitrification process. J. Membr. Sci. 217: 269-284.

2 Dendukuri, D., Karope, S. K., Kumar, A., 2005. Flow visualization through spacer filled channels by computational fluid dynamics-II: improved feed spacer designs. J. Membr. Sci. 249: 41-49.

3 Santos, J.L., Geraldes, V., Velizarov, S., Crespo, J.G., 2007. Investigation of flow patterns and mass transfer in membrane module channels filled with flow-aligned spacers using computational fluid dynamics (CFD). J. Membr. Sci. 305: 103-117.